

High-throughput microfluidic platforms applied to immunoassay-based diagnostics and environmental monitoring

THÈSE N° 7903 (2017)

PRÉSENTÉE LE 20 OCTOBRE 2017

À LA FACULTÉ DES SCIENCES ET TECHNIQUES DE L'INGÉNIEUR
LABORATOIRE DE CARACTÉRISATION DU RÉSEAU BIOLOGIQUE
PROGRAMME DOCTORAL EN MICROSYSTÈMES ET MICROÉLECTRONIQUE

ÉCOLE POLYTECHNIQUE FÉDÉRALE DE LAUSANNE

POUR L'OBTENTION DU GRADE DE DOCTEUR ÈS SCIENCES

PAR

Francesca VOLPETTI

acceptée sur proposition du jury:

Prof. G. De Micheli, président du jury
Prof. S. Maerkl, directeur de thèse
Dr G. Kaigala, rapporteur
Dr M. Meier, rapporteur
Prof. M. Lutolf, rapporteur



ÉCOLE POLYTECHNIQUE
FÉDÉRALE DE LAUSANNE

Suisse
2017

To the ones I love

Acknowledgements

First of all I would like to thank my advisor, Sebastian Maerkl, for giving me the opportunity to work in his lab and for always being a fundamental support with his ideas, suggestions and passion for science.

I would like to thank the members of my thesis committee, Prof. Giovanni de Micheli, Prof. Matthias Lutolf, Dr. Matthias Meier and Dr. Govind Kaigala, for being part of the examination jury and for evaluating the work I have done during my PhD.

My sincere thanks goes to Prof. Domenico Caputo because his passion for his work motivated me to do a PhD. I would like also to thank Prof. Joao Pedro Conde and Dr. Virginia Chu for the important experience I got in their lab.

Thank you to all the members of LBNC. Starting with the former members, I would like especially to thank Jose Garcia-Cordero for his help with microfluidics when I joined the lab and for our collaboration, Henrike, Matt and Hannes for being extremely nice and friendly since the first day. Amanda and Suzanna for the nice time we spent together. I would like to thank the current LBNC lab members Kristina, Nadanai, Ivan (for me “Vaniuska”), Barbora, Greg, Fabien and Simone, I was extremely lucky to have you as colleagues, not only from the scientific point of view but also for our friendship and the amazing time we had together. Thank you to Ekaterina for our fruitful collaboration and for these four years we have spent together in the lab. I would like to thank Craig for the great work he has done in the lab and for his attitude. A special thank you goes to my colleague and friend Francesco, for being a great collaborator and buddy, without his help it wouldn't be the same; and to Zoe, everyone who has ever met her knows she deserves a special thanks. A great thank you goes to Helen for being always helpful, kind and smiling and thank you to Martine for her help towards the end.

I am thankful to all the members of “my other Lab”, especially to Daria for spending a lot of time with me in the lab when I arrived and for becoming my really good friend afterwards. Thank you to Dmitry and Kolyo for being always helpful in the lab but mostly for our interesting and stimulating conversations. Thank you to Saj for our chatting and your

support. I thank all the remaining members of LANES: Jacopo, Simone, Dominik, Adrian, Dumitru, Yen-Chen, Ming-Wei, Oriol, Mitia, HoKwon, Alberto, Ahmet and Wei, I am glad I had the chance to meet and work with all of you.

I would like to thank people who were not in my labs but were an important part of this long journey: Adriano, Zahra, Volker, Manon, Clement, Cornelis, Miguel, Claudia, Gregoire, Elena, Enrico and members of LBEN. Thank you Francesca for our coffee breaks and our chatting/complaining.

My staying in Lausanne wouldn't have been as nice as it was without "I Vaghissimi amici", thanks to all of you I felt a bit more at home, a particular thanks goes to our wonderful mascot Alessandro.

I am grateful for my parents, my sister, Pasquale, Rosaria and Marco for being always on my side and always understanding, in any situation.

Finally, I would like to thank Nico for being with me during the last 10 years, in particular for supporting me in this last 5 years when you were able to make everyday somehow special, even if my mood was not always good.

Lausanne, 26 July 2017

Francesca Volpetti

Abstract

The research presented in this thesis is motivated by the aim to employ microfluidic devices for high-throughput analysis. Two applications, in particular, have been explored: diagnostics and environmental sensing. Miniaturization and multiplexing of laboratory procedures leads to a decrease of the cost and response time of the test. Moreover miniaturization allows the system to become portable, enabling use in the field without bulky external equipment. This need is paving the way for innovative approaches and microfluidics can be a suitable substitute for standard bench top techniques. In order to be appealing, these new technologies should have the same or even better performances over the standard techniques, not only in terms of time and cost, but also quality of results.

First, we developed a multilayer microfluidic platform for high-throughput immunoassay analysis. The device is composed of 384 units, each of them containing 4 mechanically induced trapping of molecular interactions (MITOMI) buttons, where the interaction of antibodies and antigens occurs. Therefore, the platform allows us to perform 1'536 tests, and we show that it can be useful for large scale screening in order to identify functional antibody pairs. However this system has two limitations: the experimental time (~10 hours) and the sensitivity (pM). In the second part, we presented another device modified in order to overcome the aforementioned drawbacks and to become more suitable for point of care applications.

This new version of the device has 16 independent units, and the MITOMI buttons are patterned with femtoliter wells for digital analysis. We show how digital ELISA improves the sensitivity and allows us to detect down to fM concentrations in human serum. We also show how the combination of both digital and analog detection can broaden the dynamic range. A portable automatic controller has also been built to control the valves and the flow throughout the chip and a USB microscope has been exploited in order to measure the fluorescent signal.

In the last part we present a different application for high-throughput microfluidic-based devices. A microfluidic device composed of 769 units has been developed for bacterial cell

culture and environmental monitoring. Each unit can be considered as a pixel and the entire device as a biodisplay. Each unit contains a specific bacterial strain, which is deposited using microspotting techniques. We show how different bacterial strains can be cultured over time without contamination between pixels and how they can be monitored after induction. Cells can be spotted according to a specific pattern on the chip and express fluorescent protein reporters in the presence of specific molecules allowing an easy to interpret result of the test. For example, the image of a “skull and crossbones” appears if the analyzed sample is contaminated with arsenic.

Overall, the presented work provides several microfluidic platforms for high-throughput analysis of clinical or environmental samples; these devices are useful tools for the study of a large number of proteins and molecular diagnostic applications and to characterize bacterial strains and environmental monitoring.

Keywords: microfluidics, sandwich immunoassay, digital ELISA, diagnostics, point-of-care, high-throughput, bacterial culturing, bioreporter, biopixel, environmental monitoring.

Riassunto

Il lavoro di ricerca presentato in questa tesi ha come obiettivo l'utilizzo di dispositivi microfluidici per analisi high-throughput. In particolare, sono state esplorate due applicazioni: la diagnostica e l'analisi di campioni ambientali.

La miniaturizzazione e la parallelizzazione di procedure normalmente svolte in laboratorio porta a una diminuzione dei costi e dei tempi di analisi. Inoltre la riduzione di dimensioni permette di avere un sistema portatile e di svolgere le analisi senza l'utilizzo di strumentazioni da laboratorio costose e ingombranti. La necessità di avere un tale dispositivo apre la strada ad approcci alternativi e la microfluidica è una buona candidata per soddisfare tale richiesta. Queste nuove tecnologie, per essere prese in considerazione, devono fornire uguali se non migliori prestazioni, non solo in termini di costi e tempi di analisi, ma anche per quanto riguarda la qualità dei risultati.

Inizialmente abbiamo sviluppato un dispositivo microfluidico multistrato che permette di realizzare molteplici analisi immunologiche in parallelo. Il dispositivo è composto da 384 unità, ogni unità contiene 4 membrane circolari, chiamate MITOMI, che servono ad intrappolare meccanicamente su un substrato vetroso le molecole e a studiare l'interazione tra antigene e anticorpo. Il dispositivo permette di eseguire 1'5536 test, e può essere utilizzato per analizzare un numero elevato di proteine contemporaneamente e studiare la funzionalità di differenti coppie di anticorpi. Questo dispositivo ha due limitazioni: il tempo necessario per compiere l'analisi (all'incirca 10 ore) e la sensibilità (pM). Nella seconda parte della tesi verrà descritto, quindi, un innovativo design del dispositivo, realizzato per ovviare a queste due limitazioni.

La nuova versione del dispositivo contiene 16 unità; in questo caso le membrane MITOMI hanno delle camerette della dimensione dei femtolitri dove verranno effettuati saggi di immunoassorbimento legato ad enzimi (ELISA) digitali dei campioni. Abbiamo mostrato come questa tecnica permette di migliorare la sensibilità, raggiungendo una risoluzione di fM in siero umano, e che la combinazione di saggio immunologico digitale e analogico ha portato ad un aumento dell'intervallo dinamico. È stato inoltre realizzato un

controllore automatico e portatile per manipolare le valvole e fluire i liquidi nel dispositivo microfluidico. Per l'acquisizione del segnale fluorescente è stato utilizzato un microscopio commerciale USB.

Nell'ultima parte, sarà presentato un dispositivo microfluidico utilizzato per un'applicazione diversa dal dosaggio immunologico. Il dispositivo contiene 769 unità ed è stato sviluppato per eseguire colture batteriche e per il monitoraggio di campioni ambientali. L'intero dispositivo può essere considerato come un display e ogni unità come dei pixel, nei quali differenti ceppi batterici sono depositati attraverso un robot. Questi differenti tipi di cellule possono crescere durante un esteso periodo, senza avere contaminazioni tra le diverse unità, e possono essere monitorate dopo essere state indotte. Le cellule, modificate geneticamente per esprimere una proteina fluorescente alla presenza di determinate molecole, possono essere poste nelle diverse unità secondo uno specifico pattern. Ad esempio l'immagine di un teschio può essere visualizzata se dell'arsenico è presente nel campione analizzato con il dispositivo.

Nel complesso, il lavoro presentato in questa tesi consiste nella realizzazione di dispositivi microfluidici per eseguire analisi high-throughput di campioni clinici e ambientali; questi dispositivi sono strumenti utili per lo studio di un numero elevato di proteine, la diagnostica e per l'analisi di un numero elevato di differenti ceppi batterici e per monitoraggio ambientale.

Parole chiave: microfluidica, dosaggio immunologico, ELISA digitale, diagnostica, point-of-care, high-throughput, coltura batterica, bioreporter, biopixel, monitoraggio dell'ambiente.

Résumé

Les travaux de recherche présentés dans cette thèse ont pour objectif l'utilisation de dispositifs microfluidiques à des fins d'analyse en « high-throughput » (haut débit). En particulier, deux applications ont été explorées: le diagnostic médical et l'analyse des échantillons environnementaux.

La miniaturisation et la parallélisations des procédures normalement effectuées dans le laboratoire conduit à une diminution des coûts et des durées d'analyse. En outre, la réduction de la taille permet d'avoir un système portable et d'effectuer l'analyse sans l'utilisation d'instruments de laboratoire coûteux et encombrants. La nécessité d'avoir un tel dispositif au développement d'approches alternatives, et la microfluidique est une technologie prometteuse pour remplacer des techniques actuelles en répondant aux critères évoqués plus haut. Afin que ces nouvelles technologies soient attrayantes, elles se doivent de fournir une performance égale ou supérieure, non seulement en termes de coût et de temps d'analyse, mais également en ce qui concerne aussi la qualité des résultats.

Nous avons développé initialement un dispositif microfluidique multicouche qui permet d'effectuer plusieurs tests immunologiques en parallèle. Le dispositif se compose de 384 unités, chaque unité comprenant 4 boutons membranes circulaires, appelés MITOMI, qui servent à piéger mécaniquement sur un substrat de verre des molécules et ainsi étudier l'interaction entre un antigène et un anticorps. Le dispositif permet d'effectuer 1'536 tests. Il peut donc être utilisé pour analyser un grand nombre de protéines et en même temps étudier la fonctionnalité de différentes paires d'anticorps. Ce dispositif a toutefois deux limites: le temps nécessaire pour effectuer l'analyse (environ 10 heures) et la sensibilité du test immunologique (pM).

Dans la deuxième partie de la thèse, une conception innovante du dispositif est décrite, conçue pour surmonter les deux limites évoquées. La nouvelle version du dispositif contient 16 unités; dans ce cas, les boutons MITOMI comportent des puits de quelques femtolitres dans lesquels seront effectués des dosages d'échantillons par méthode immuno-enzymatique ELISA sous forme digitale. Nous montrons que cette technique améliore la sensibilité, avec

une résolution atteignant de fM dans le sérum humain, et que la combinaison des analyses digitale et analogique conduit à une augmentation de la gamme dynamique du test immunologique. Nous présentons également un dispositif de commande automatique et portable pour manipuler les valves et le débit du liquide dans le dispositif microfluidique, ainsi que l'utilisation d'un microscope commercial USB pour l'acquisition du signal fluorescent. Dans la dernière partie, nous présentons un dispositif microfluidique utilisé pour une application qui diffère du dosage immuno-enzymatique. Le dispositif, contenant 769 unités, a été développé pour effectuer des cultures bactériennes et pour la surveillance des échantillons environnementaux (par exemple d'eau). L'ensemble du dispositif peut être considéré comme un écran, et chaque unité comme un pixel, dans lesquels les différentes souches bactériennes sont déposées par l'intermédiaire d'un robot « spotter ». Ces différents types de bactéries peuvent se développer sur une longue période, sans contamination entre les différentes unités, et peuvent être surveillées après induction. Les bactéries génétiquement modifiées pour exprimer une protéine fluorescente en présence de certaines molécules peuvent être placées dans les différentes unités selon un motif spécifique. Par exemple, le symbole de la tête de mort peut être affiché si l'arsenic est présent dans l'échantillon analysé avec l'appareil.

Dans l'ensemble, les travaux présentés dans cette thèse consistent en la réalisation de dispositifs microfluidiques pour l'analyse à haut débit d'échantillons cliniques, utiles pour l'étude d'un grand nombre de protéines et pour l'analyse diagnostique; ainsi qu'environnementaux pour la surveillance environnemental et l'étude de souches bactériennes.

Mots-clés: microfluidique, test immunologique, ELISA numérique, diagnostic, point-of-care, high-throughput, culture bactérienne, bioreporter, biopixel, surveillance de l'environnement.

Contents

Chapter 1 Introduction	1
1.1 - Multilayer microfluidics	2
1.2 - Microfluidic for immunoassay-based diagnostic	2
1.2.1 - Digital immunoassay	4
1.3 - Microfluidic for cell biology	6
1.4 - Summary of the thesis	7
Chapter 2 A microfluidic platform for high-throughput multiplexed protein quantitation	13
2.1 - Introduction	13
2.2 - Results and Discussion	15
2.2.1 - Assay workflow	15
2.2.2 - Assay optimization.....	17
2.2.3 - Multiplex assay	18
2.2.4 - Combinatoric screen to identify functional antibody combinations	20
2.2.5 - Stability test	24
2.3 - Conclusions	25
2.4 - Materials and methods	26
2.4.1 - Device fabrication	26
2.4.2 - Epoxy-silane coated glass slide	26
2.4.3 - Microarray spotting.....	27
2.4.4 - Antibodies and proteins	27
2.4.5 - Device operation	27
2.4.6 - Data analysis	28
2.5 - Supplementary	28
2.5.1 - Representative fluorescent image of the unit cell of the multiplex detection	28
2.5.2 - Multiplexed assay spotting 2 nM concentration secondary antibody	29
2.5.3 - Stability on the surface chemistry	30
Chapter 3 A digital-analog microfluidic platform for patient-centric multiplexed biomarker diagnostics of ultra-low volume samples	33
3.1 - Introduction	34

3.2 - Results and Discussion	36
3.2.1 - Microfluidic digital-analog device	36
3.2.2 - Digital-MITOMI characterization	39
3.2.3 - Multiplexed digital assay in serum.....	41
3.2.4 - Portable microfluidic diagnostic system	43
3.2.5 - Multiplexed Ebola diagnostic in whole blood sample	46
3.3 - Conclusions	48
3.4 - Methods	49
3.4.1 - Reagents, antibodies, proteins, and clinical samples	49
3.4.2 - Blood specimens	49
3.4.3 - Microfabrication	49
3.4.4 - MicroFluidic Diagnostic System.....	50
3.4.5 - Device function and operation	52
3.4.6 - Digital enzyme measurements	52
3.4.7 - Microfluidic digital and analog immunoassay	52
3.4.8 - Multiplexed digital detection of anti-EBOLA antibodies in human serum	53
3.4.9 - Detection of human IL-6 in human serum	53
3.4.10 - Multiplexed detection of anti-Ebola IgG in whole blood	53
3.4.11 - Image acquisition, quantification and data analysis	54
3.5 - Supplementary	55
3.5.1 - Single enzyme counting and activity traces	55
3.5.2 - Microfluidic control system	56
3.5.3 - Microfabricated diagnostic design	57
3.5.4 - Platform technologies for biomarker diagnostic	58
3.5.5 - Digital-MITOMI immunoassay steps	58
3.5.6 - IL-6 immunoassay steps	59
3.5.7 - Multiplex Ebola immunoassay steps.....	59
Chapter 4 A microfluidic biodisplay	63
4.1 - Introduction	63
4.2 - Results and Discussion	65
4.2.1 - Biodisplay programming, culturing, sampling and readout	65
4.2.2 - Multiplexed characterization of bacterial strains	67
4.2.3 - Biodisplay.....	70
4.2.4 - Spores enable long-term storage	72
4.3 - Conclusions	73
4.4 - Methods	75
4.4.1 - Materials.....	75
4.4.2 - Device fabrication	76
4.4.3 - Cell culture, transformation and spore formation	76
4.4.4 - Cell arraying	76
4.4.5 - Cell-display culturing	77
4.4.6 - Imaging.....	77
4.5 - Supplementary	78
4.5.1 - Biodisplay for strain characterization at 37°C	78
4.5.2 - Arsenic responsive <i>E. coli</i>	79
4.5.3 - Arsenic biodisplay –different arsenic concentrations	80
4.5.4 - Arsenic biodisplay over time.....	81
4.5.5 - Cellphone image acquisition	82
4.5.6 - Embedded device	83

4.5.7 - List of strains used in this work	84
Chapter 5 Conclusions and outlook	89
5.1 - Microfluidics for high-throughput immunoassay analysis.....	89
5.2 - Bacteria biodisplay	91
Appendix A	95
A.1 - Multiplexed serological detection of IgE and IgG for Allergy detection	95
A.1.1 - Materials and Methods	96
Curriculum vitae	99

List of figures

Figure 1.1: Digital detection.	5
Figure 2.1: Workflow schematic.....	16
Figure 2.2: Optimization of antibody concentration.....	18
Figure 2.3: Multiplexed assay and antibody cross-reactivity testing.....	19
Figure 2.4: Screening of antibody combinations for PSA detection: secondary and tertiary antibodies were spotted.	21
Figure 2.5: Screening of antibody combinations for PSA detection: primary and secondary antibodies were spotted.	22
Figure 2.6: Combinatoric antibody screen.....	23
Figure 2.7: Stability test.....	24
Figure 3.1: The digital-analog hybrid, multiplexed microfluidic diagnostic device.	37
Figure 3.2: Serpentine-shape (S-shape) delay peristaltic pump.....	38
Figure 3.3: Single enzyme counting with digital-MITOMI.....	40
Figure 3.4: Digital-MITOMI Immunoassay.	41
Figure 3.5: Multiplexed digital Ebola diagnostics in human serum..	42
Figure 3.6: Portable, low-cost μ Fluidic Diagnostics System.....	43
Figure 3.7: Graphical user interface.....	44
Figure 3.8: GFP analog-amp and analog MITOMI assay.....	45
Figure 3.9: IL-6 detection	46
Figure 3.10: Multiplexed Ebola diagnostics in whole blood using the μ FDS.	47
Figure 4.1: Biodisplay schematic and use.....	65
Figure 4.2: Using the biodisplay for strain characterization.	68
Figure 4.3: One delayed arabinose induction.....	69
Figure 4.4: Biodisplay for arsenic sensing.....	70
Figure 4.5: Biodisplay for arabinose and arsenic sensing.....	71
Figure 4.6: Spore biodisplay	73
Figure A.1: Allergy detection	96

Figure SI 2.1: Fluorescent images of some of the unit cells on the device.....	28
Figure SI 2.2: Multiplexed assay and antibody cross-reactivity testing..	29
Figure SI 2.3: Stability on the surface chemistry.....	30
Figure SI 3.1: Activity traces and observed turnover rates of enzymes for the β G assay.	55
Figure SI 3.2: 3D rendering, of the MSC.....	56
Figure SI 3.3: Microfabricated diagnostic devices used in this study.....	57
Figure SI 4.1: Biodisplay for strain characterization at 37°C.	78
Figure SI 4.2: Arsenic-responsive E. coli.	79
Figure SI 4.3: Arsenic biodisplay.....	80
Figure SI 4.4: Arsenic biodisplay over time.	81
Figure SI 4.5: Cellphone image acquisition.....	82
Figure SI 4.6: Embedded spore biodisplay..	83

List of tables

Table 2.1: List of antibodies.	20
Table 3.1: Cost table of μ Fluidic Diagnostic System.	51
Table 3.2: Comparison of the μ FDS with the microfluidic platform technologies for biomarker diagnostics.	58
Table 3.3: Liquid handling sequence for the digital-MITOMI immunoassay	58
Table 3.4: Liquid handling sequence for the analog-amp IL-6 MITOMI immunoassay	59
Table 3.5: Liquid handling sequence for the multiplex MITOMI immunoassay	59
Table 4.1: List of plasmids and strains used in this work.	84

Chapter 1

Introduction

The detection and quantification of proteins is extremely important to describe biological processes and for clinical analysis. In particular for clinical analysis the quantitation of biomarkers is crucial for diagnosis, monitoring health conditions and verifying the efficacy of a drug. With standard laboratory test equipment significant consumption of reagents, sample and time are required in order to perform the analysis. In order to overcome those limitations, the development of a miniaturized system, able to perform procedures that are usually done in a laboratory became highly attractive. Miniaturized devices speed up the analysis test and dramatically reduce the overall cost of the process, making the practice of diagnostics faster, cheaper and more accessible to people. Moreover, the possibility to have information about multiple biomarkers has stimulated the development of analysis that provides parallel protein measurement in the same specimen [1].

Microfluidics in the last decades has been extensively explored and is a good candidate to replace standard laboratory techniques [2]. Microfluidics manipulates and controls liquids in a range of microliters to picoliters, having channels with dimensions in the micro-scale, and all the fluidic components are miniaturized and integrated in the same device. Small dimensions lead not only to small volumes of reagents but also to specific physical properties: mass transport is dominated by diffusion, there is no turbulence, extremely well-designed and predictable laminar flow is attainable and it is possible to guarantee homogenous experimental conditions within different units of the same chip [3], [4].

The number of publications, based on microfluidic research, especially in engineering journals, is increasing more and more over the years [5], showing how microfluidics has been applied to a variety of fields: single molecule analysis [6], diagnostics [7], organ on a chip [8], synthetic biology [9], [10], genomics and biomaterials [11]. Despite the effort on microfluidic-based research, there is still room for improving the technology in order to commercialize such devices.

1.1 - Multilayer microfluidics

Microfluidics consists of an analytical system for the manipulation of small volumes of liquids (pL or nL). As already mentioned, small dimensions lead to small sample volumes but also to an improvement in the performance compared to the macroscale system, and most importantly increase the number of individual experiments per time.

Microfluidic components can be fabricated with the same techniques developed for microelectronics and semiconductor-processing industries. The dimensions of the features are not highly critical (μm) and the process flow is straightforward. Different materials can be employed for the fabrication of microfluidic devices: glass, silicon, paper, hydrogels and elastomers [12]. Glass and silicon are normally processed with standard photolithography. Glass is transparent, electrically insulating and not permeable to gas. Some advantages over other materials include its compatibility with solvents and thermo stability; however there are some disadvantages such as the complexity and cost of fabrication. Hydrogels are widely used to embed cells, since they can mimic the extracellular matrix. Thus, their aqueous nature, permeability and biocompatibility make them suitable for 3D cell culture. Paper devices are made on a porous matrix of cellulose; their mode of operation is based on capillary effect. Modifying some areas of the paper, it is possible to guide the liquid. These devices are simple, they can be employed for fast analysis and they do not need an external pump to flow the liquid, but on the other hand they are low-throughput and they have low sensitivity. It is also possible to combine the different materials into a hybrid chip and benefit from their individual advantages [13], [14].

Polymer-based chips were introduced several years after glass microfluidic devices. They are less expensive, compared to glass devices and thanks to soft-lithography, they are rapidly fabricated and can be easily replicated using the same mold. One of the most popular elastomers is polydimethylsiloxane (PDMS) [11]. One advantage of PDMS is its high elasticity, which allows the integration of pneumatic valves in the chip, enabling precise control of multiple liquids in the device [16]. The valves are obtained by bonding multiple patterned layers of PDMS and aligning the channels of one layer (the control) perpendicular to the channels of the other layer (flow layer). Since PDMS is a soft material, it is possible to obtain large deflections by applying small forces, thus applying pressure in the control line causes the PDMS membrane to bend and pinch the flow channel underneath. Thousands of different valves can be integrated in a single device yielding a microfluidic large-scale integration (MLSI) device [17]. PDMS has other advantages like optical transparency, thus it is suitable for optical detection, and it is permeable to gas and biocompatible. Despite all these qualities, PDMS has also some limitations, such as incompatibility with organic solvents.

1.2 - Microfluidic for immunoassay-based diagnostic

Immunoassays are widely used for medical diagnostics; they are based on the high affinity and specificity between antigen and antibody. Immunoassays rely on the ability of an antibody to specifically bind target molecules, the antigens. Once the target molecule binds the primary antibody, a secondary labeled antibody is added in order to detect the

immunocomplex. Possible labels for the secondary antibodies are: enzymes, radioactive isotopes, DNA reporters, fluorogenic reporters or electrochemiluminescent tags. Immunoassays are usually performed on a microwell plate, but they could be significantly improved with microfluidics. There are important characteristics a device should have to perform a good diagnosis and compete with standard diagnostic techniques: multiplexing, sensitivity, broad dynamic range, low sample consumption and portability.

Multiplexing enables the analysis of different samples or the identification of different biomarkers within the same sample [18] but also the study of the interactions between multiple proteins and the discovery of new biomarkers [19]. There are two approaches for multiplex assay using microfluidics: bead based-immunoassay [20] or a planar assay [21]–[23].

One example of bead-based assays is the Luminex technology [24]. In this approach beads are dyed with different intensity in order to differentiate them from each other and individual sets of bead are coated with a specific primary antibody. The beads are then incubated with the target molecule allowing the binding with a specific antibody. Then secondary labeled antibodies bind the target analyte and the signal is read through flow cytometry. The readout is performed in order to identify the color specific to each bead corresponding to the specific target and the signal from the secondary antibody to detect the immunocomplex. Multiplexing is achieved using a color code for each bead, enabling the discrimination of different antigens.

For the planar assay (for example using microspotting techniques) the multiplexing is given by the position of the immunocomplex on the surface. In this case, in different positions it is possible to localize different antibodies, thus overcoming the intrinsic limitation of having a limited number of colors. Two examples of planar assays are the barcode [22] and the mosaic immunosensors [9], [13]. In the former, multiple analytes in a blood sample are detected, where the immunoassay area is a microscopic barcode. The latter is one of the first examples of a planar assay performed using microfluidics. The surface where the assay occurs was patterned using microchannels to guide the solution containing a specific antigen in a specific position of the substrate.

Another approach for planar assay is the Mechanically Induced Trapping of Molecular Interaction (MITOMI)[26]. This technique combines both microarrays and a new microfluidic detection mechanism [27]. Nanoliter-volumes of biological solution are spotted on a glass slide and the spots are then aligned with a microfluidic device. The units of the microfluidic chip have some characteristic components: a spotting chamber, a detection chamber, a “neck valve” that separates the two chambers and a “sandwich valve” that separates each unit from the neighboring ones. Inside the detection area there are one or more button membranes that physically trap molecules that bind the surface between the substrate and the PDMS. MITOMI has been originally used to study the affinity and the kinetic interactions between molecules, but it has also been used as a diagnostic tool for immunoassay tests [6], [10], [15].

Both bead and planar approaches have enabled multiplex analysis but they require the detection of the signal from a large number of reporter molecules, which limits their

sensitivity. Moreover a large number of secondary antibodies is needed to increase the signal above the background for detection. As it will be explained in detail in the next paragraph, a possible solution to increase the limit of detection (LOD) involves using digital enzyme-linked immunoassorbent assay (ELISA).

A miniaturized immunoassay based-device can be employed as a point of care (POC), usually referring to small portable devices that can autonomously carry out immunoassays without bulky external equipment. Microfluidic-based immunoassays are emerging as good candidates that can accomplish this requisite [30]. For example an automated microfluidic liquid handling system controlled by a smartphone has been developed [31]. The controller is able to manipulate valves and liquids within an elastomeric microfluidic device; the system is portable and powered by a 12.8 V 1500 mAh Lithium battery.

Another important requirements for POC applications is the possibility to utilize small sample volumes and avoid any pre-treatment of the sample. Thanks to microfluidic techniques, it is possible to drastically reduce sample consumption, because of the small device dimensions and the capability to perform several different tests on the same device. Ideally a POC device should required only one drop of blood (~5 μ l) obtainable by a simple pin-prick to perform the test.

1.2.1 - Digital immunoassay

As already mentioned, one challenge for diagnostics using microfluidics is the capability of detecting low concentrations of analyte to identify the early onset of a disease.

A method to obtain high sensitivity is digital ELISA. ELISA is an enzyme immunoassay, where the detection antibody is linked to an enzyme. After the immunocomplex with the antigen is formed, the conjugate enzyme is incubated with substrate and the product activity is monitored. The idea is to compartmentalize the immunocomplex in a small volume (femtoliters, fl) chamber and monitor the activity of the enzyme over time. If the reaction volume is small, a small number of fluorophores produced by the enzymatic reaction, is enough to have a signal above the background [32]. Thus, confining the molecules in a small volume leads an increase in concentration and thus in sensitivity (Figure 1.1a).

If the sample has a low concentration of analyte, the ratio of the target molecule to the number of binding sites (captured antibodies) is small and the probability that a reaction volume contains a labeled immunoassay complex follows a Poisson distribution. According to this distribution, an event (in our case the formation of the immunocomplex) can occur 0, 1, 2, ... times in an interval. If λ is the average number of events in an interval, the probability of observing k events in an interval (in our case the number of target molecules) is given by the equation:

$$p(k) = \frac{\lambda^k e^{-\lambda}}{k!} \quad \text{Equation 1-1}$$

According to Poisson distribution, when we decrease the concentration of the analyte, the probability of having, in each reaction volume, either 1 or 0 immunocomplex, increases. Each small volume reaction can then be categorized as “on” for a reactor containing one enzyme and “off” for one where the biomolecule is not present (Figure 1.1b) [33]–[35]. Time-lapses are taken and the concentration of the analyte is calculated according to the number of “on” wells over the total number of wells. The activity traces of enzymes are plotted over time and the slope for each curve is observed (the greater number of enzymes, the steeper the slope). A histogram with the observed turnover rate for each well versus the number of wells can be plotted [36]. It is then possible to approximate each histogram peak with a Gaussian distribution and calculate the probability to have 0, 1, 2, 3... molecules (Figure 1.1c).

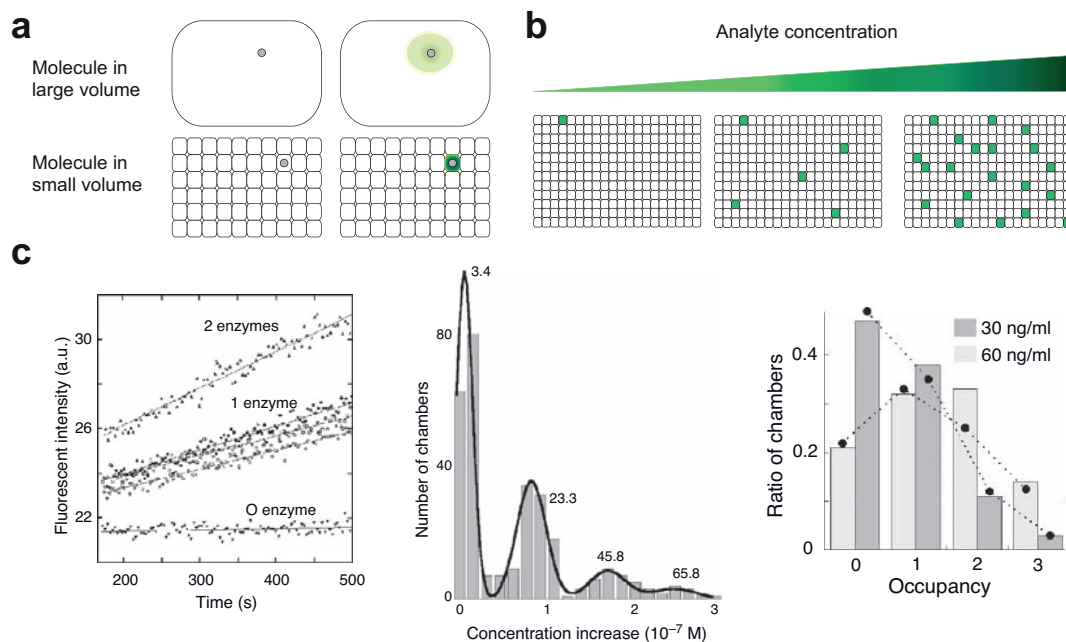


Figure 1.1 **Digital detection:** a) Representation of the difference in fluorescence signal between a molecule in a large (top) and small volume (bottom). b) Schematic of the digital signal related to increasing concentration. c) Activity of the enzyme molecules: recording of the enzyme activity in different wells (on the left), histogram of the number of chambers plotted versus the increase in concentration over 60 s, the value displayed next to each peak is the center of the Gaussian (in the center), four peaks can be attributed to an occupancy of 0,1,2,or 3 enzyme(s) per chamber (on the right). Panel (c) is adapted from *Nat. Biotechnol.*, vol. 23, no. 3, pp. 361–365 © (2005).

To reach a low LOD, a sufficient number of wells has to be interrogated. Other important parameters to obtain a low LOD are the antibodies used [37] and enzyme substrate concentration, which both should be optimized to achieve high sensitivity.

One method to perform digital ELISA is to have microfabricated wells, to form a large array of femtoliter-sized reaction chambers and load them with beads where a sandwich

antibody complex is formed out of the device [34]. The immunocomplex is formed covering the bead with the capture antibody and subsequent incubation with the target molecule, pbiotinylated detection antibody and streptavidin enzyme label. The size of the femtowell matches the bead's size in order to have one bead per well. If the number of analytes is much lower than the beads, it is possible to have single molecule detection.

As it has been mentioned already, multiplex detection is useful for the identification of multiple biomarkers in the same sample. For example the detection of multiple cytokines, which play an important role for prognosis, diagnosis and response to therapy. Digital immunoassay has been also performed for the detection of multiple biomarkers in human serum. In this case multiple subpopulations of beads each with a different fluorescent signature and specific antibody are incubated together with the sample [38]: four cytokines in plasma have been measured using this approach.

One limitation of the digital immunoassay is the dynamic range, which is limited by the number of interrogated wells. When the concentration is such that all wells will be “on”, any higher value in concentration cannot be discriminated. In order to overcome these limits the sample can be diluted or a combination of digital and analog detection can be implemented.

1.3 - Microfluidic for cell biology

Cells have dimensions on the order of microns, so they can be easily manipulated and tested using microtechnology [39]. Studying biological systems through microfluidic devices has several advantages over conventional bench-top systems: low reagent and sample volume, precise control and tailored cellular microenvironments, long term monitoring of cells and low-cost devices [40], [41]. The small dimension of microfluidics allows to assembly multiple cell culture chambers on a single device. Thus, allows high parallelization of analysis and high throughput of sample while reducing reagents cost.

Indeed, in the field of microbiology, microfluidics has been used for several applications, for example: culturing and monitoring of cells [42], impedance-based bacterial detection and identification [43], bacterial persistence [44], and live cell bacterial sensor [45]. Moreover, it has been shown that cells can be locally and selectively sampled using microfluidic probes [46] or microfluidic devices [47]; it is possible to create gradients, study chemotaxis [48]–[50] and adjust precisely the concentration of nutrients or inducers. Thanks to microfluidics it is also possible to mimic *in vivo* conditions [51]–[53] and obtain a 3D stem cell culture system.

Microfluidics is especially suitable for screening large numbers of cells, in fact the technologies for high-throughput screening usually involve robotic liquid handling, high-density microplates, and sophisticated detection schemes. Using microfluidics enables different modes to be employed: perfusion flow mode, droplet mode and microarray mode [39]. In the perfusion mode the devices have components for introducing the reagents and samples into the chip, moving them in different microchannel networks, combining and mixing them. For the droplet mode, the reagents are compartmentalized into nanoliter or picoliter volumes using a system of water-in-oil emulsion droplets. Finally, the microarray

mode consists of a 2D support where materials, such as antibodies, proteins or lipids, which interact with the cells, allow their capture and subsequent interrogation [54] or cells are directly spotted on the surface [47], [55], [56]. Some examples of microfluidic high-throughput screening are the study of: cell-cell communication[57], molecular mechanisms for signal transduction [58], model transcriptional regulator [47], [59], or protein localization [47].

The possibility to engineer bacteria to recognize the presence of specific molecules in the environment can provide advantages over the conventional chromatography technologies that are tedious and not portable. Bioreporters produce an easily detectable signal that changes upon the level of exposure to the target compound [60], [61]. The bacteria are genetically modified in order to couple a sensing element to a reporter gene, which upon expression produces a measurable signal. The amount or activity of the protein reporter is an indication of the cellular response to the target molecule.

Having a device that creates an interface between the environment and the biosensor is an important tool for environmental sensors, for example for heavy metal detection [62], [63]. To employ this system in the field, it is necessary to have a safe interface between the genetically modified cells, the user and the environment; furthermore the micro device should provide fresh medium and sample to the bacteria over time, in order to achieve continuous growth and monitoring.

1.4 - Summary of the thesis

Microfluidics has the possibility to change the way of sensing analytes, from proteins to heavy metals. We developed and characterized microfluidic platforms for high-throughput analysis. In particular we have employed multilayer PDMS chips for multiplex immunoassays and for monitoring bacterial colonies under different environmental conditions.

Following the overview of the state of art of the high-throughput microfluidic devices provided in the introduction, **Chapter 2** of the thesis presents a microfluidic platform containing 384 unit cells, in which 1'536 independent immunassays can be performed in parallel. It can be applied to monitor several cytokines over time, yielding information about different factors such as inflammation, cell differentiation, etc. Using microarraying, we immobilized different primary and secondary antibody pairs into different units and we detected several biomarkers in 4 different samples. The platform has been optimized in terms of the concentration at which antibodies were spotted, for both primary and secondary antibodies. Moreover a stability test has been performed in order to proof the possibility to store the device for extended period of time. The platform has also been used in order to perform a combinatory study of antibody pairs purchased from different companies to identify optimal antibody combinations.

After showing the possibility to perform multiplex immunoassays using MITOMI buttons we designed a new device that allowed us to decrease the experimental time, enhance sensitivity, dynamic range (digital-analog detection), and perform multiplexed analysis on

small sample volumes. In **Chapter 3** we present a multiplexed digital-analog microfluidic platform for the rapid and highly sensitive detection of 3-4 biomarkers in quadruplicate in 16 independent and isolated microfluidic unit cells requiring only a single 5 μ l whole blood sample. A peristaltic pump has been introduced in the chip in order to shorten the mixing time of the antibody in comparison to the first generation chip in which mixing occurred via diffusion. The MITOMI buttons have been patterned with femtoliter wells for digital detection. The digital analysis allowed us to reach a LOD in the low femtomolar range in human serum. Moreover, by integrating digital and analog detection we were able to achieve a dynamic range of up to 5 orders of magnitude. Finally, we eliminated the need of bulky equipment around our microfluidic platform by developing a low-cost, portable hardware system to control and readout the microfluidic device and detect anti-Ebola IgG in ultra-low volumes of whole blood samples in a multiplexed assay format. This approach can overcome one of the limitations preventing the application of microfluidics in the field, where bulky and expensive lab equipment might not be available, moving the microfluidic approach beyond the clinical point of care settings.

In **Chapter 4** we designed a two-layer microfluidic platform to obtain a bacterial display. The display has 768 units where different strains can be cultured and interpreted as a pixel. We used microarray spotting in order to address the strains to each chamber. It is possible to culture the bacteria for several days providing a continuous supply of fresh medium. Moreover using a set of valves placed in the inlets and outlets of the chip, it is possible to sample different solutions and switch between them, allowing induction in dynamic conditions. Finally we also showed that it is possible to spot the strain in a pattern, which is easy to interpret, in order to verify if a given analyte is present in the sample (e.g. arsenic in tap water).

Bibliography

- [1] A. Mantovani, P. Allavena, A. Sica, and F. Balkwill, “Cancer-related inflammation,” *Nature*, vol. 454, no. 7203, pp. 436–444, Jul. 2008.
- [2] G. M. Whitesides, “The origins and the future of microfluidics,” *Nature*, vol. 442, no. 7101, pp. 368–373, Jul. 2006.
- [3] T. M. Squires and S. R. Quake, “Microfluidics: Fluid physics at the nanoliter scale,” *Rev. Mod. Phys.*, vol. 77, no. 3, pp. 977–1026, Oct. 2005.
- [4] D. T. Chiu *et al.*, “Small but Perfectly Formed? Successes, Challenges, and Opportunities for Microfluidics in the Chemical and Biological Sciences,” *Chem*, vol. 2, no. 2, pp. 201–223, Feb. 2017.
- [5] E. K. Sackmann, A. L. Fulton, and D. J. Beebe, “The present and future role of microfluidics in biomedical research,” *Nature*, vol. 507, no. 7491, pp. 181–189, Mar. 2014.
- [6] A. R. Wheeler *et al.*, “Microfluidic device for single-cell analysis,” *Anal. Chem.*, vol. 75, no. 14, pp. 3581–3586, Jul. 2003.
- [7] B. Weigl, G. Domingo, P. LaBarre, and J. Gerlach, “Towards non- and minimally instrumented, microfluidics-based diagnostic devices,” *Lab. Chip*, vol. 8, no. 12, pp. 1999–2014, 2008.
- [8] S. N. Bhatia and D. E. Ingber, “Microfluidic organs-on-chips,” *Nat. Biotechnol.*, vol. 32, no. 8, pp. 760–772, Aug. 2014.
- [9] N. Szita, K. Polizzi, N. Jaccard, and F. Baganz, “Microfluidic approaches for systems and synthetic biology,” *Curr. Opin. Biotechnol.*, vol. 21, no. 4, pp. 517–523, Aug. 2010.
- [10] “Rapid cell-free forward engineering of novel genetic ring oscillators | eLife.” [Online]. Available: <https://elifesciences.org/content/4/e09771>. [Accessed: 01-May-2017].
- [11] S. Kobel and M. P. Lutolf, “Biomaterials meet microfluidics: building the next generation of artificial niches,” *Curr. Opin. Biotechnol.*, vol. 22, no. 5, pp. 690–697, Oct. 2011.
- [12] K. Ren, J. Zhou, and H. Wu, “Materials for Microfluidic Chip Fabrication,” *Acc. Chem. Res.*, vol. 46, no. 11, pp. 2396–2406, Nov. 2013.
- [13] W. H. Grover, A. M. Skelley, C. N. Liu, E. T. Lagally, and R. A. Mathies, “Monolithic membrane valves and diaphragm pumps for practical large-scale integration into glass microfluidic devices,” *Sens. Actuators B Chem.*, vol. 89, no. 3, pp. 315–323, Apr. 2003.
- [14] H. Wu, B. Huang, and R. N. Zare, “Generation of Complex, Static Solution Gradients in Microfluidic Channels,” *J. Am. Chem. Soc.*, vol. 128, no. 13, pp. 4194–4195, Apr. 2006.
- [15] S. R. Quake and A. Scherer, “From Micro- to Nanofabrication with Soft Materials,” *Science*, vol. 290, no. 5496, pp. 1536–1540, Nov. 2000.
- [16] M. A. Unger, H.-P. Chou, T. Thorsen, A. Scherer, and S. R. Quake, “Monolithic Microfabricated Valves and Pumps by Multilayer Soft Lithography,” *Science*, vol. 288, no. 5463, pp. 113–116, Apr. 2000.
- [17] T. Thorsen, S. J. Maerkl, and S. R. Quake, “Microfluidic Large-Scale Integration,” *Science*, vol. 298, no. 5593, pp. 580–584, Oct. 2002.
- [18] S. I. Stoeva, J.-S. Lee, J. E. Smith, S. T. Rosen, and C. A. Mirkin, “Multiplexed detection of protein cancer markers with biobarcode nanoparticle probes,” *J. Am. Chem. Soc.*, vol. 128, no. 26, pp. 8378–8379, Jul. 2006.
- [19] N. Rifai, M. A. Gillette, and S. A. Carr, “Protein biomarker discovery and validation: the long and uncertain path to clinical utility,” *Nat. Biotechnol.*, vol. 24, no. 8, pp. 971–983, Aug. 2006.
- [20] C. T. Lim and Y. Zhang, “Bead-based microfluidic immunoassays: the next generation,” *Biosens. Bioelectron.*, vol. 22, no. 7, pp. 1197–1204, Feb. 2007.
- [21] A. Bernard, B. Michel, and E. Delamarche, “Micromosaic Immunoassays,” *Anal. Chem.*, vol. 73, no. 1, pp. 8–12, Jan. 2001.
- [22] R. Fan *et al.*, “Integrated barcode chips for rapid, multiplexed analysis of proteins in microliter quantities of blood,” *Nat. Biotechnol.*, vol. 26, no. 12, pp. 1373–1378, Dec. 2008.
- [23] J. L. Garcia-Cordero, C. Nembrini, A. Stano, J. A. Hubbell, and S. J. Maerkl, “A high-throughput nanoimmunoassay chip applied to large-scale vaccine adjuvant screening,” *Integr. Biol. Quant. Biosci. Nano Macro*, vol. 5, no. 4, pp. 650–658, Apr. 2013.

- [24] C. A. Ray *et al.*, “Development, validation, and implementation of a multiplex immunoassay for the simultaneous determination of five cytokines in human serum,” *J. Pharm. Biomed. Anal.*, vol. 36, no. 5, pp. 1037–1044, Jan. 2005.
- [25] E. Delamarche, A. Bernard, H. Schmid, B. Michel, and H. Biebuyck, “Patterned delivery of immunoglobulins to surfaces using microfluidic networks,” *Science*, vol. 276, no. 5313, pp. 779–781, May 1997.
- [26] S. J. Maerkl and S. R. Quake, “A Systems Approach to Measuring the Binding Energy Landscapes of Transcription Factors,” *Science*, vol. 315, no. 5809, pp. 233–237, Jan. 2007.
- [27] J. L. Garcia-Cordero and S. J. Maerkl, “Mechanically Induced Trapping of Molecular Interactions and Its Applications,” *J. Lab. Autom.*, vol. 21, no. 3, pp. 356–367, Jun. 2016.
- [28] J. L. Garcia-Cordero and S. J. Maerkl, “A 1024-sample serum analyzer chip for cancer diagnostics,” *Lab. Chip*, Dec. 2013.
- [29] C. Zheng *et al.*, “High-throughput immunoassay through in-channel microfluidic patterning,” *Lab. Chip*, vol. 12, no. 14, pp. 2487–2490, Jul. 2012.
- [30] L. Mou and X. Jiang, “Materials for Microfluidic Immunoassays: A Review,” *Adv. Healthc. Mater.*, p. n/a-n/a, Mar. 2017.
- [31] B. Li *et al.*, “A smartphone controlled handheld microfluidic liquid handling system,” *Lab. Chip*, vol. 14, no. 20, pp. 4085–4092, Oct. 2014.
- [32] M. E. Vincent, W. Liu, E. B. Haney, and R. F. Ismagilov, “Microfluidic stochastic confinement enhances analysis of rare cells by isolating cells and creating high density environments for control of diffusible signals,” *Chem. Soc. Rev.*, vol. 39, no. 3, pp. 974–984, Feb. 2010.
- [33] S. H. Kim, S. Iwai, S. Araki, S. Sakakihara, R. Iino, and H. Noji, “Large-scale femtoliter droplet array for digital counting of single biomolecules,” *Lab. Chip*, vol. 12, no. 23, pp. 4986–4991, Dec. 2012.
- [34] D. M. Rissin *et al.*, “Single-molecule enzyme-linked immunosorbent assay detects serum proteins at subfemtomolar concentrations,” *Nat. Biotechnol.*, vol. 28, no. 6, pp. 595–599, Jun. 2010.
- [35] D. M. Rissin and D. R. Walt, “Digital concentration readout of single enzyme molecules using femtoliter arrays and Poisson statistics,” *Nano Lett.*, vol. 6, no. 3, pp. 520–523, Mar. 2006.
- [36] Y. Rondelez *et al.*, “Microfabricated arrays of femtoliter chambers allow single molecule enzymology,” *Nat. Biotechnol.*, vol. 23, no. 3, pp. 361–365, Mar. 2005.
- [37] D. Wu, M. D. Milutinovic, and D. R. Walt, “Single molecule array (Simoa) assay with optimal antibody pairs for cytokine detection in human serum samples,” *The Analyst*, vol. 140, no. 18, pp. 6277–6282, Sep. 2015.
- [38] D. M. Rissin *et al.*, “Multiplexed single molecule immunoassays,” *Lab. Chip*, vol. 13, no. 15, pp. 2902–2911, Jul. 2013.
- [39] G. Du, Q. Fang, and J. M. J. den Toonder, “Microfluidics for cell-based high throughput screening platforms—A review,” *Anal. Chim. Acta*, vol. 903, pp. 36–50, Jan. 2016.
- [40] E. W. K. Young and D. J. Beebe, “Fundamentals of microfluidic cell culture in controlled microenvironments,” *Chem. Soc. Rev.*, vol. 39, no. 3, pp. 1036–1048, Mar. 2010.
- [41] M. Mehling and S. Tay, “Microfluidic cell culture,” *Curr. Opin. Biotechnol.*, vol. 25, pp. 95–102, Feb. 2014.
- [42] R. Gómez-Sjöberg, A. A. Leyrat, D. M. Pirone, C. S. Chen, and S. R. Quake, “Versatile, fully automated, microfluidic cell culture system,” *Anal. Chem.*, vol. 79, no. 22, pp. 8557–8563, Nov. 2007.
- [43] M. S. Mannoor, S. Zhang, A. J. Link, and M. C. McAlpine, “Electrical detection of pathogenic bacteria via immobilized antimicrobial peptides,” *Proc. Natl. Acad. Sci. U. S. A.*, vol. 107, no. 45, pp. 19207–19212, Nov. 2010.
- [44] N. Q. Balaban, J. Merrin, R. Chait, L. Kowalik, and S. Leibler, “Bacterial persistence as a phenotypic switch,” *Science*, vol. 305, no. 5690, pp. 1622–1625, Sep. 2004.
- [45] C. Roggo and J. R. van der Meer, “Miniaturized and integrated whole cell living bacterial sensors in field applicable autonomous devices,” *Curr. Opin. Biotechnol.*, vol. 45, pp. 24–33, Jun. 2017.

- [46] A. Kashyap, J. Autebert, E. Delamarche, and G. V. Kaigala, “Selective local lysis and sampling of live cells for nucleic acid analysis using a microfluidic probe,” *Sci. Rep.*, vol. 6, p. 29579, Jul. 2016.
- [47] N. Déneraud *et al.*, “A chemostat array enables the spatio-temporal analysis of the yeast proteome,” *Proc. Natl. Acad. Sci. U. S. A.*, vol. 110, no. 39, pp. 15842–15847, Sep. 2013.
- [48] Z. Tatárová, J. P. Abbuehl, S. Maerkl, and J. Huelsken, “Microfluidic co-culture platform to quantify chemotaxis of primary stem cells,” *Lab. Chip*, vol. 16, no. 10, pp. 1934–1945, May 2016.
- [49] “Microfluidic Gradient Platforms for Controlling Cellular Behavior,” *PubMed Journals*. [Online]. Available: <https://ncbi.nlm.nih.gov/labs/articles/20734372/>. [Accessed: 19-Apr-2017].
- [50] F. Piraino *et al.*, “Polyester μ -assay chip for stem cell studies,” *Biomicrofluidics*, vol. 6, no. 4, p. 44109, Nov. 2012.
- [51] S. Allazetta, L. Kolb, S. Zerbib, J. ’an Bardy, and M. P. Lutolf, “Cell-Instructive Microgels with Tailor-Made Physicochemical Properties,” *Small Weinh. Bergstr. Ger.*, vol. 11, no. 42, pp. 5647–5656, Nov. 2015.
- [52] S. Cosson and M. P. Lutolf, “Hydrogel microfluidics for the patterning of pluripotent stem cells,” *Sci. Rep.*, vol. 4, p. 4462, Mar. 2014.
- [53] S. Lopa *et al.*, “Fabrication of multi-well chips for spheroid cultures and implantable constructs through rapid prototyping techniques,” *Biotechnol. Bioeng.*, vol. 112, no. 7, pp. 1457–1471, Jul. 2015.
- [54] Z. Tong *et al.*, “Crossed flow microfluidics for high throughput screening of bioactive chemical–cell interactions,” *Lab. Chip*, vol. 17, no. 3, pp. 501–510, Jan. 2017.
- [55] O. I. Berthuy, S. K. Muldur, F. Rossi, P. Colpo, L. J. Blum, and C. A. Marquette, “Multiplex cell microarrays for high-throughput screening,” *Lab. Chip*, vol. 16, no. 22, pp. 4248–4262, Nov. 2016.
- [56] K. Woodruff, L. M. Fidalgo, S. Gobaa, M. P. Lutolf, and S. J. Maerkl, “Live mammalian cell arrays,” *Nat. Methods*, vol. 10, no. 6, pp. 550–552, Jun. 2013.
- [57] A. Prindle, P. Samayoa, I. Razinkov, T. Danino, L. S. Tsimring, and J. Hasty, “A sensing array of radically coupled genetic ‘biopixels,’” *Nature*, vol. 481, no. 7379, pp. 39–44, Dec. 2011.
- [58] M. Blazek, T. S. Santisteban, R. Zengerle, and M. Meier, “Analysis of fast protein phosphorylation kinetics in single cells on a microfluidic chip,” *Lab. Chip*, vol. 15, no. 3, pp. 726–734, Feb. 2015.
- [59] A. S. Rajkumar, N. Déneraud, and S. J. Maerkl, “Mapping the fine structure of a eukaryotic promoter input-output function,” *Nat. Genet.*, vol. 45, no. 10, pp. 1207–1215, Oct. 2013.
- [60] J. R. van der Meer and S. Belkin, “Where microbiology meets microengineering: design and applications of reporter bacteria,” *Nat. Rev. Microbiol.*, vol. 8, no. 7, pp. 511–522, Jul. 2010.
- [61] S. Daunert, G. Barrett, J. S. Feliciano, R. S. Shetty, S. Shrestha, and W. Smith-Spencer, “Genetically Engineered Whole-Cell Sensing Systems: Coupling Biological Recognition with Reporter Genes,” *Chem. Rev.*, vol. 100, no. 7, pp. 2705–2738, Jul. 2000.
- [62] M. Kim, J. W. Lim, H. J. Kim, S. K. Lee, S. J. Lee, and T. Kim, “Chemostat-like microfluidic platform for highly sensitive detection of heavy metal ions using microbial biosensors,” *Biosens. Bioelectron.*, vol. 65, pp. 257–264, Mar. 2015.
- [63] N. Buffi *et al.*, “Development of a microfluidics biosensor for agarose-bead immobilized *Escherichia coli* bioreporter cells for arsenite detection in aqueous samples,” *Lab. Chip*, vol. 11, no. 14, pp. 2369–2377, Jul. 2011.

Chapter 2

A microfluidic platform for high-throughput multiplexed protein quantitation

Adapted from: Francesca Volpetti, Jose Garcia-Cordero and Sebastian J. Maerkl (2015) PLoS ONE vol.10 p. e0117744.

We present a high-throughput microfluidic platform capable of quantitating up to 384 biomarkers in 4 distinct samples by immunoassay. The double layers microfluidic device contains 384 unit cells, which can be individually programmed with pairs of capture and detection antibody. Samples are quantitated in each unit cell by four independent MITOMI detection areas, allowing four samples to be analyzed in parallel for a total of 1'536 assays per device. We show that the device can be pre-assembled and stored for weeks at elevated temperature (40°C) and we performed proof-of-concept experiments simultaneously quantitating IL-6, IL-1 β , TNF- α , PSA, and GFP. Finally, we show that the platform can be used to identify functional antibody combinations by screening 64 antibody combinations requiring up to 384 unique assays per device.

2.1 - Introduction

The precise quantitation of proteins is important in systems biology and is becoming of interest in clinical studies. In both cases it is increasingly necessary to monitor dozens if not hundreds of proteins per sample, to provide an overview of protein levels in signalling networks [1], or to derive higher order correlations in clinical samples [2], [3]. Techniques for multiplexed analysis of proteins have therefore attracted considerable attention [4].

The classical and still widespread approach for quantitating proteins is based on immunoassays, particularly ELISA, which provides high-specificity, sensitivity and dynamic range, but is relatively low-throughput and extremely cost-ineffective due to large reagent

and sample consumption. To alleviate some of these problems low to medium throughput microfluidic methods have been developed for protein quantitation [5]–[7]. Multiplexed alternatives to ELISAs have recently been developed including array based detection schemes [2], [8] and bead based detection [9]–[11]. These approaches enabled the parallel analysis of large numbers of biomarkers. One significant difference between multiplexed bead assays and standard ELISAs is the fact that all antibody pairs are allowed to cross-react in the multiplexed bead assay, giving rise to potential off-target effects. A recent refinement of an array based approach circumvented these limitations using a method called antibody co-localization microarray (ACM) which specifically co-localizes antibody pairs using a microarrayer and has been used to analyse up to 50 proteins in parallel [12]. Although the ACM approach solved the problem of cross-reactivity, showed low limits of detection (LODs) and a high dynamic range, it remains difficult to implement. Microwestern arrays (MWA) were developed to alleviate some of the various shortcomings of bead-based multiplexed analysis, reverse-phase lysate arrays, and mass spectrometry based approaches [13]. MWAs are miniaturized and partially automated western blots. With MWAs it is possible to analyse 192 proteins in 6 samples for a total of 1'152 measurements. Nonetheless, MWAs are difficult to fully automate as all processing steps required for a standard western blot such as electrophoretic separation, transfer to a nitrocellulose membrane, and development with antibodies are still necessary and the entire process requires 14-24 hours.

Microfluidic based approaches are appealing alternatives to these existing methods, as all fluid handling steps can be integrated and thus automated. A recent microfluidic device based on mechanically induced trapping of molecular interactions (MITOMI) [14] could analyse 4 biomarkers in 8 samples, or vice versa [6]. We have recently reported highly-integrated and parallelized microfluidic nanoimmunoassays based on MITOMI coupled to sample microarrays, allowing the analysis of 4 biomarkers in 384 samples per device [15] and more recently 4 biomarkers in 1'024 human clinical serum samples, for a total of 4'096 measurements, requiring as little as 5 nL per sample [16]. Here we demonstrate a new functional mode enabling the parallel analysis of up to 384 biomarkers in 4 samples, for a total of 1'536 measurements per device. In our approach, each antibody pair is isolated in its own unit cell, completely eliminating cross-talk. We show that we can achieve good sensitivity and high-dynamic range with MITOMI. The approach requires ~5-25 nl (0.45-2.25 ng) of antibody per assay and is thus extremely cost effective. Antibody suppliers generally provide 100 mg of antibody, which is sufficient for ~100'000 assays using our approach. We also demonstrate that the device and antibody array can be assembled and consequently stored for weeks in ambient conditions prior to use. All processing steps are fully integrated on the microfluidic device and can be automated [17]. We measured IL-6, IL-1 β , TNF- α , PSA, and GFP, in buffer and determined the limit of detection (LOD, > mean + 2 std. deviations of the control) for these 5 proteins to be 4, 4, 30, 15, and 4 pM, respectively. We go on to show that the platform can be applied to identify optimal antibody combinations of a 3 antibody immunosandwich assay by screening all 64 combinations of 4 primary biotinylated anti-PSA mouse monoclonal antibodies, 4 secondary anti-PSA rabbit poly- and monoclonal antibodies, and 4 tertiary anti-rabbit IgG fluorophore conjugated antibodies. We tested multiple titrations of the secondary antibody for each of the antibody

combinations to derive precise, quantitative information on the relative binding strength for all 64-antibody combinations. We found that many antibody combinations were incompatible and thus non-functional, but nonetheless were able to identify several antibody combinations that performed well. The platform should thus find applications where it is necessary to perform multiplexed biomarker analysis or in combinatoric screens.

2.2 - Results and Discussion

2.2.1 - Assay workflow

The device is fabricated by multilayer soft-lithography [18] and is comprised of two PDMS layers (control and flow layer) aligned to an epoxy functionalized glass slide pre-arrayed with antibody pairs (Figure 2.1a). A DNA microarrayer was used to array the pairs of primary and secondary antibodies, which subsequently are aligned to the unit cells so that a microfluidic chamber encloses each antibody spot. The aligned device is bonded to the epoxy-coated glass slide by incubating overnight at 40°C (Figure 2.1b).

The microfluidic design is composed of 384 unit cells [15]. Each unit cell consists of two 1.7 nl antibody chambers, one for the primary antibody and the other for the secondary antibody. A detection chamber is located between the two antibody storage chambers and includes 4 detection regions created by MITOMI buttons (120 µm diameter). Each unit cell can be isolated with a microfluidic valve, and the antibody chambers are separated from the reaction chamber when the sample is flown through the main channel (Figure 2.1a).

MITOMI is a micro-mechanical method recently developed to allow the quantitative analysis of molecular interactions [14], [19]. MITOMI consists of a freestanding “button” membrane, which can be actuated by pneumatic or hydraulic pressure, similarly to standard micro-mechanical valves generated by multilayer soft-lithography [18]. When the button membrane is actuated it physically contacts a circular area on the glass surface of the microfluidic device. When the button membrane is in contact with the glass surface it protects the surface from solute and solvent molecules and can thus be used for surface patterning [20]. In addition to surface patterning, MITOMI is primarily used to mechanically trap surface bound molecules between the derivatized glass surface and the PDMS button membrane preventing dissociation of these molecules and thus allowing the precise measurement of transient molecular interactions. MITOMI has previously been applied to characterizing protein-DNA [14], [21]–[24], protein-RNA [25], [26], protein-protein [27], protein – small molecule interactions [26] and kinetic measurements [23], [27].

The assay itself is composed of four steps: i) functionalization of the surface, ii) surface immobilization of the primary antibody, iii) flow of the sample, iv) incubation with the secondary antibody, and readout (Figure 2.1c). To functionalize the surface, a solution of 2 mg/ml biotin-BSA was flowed through the detection chambers for 20 minutes with the buttons open, followed by a wash with 0.005% Tween PBS for 10 minutes. Next 0.5 mg/ml neutravidin PBS was flowed for 20 minutes, followed again by a wash step. After this step the buttons were actuated in order to specifically protect the detection areas while the

remaining surface was passivated with biotin-BSA, which was flowed for 20 minutes followed by a wash step.

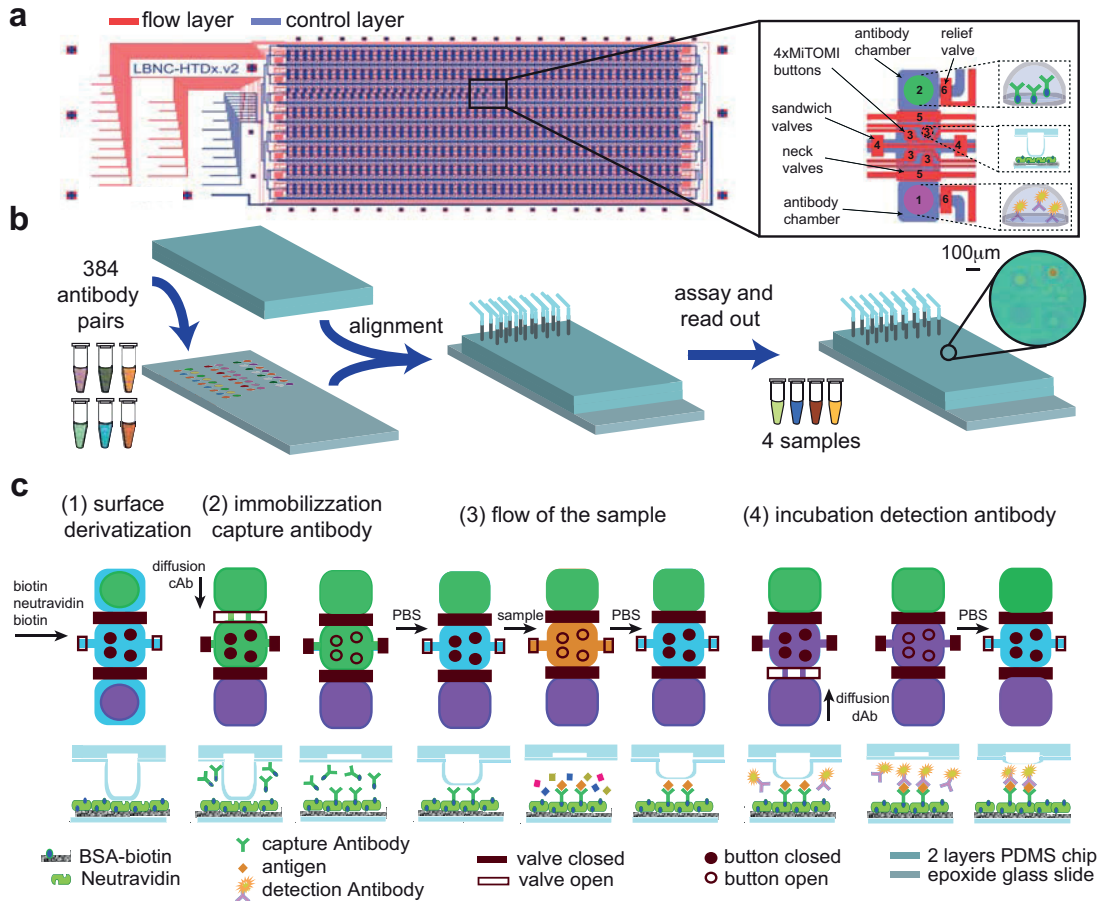


Figure 2.1: **Workflow schematic.** a) Microfluidic design: the device consists of two PDMS layers: flow (blue) and control (red). The chip is an array of eight rows by 48 columns for 384 unit cells. Each unit cell is composed of: two antibody chambers divided by a reaction chamber (1-2), 4 MITOMI buttons (3), a valve that segregates the unit cells (4), a valve that separates antibody and reaction chambers (5) and a valve for releasing pressure in the antibody chambers (6). b) The PDMS chip is aligned to an epoxy-functionalized slide onto which primary and secondary antibodies were spotted. c) Assay details: schematic of the unit cell and cross section of a button region: i) functionalization of the surface: BSA-biotin is flowed through the chip followed by neutravidin. Next, the buttons are closed and BSA-biotin flowed again to passivate all neutravidin molecules except for those located underneath the MITOMI buttons, ii) the biotinylated primary antibody is allowed to diffuse into the MITOMI detection chamber and is bound by neutravidin immobilizing it in the MITOMI detection regions, iii) the sample is flown through the device and antigens are captured by the surface immobilized antibodies, iv) finally, the fluorescently labeled secondary antibody is allowed to diffuse into the MITOMI area, binds to the antigen if present, and is trapped by MITOMI. The entire device is then quantitated using a DNA microarray scanner

Next, the unit cells were isolated and the biotinylated primary antibody allowed to diffuse into the reaction chamber. The buttons were kept closed until the antibody equilibrated to

allow a homogeneous immobilization of the primary antibody. After 2.5 hours the buttons were opened for 30 minutes and the biotinylated antibodies were immobilized to the four neutravidin coated detection regions. We then closed the MITOMI buttons to protect the detection regions from cross-contamination, opened the sandwich valves that previously isolated the unit cells, closed the primary antibody chamber, and washed the detection region with 0.005% Tween PBS. Four different samples can be measured on the device as each of the four MITOMI buttons can be independently actuated. It is thus possible to either measure one sample at 4 different dilutions, which increases the dynamic range of the assay, or 4 independent samples. Each sample is flowed for 20 minutes, followed by a 10 minutes wash step. The MITOMI buttons are actuated during the wash step to prevent dissociation and thus loss of antigen, and cross-contamination. Finally, the unit cells are once again isolated, and the secondary antibody allowed to diffuse into the detection area for 2.5 hours. Each button is then opened sequentially for 20 minutes to allow association of the secondary antibody. The sequential opening at this step further reduces any possibility of cross-contamination between buttons, which is particularly important if independent samples are tested. The entire device is then scanned with a standard DNA microarray scanner, and antigen is detected and quantitated via the fluorescently labeled secondary antibody.

2.2.2 - Assay optimization

The concentrations of the primary and secondary antibody were optimized in order to achieve optimal device performance and low limits of detection. We spotted 10 different concentrations of primary antibody to maximize signal while minimizing the required antibody amounts. After surface functionalization, the primary antibodies were re-hydrated and allowed to diffuse into the reaction chamber. We then flowed 30 nM of GFP over all four buttons in the open state for 20 minutes. GFP pull-down saturated at a spotted antibody concentration of 600 nM (Figure 2.2a), and we consequently spotted all primary antibodies at a concentration of 600 nM. Special care was taken to ensure that all four buttons were uniformly derivatized with primary antibody, which required keeping the buttons closed while the primary antibody was allowed to equilibrate for ~2 hours. Failure to do so gave rise to higher antibody densities on the two buttons near the antibody source chamber, which could not be remedied with longer incubation times, indicating that the amount of spotted antibody is not significantly larger than the amount that can be surface immobilized.

We next optimized the secondary antibody concentration. Different dilutions of anti-GFP secondary antibodies labeled with Alexa Fluor 647 and GFP were spotted on the glass slide to simultaneously assess the impact of antigen and secondary antibody concentration. For this experiment we simply flowed the primary antibody for 20 minutes at a concentration of 30 nM. The fluorescence signal from the antibody-antigen-antibody complex (Figure 2.2b) began to saturate when the concentration of the secondary antibodies reached a value of 28 nM. The limit of detection (LOD) is ~10 pM ($>$ mean + 2 std. deviations of the control) and a dynamic range of 3 orders of magnitude can be achieved in the range of 1.2-140 nM for the secondary antibody. Since the LOD was not significantly different over a secondary antibody range of 1.2 – 140 nM we opted to use a concentration of 6 nM, which resulted in low levels of non-specific signal, a low LOD, and a good dynamic range. Higher secondary

antibody concentrations give rise to higher signal but didn't improve the LOD. Furthermore, the use of lower antibody concentrations can result in cost savings when a very large number of assays are to be performed. But since our platform already uses very small quantities of antibody per assay these considerations are secondary as a single vial of antibody (100 μ g) is sufficient for \sim 100'000 assays. Nonetheless, higher secondary antibody concentrations do perform better when high biomarker levels are to be quantitated, and our platform does allow for the parallel use of multiple antibody concentrations in different microfluidic unit cells, which is appealing if high-dynamic range samples are to be quantitated. For the following multiplex experiments we chose 600 nM and 6 nM for the primary antibody and the secondary antibody concentrations, respectively.

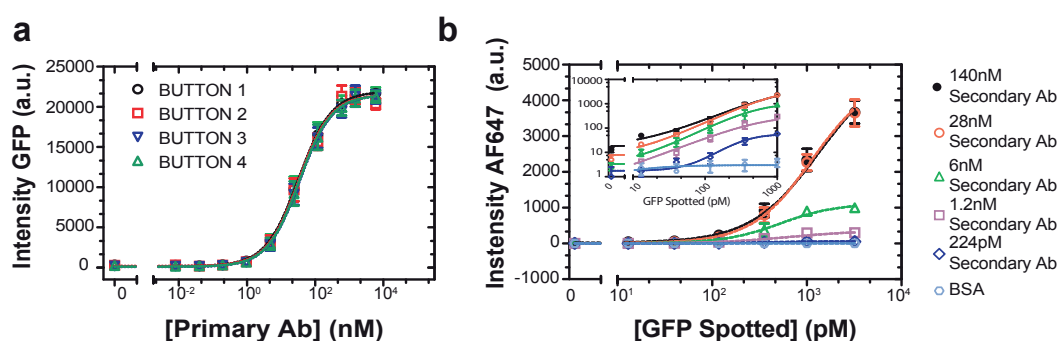


Figure 2.2: **Optimization of antibody concentration.** a) Different concentrations of anti-GFP primary antibody were spotted and 30 nM of GFP was detected with the four buttons (error bars are std. dev., n=9). All 4 buttons show identical response profiles and 600 nM was chosen as the optimal primary antibody concentration. b) Intensity of fluorescent signal as a function of spotted GFP concentration at 5 different secondary antibody concentrations, the primary antibody was flowed at a concentration of 60 nM. The inset shows the same data on a log-log scale (error bars are std. dev. n=3).

2.2.3 - Multiplex assay

To demonstrate the multiplexing capability of the platform, we tested various combinations between 5 antibody pairs on a single device for 1'408 experiments (Figure 2.3). GFP primary antibody was tested against all 5 secondary antibodies each at two different concentrations 2 nM and 6 nM, and a BSA negative control, for a total of 11 combinations. These combinations were spotted 4 times requiring 44 unit cells. The remaining 4 primary antibodies (IL-6, IL-1 β , TNF- α , PSA) were tested against 5 different secondary antibodies each at two concentrations and one BSA control, but spotted in 7 replicates, requiring a total of 308 unit cells. In total, 352 unit cells on the device were used in this experiment. We measured a negative control and an antigen cocktail containing 5 proteins in buffer (IL-6, IL-1 β , TNF- α , PSA, GFP) each at two concentrations and one BSA control, but spotted in 7 replicates giving rise to 1'408 experiments.

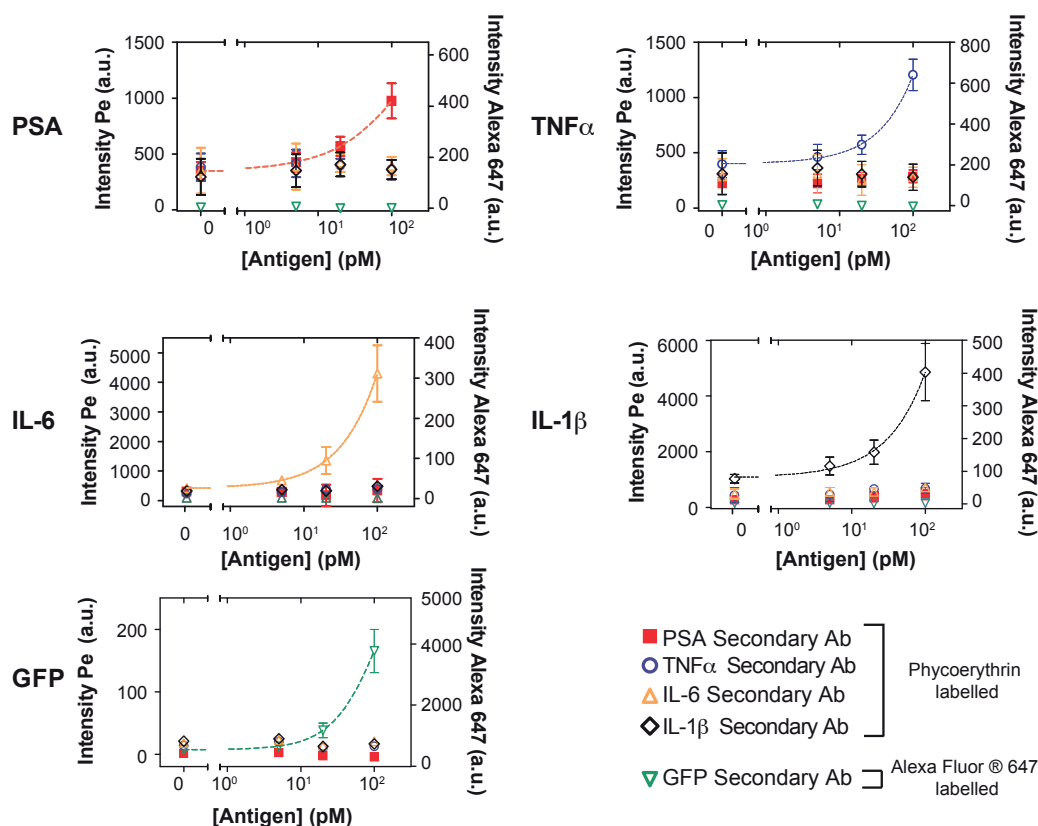


Figure 2.3: **Multiplexed assay and antibody cross-reactivity testing.** Fluorescent signal and binding curves for 5 different proteins (PSA, TNF- α , IL-6, IL-1 β , and GFP) quantitated in parallel on a single device. Concentrations for the primary and secondary antibodies used in this experiment were 600 nM and 6 nM, respectively. Each panel shows the signal obtained from the specific primary antibody to the given antigen detected with the various secondary fluorescently labeled detection antibodies. The results show that each antigen was specifically detected by the correct antibody pair and that no significant cross reactivity occurred between the antigens and antibodies tested in this experiment. Left y-axis: phycoerythrin labeled secondary antibody signal; right y-axis: Alexa Fluor 647 labeled secondary antibody signal (error bars are std. dev. $n=7$).

The solutions were introduced on-chip starting with the BSA control and then from the lowest to the highest concentration of the antigen cocktail, one for each button. As shown in Figure 2.3 and Figure SI 2.2 the specific signal from each reaction is considerably higher than the non-specific signal, indicating that, at least for these antibody combinations, no considerable cross-reactivity was observed.

Depending on the antigen the LOD varies from 4 pM to 30 pM. In our previous work [16] LODs of 3.67 pM, 742 fM, 897 fM and 1.04 pM were achieved for TNF- α , IL-6, IL-1 β and PSA, respectively. These LODs are comparable to other microfluidic methods. Zheng et al. report a MITOMI device capable of detecting 10-100 pg/ml (55.6 – 556 fM) of CEA [6], Fan et al. report a sensitivity of <1-30 pM for various cytokines using a barcode based microfluidic platform [2], and Pla-Roca et al. measured LODs for TNF- α = 15.6 pg/ml (917

fM), IL-6 = 42.9 pg/ml (2.04 pM), and IL-1 β = 12.3 pg/ml (683 fM) [12]. Commercially available macroscale assays often exhibit higher sensitivities. Meso Scale Discovery reports the following sensitivities: TNF- α = 1.1 pg/ml (64.7 fM), IL-6 = 0.7 pg/ml (33.3 fM), and IL-1 β = 2.4 pg/ml (133.3 fM), and Luminex: TNF- α = 25 pg/ml (1.47 pM), IL-6 = 5 pg/ml (238.1 fM), and IL-1 β = 15 pg/ml (833.3 fM)

2.2.4 - Combinatoric screen to identify functional antibody combinations

Immunoassays generally require two or three antibodies, two of which directly bind to the biomarker of interest, while the third is required for readout. It can thus be non-trivial to identify combinations of antibodies that function in concert, particularly the two antibodies that are required to bind to the same protein biomarker. In addition to this combinatoric problem of identifying antibodies that work well together, it is also of interest to identify those antibodies that have the highest affinity for their antigen. Our multiplexed immunoassay platform is ideally suited to conduct large-scale screens to address these issues.

To test whether our platform can be used to identify functional antibody combinations we chose to optimize a 3-antibody immunoassay for PSA. We acquired 4 primary biotinylated anti-PSA monoclonal antibodies, 4 secondary anti-PSA antibodies, and 4 tertiary anti-rabbit IgG antibodies labeled either with phycoerythrin or Alexa-Fluor 546 (Table 2.1), originating from 4 different antibody suppliers. In addition to testing all 64 antibody combinations we also decided to titrate the secondary antibody, to derive relative binding affinities of these antibodies.

	Description	Species	Clonality	Supplier	Catalog Number
A	anti-PSA biotin conjugated	Mouse	monoclonal	Abcore	1B-289
B	anti-PSA biotin conjugated	Mouse	monoclonal	Abcam	ab77310
C	anti-PSA biotin conjugated	Mouse	monoclonal	Abcam	ab182031
D	anti-PSA biotin conjugated	Mouse	monoclonal	Abcam	ab182030
1	anti-PSA	Rabbit	polyclonal	Fitzgerald	70R-35481
2	anti-PSA	Rabbit	monoclonal	Abcam	ab76113
3	anti-PSA	Rabbit	polyclonal	Abcam	ab53774
4	anti-PSA	Rabbit	polyclonal	Abcam	ab19554
α	Goat anti-rabbit IgG PE conjugated	Goat		Life Technologies	P-2771MP
β	Goat anti-rabbit IgG Alexa Fluor 546 conjugated	Goat		Life Technologies	A-11010
γ	Goat anti-rabbit IgG PE conjugated	Goat	polyclonal	Abcam	ab72465
δ	Goat anti-rabbit IgG PE conjugated	Goat	polyclonal	Abcam	ab97070

Table 2.1: **List of antibodies.** The table lists the 12 antibodies tested. Description, species, clonality, supplier and catalog number are provided for each antibody (Life-Technologies did not provide the clonality for antibodies α and β but they are likely polyclonal antibodies). The first set (A-D) includes the biotinylated primary antibodies, the second set (1-4) the secondary antibodies, and the third set (α - δ) the tertiary antibodies conjugated with phycoerythrin or Alexa Fluor 546.

We performed the combinatoric screen in 3 different ways. In the first experiment we spotted the 4 secondary antibodies, each at 6 different concentrations (including a no-antibody control), and the 4 tertiary antibodies generating 96 unique combinations (4x4x6) in quadruplicate requiring all 384 unit cells on the device. We then surface immobilized the 4 biotinylated primary antibodies on the 4 MITOMI detection areas to generate 384 unique conditions performed in quadruplicate for a total of 1'536 assays. We then tested the antibody combinations for their ability to detect 100 pM of PSA (Figure 2.4).

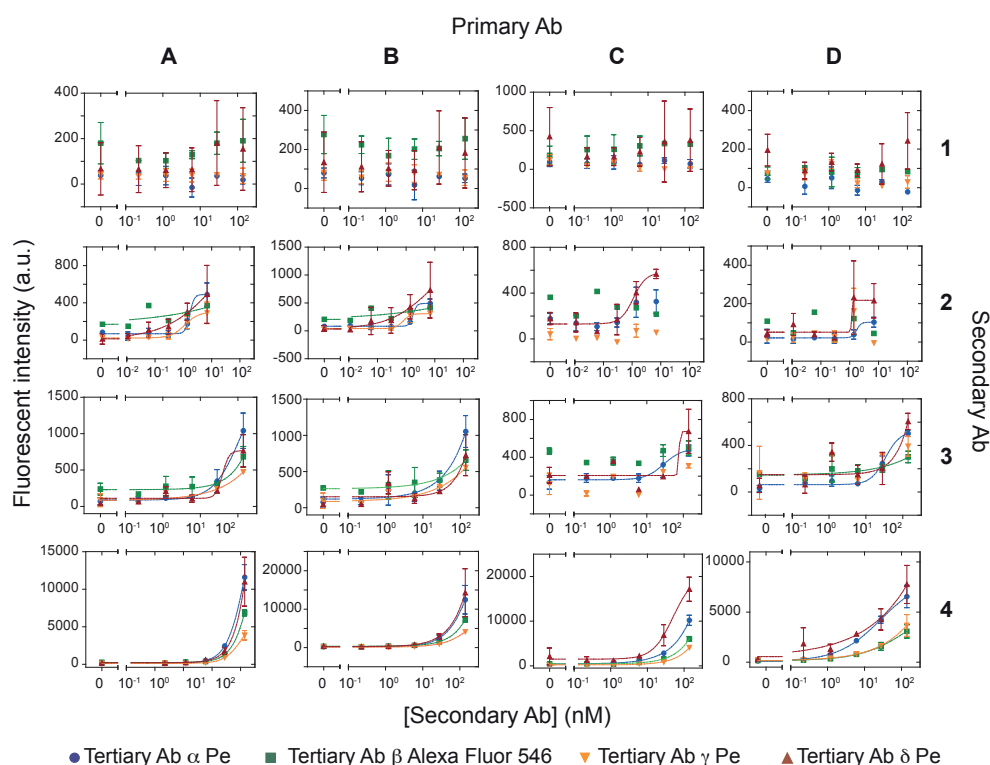


Figure 2.4: **Screening of antibody combinations for PSA detection: secondary and tertiary antibodies were spotted.** Different combinations of four secondary antibodies (1-4) and four tertiary antibodies (α - δ) were spotted. The secondary antibodies were spotted at six different concentrations, and the tertiary antibody at a concentration of 30 nM. After surface derivatization, four different primary antibodies (A-D) were flowed in sequence, one for each button, followed by 100 pM PSA in a buffer solution. Next the secondary antibody was allowed to diffuse in the reaction chamber and finally, the tertiary (α - δ) antibodies diffused in reaction chamber.

This experiment provided a global overview of the performance of the various antibody combinations, and showed that two of the secondary antibodies (#1 and #2) were non-functional, or performed poorly. We next repeated the experiment with spotted primary and secondary antibodies and testing 3 of the 4 tertiary antibodies (Figure 2.5). We opted to remove the δ tertiary antibody from this screen as it gave consistently high non-specific

fluorescent background. This second screen returned qualitatively the same results as the first screen.

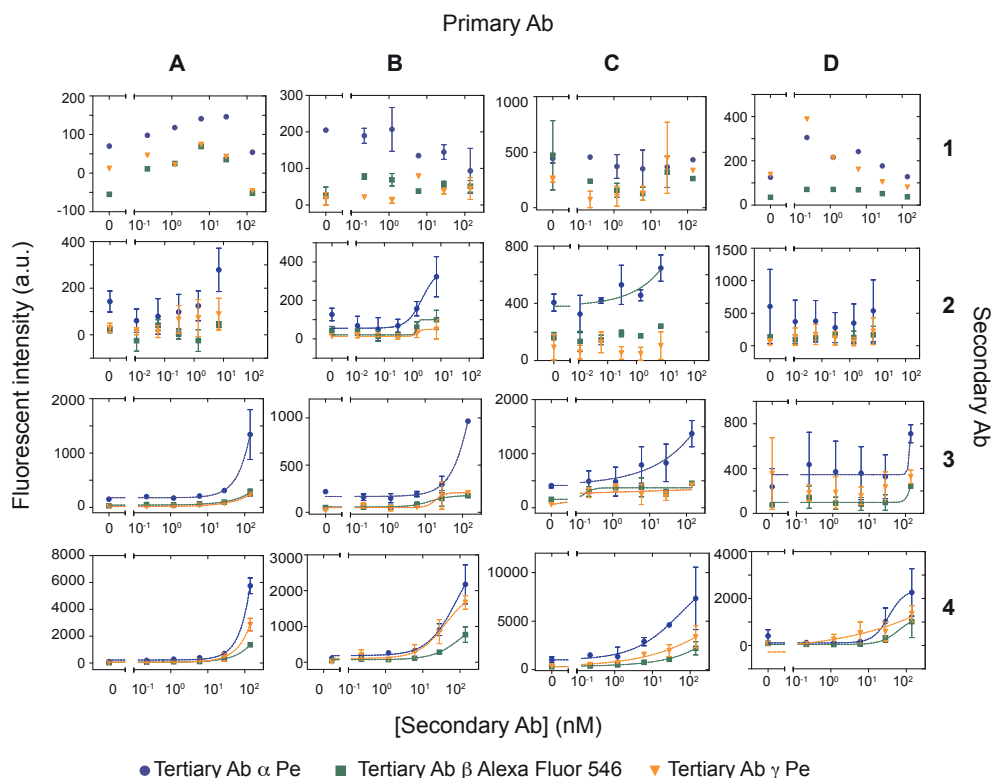


Figure 2.5: **Screening of antibody combinations for PSA detection: primary and secondary antibodies were spotted.** 16 different combinations of antibodies were spotted: four primary antibodies (A-B) and four secondary antibodies (1-4). The secondary antibodies were spotted at six different concentrations (0, 0.2, 1.2, 6, 28 and 140 nM), and the primary antibody at a concentration of 600 nM. After the surface derivatization, the primary antibody was allowed to diffuse and immobilize to the surface, then 100 pM PSA was flowed in the chip. Next the secondary antibody was allowed to diffuse in the reaction chamber and finally, three different tertiary antibodies (α , β , γ) were sequentially flowed, one for each button.

We then repeated the screen on 4 separate devices by spotting 12 concentrations of the secondary antibody, immobilizing one of the 4 biotinylated antibodies in all four MITOMI detection areas, and testing each fluorescently labeled tertiary antibody on a separate MITOMI button for a total of 768 unique conditions (12x4x4x4) with 8 repeats gathering a total of 6144 data points (Figure 2.6).

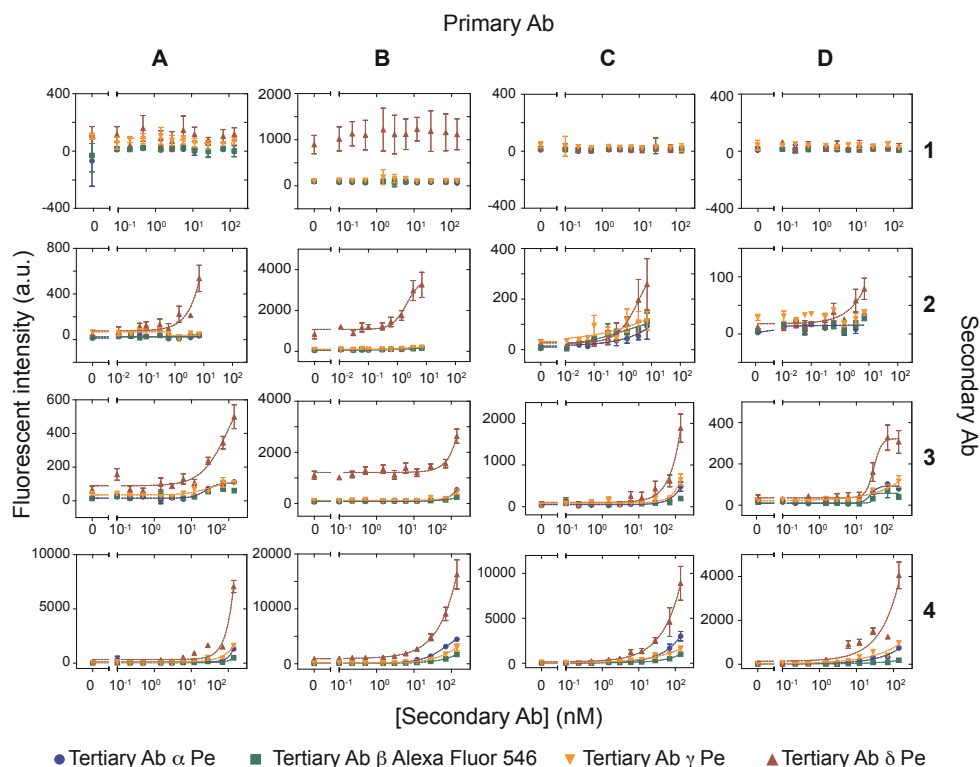


Figure 2.6: **Combinatorial antibody screen.** Four different secondary antibodies (1-4) were spotted at 12 different concentrations on four epoxy glass slides and aligned to PDMS chips. For each device one of the four primary antibodies (A-B) was flowed at a concentration of 30 nM through the device and immobilized on the four MITOMI detection regions. Next, PSA was flowed at a concentration of 100 pM. Then, the secondary antibodies were allowed to diffuse into the reaction chamber. Finally, the four different tertiary antibodies (α - δ) were flowed sequentially at a concentration of 30 nM one for each MITOMI button. (error bars are std. dev. n=8).

We found no major differences in performance between the 4 primary antibodies tested, but observed a considerable variation in the secondary and tertiary antibody performances. The secondary polyclonal antibody #1 from Fitzgerald repeatedly failed in all combinations tested and the two polyclonal antibodies (#3 and #4) from Abcam consistently outperformed the monoclonal antibody #2 from the same supplier. Both tertiary antibodies (γ and δ) from Abcam gave non-specific signal, apparently because of poor antibody purification after conjugation to phycoerythrin. Nonetheless tertiary antibody δ performed exceedingly well in our screen, but did give rise to considerable non-specific signal when used in combination with primary antibody B. The second best performer of the tertiary antibodies was antibody α from Life-Technologies. These results show that there is a significant variability in antibody performance, but that it is possible to identify functional antibody combinations rapidly, and cost effectively on our multiplexed immunoassay platform.

2.2.5 - Stability test

We envision these immunoassay devices to ultimately be used either in research or clinical settings, which requires that the assembled microfluidic device and reagents contained therein be stable for extended periods of time, preferably at ambient conditions. We therefore performed a stability test to determine how long the device maintained its functionality. Six slides were spotted with primary and secondary antibodies against GFP. After bonding the PDMS device with the spotted glass slides the assembled devices were stored at 40°C for up to one month. We tested devices periodically after one, two, and four weeks under the same experimental conditions. After one week at 40°C we observed no significant decrease in signal from the stored chip as compared to a new device (Figure 2.7). After two weeks the signal decreased by ~20% and after one month the signal decrease by about 50%. This study indicates that assembled devices are indeed functional after 1 month stored at elevated temperatures and that after four weeks the decrease in signal is within acceptable limits.

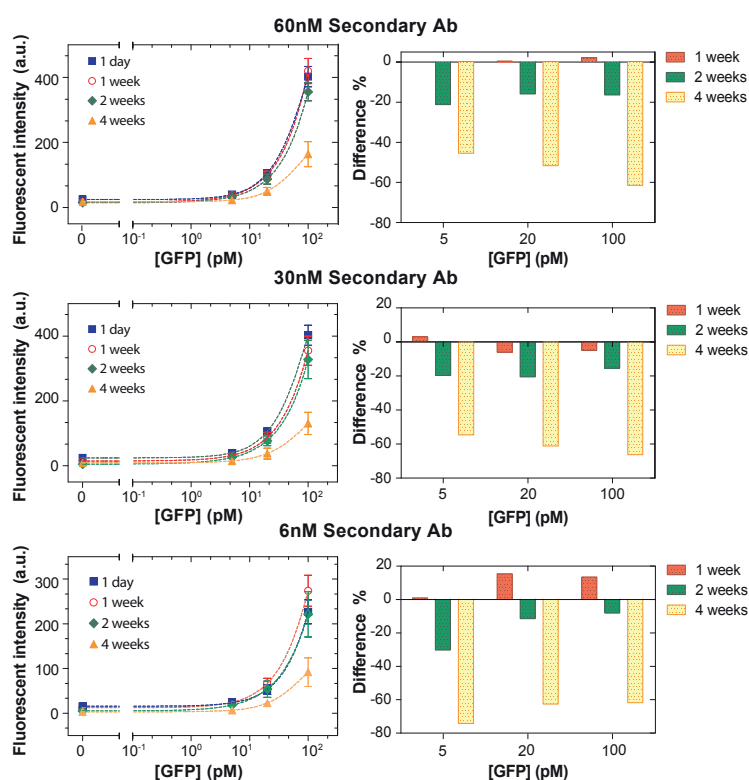


Figure 2.7: **Stability test.** (left column) Intensity of the fluorescent signal as a function of the GFP concentration flowed through the channel, using a new device and devices stored at 40°C for 1, 2, and 4 weeks. (Right column) Percentage difference between the mean signals measured on the new device and those stored for different amounts of time.

In this series of experiments we assembled the devices, stored them at elevated temperatures, and then performed all fluidic operations. This still requires the use of

biotinylated-BSA, and neutravidin. These reagents should be reasonably stable in solution or in lyophilized form, and thus no hindrance to applications in a variety of environments. We nonetheless tested whether it is possible to assemble a device, perform the surface chemistry, dry and store the device. The use of oil (Fluorinert FC-40) in the control layers prevented premature re-hydration of the spotted antibodies. We observed that the low-viscosity oil could slowly seep through the PDMS, leading to fouling of the flow layer and the surface chemistry. Storing the device in vacuum over-night eliminated this problem and allowed us to perform a functional immunoassay one day after generating the surface chemistry and drying the device. A better solution would be to remove the oil from the control lines after generating the surface chemistry, eliminating the need for vacuum storage. The signals obtained from this device were lower than from devices with a freshly prepared surface (Figure SI 2.3), but sufficiently high to conduct quantitative measurements. It is thus possible to decouple surface preparation from the actual assay with good results (LOD of 10 pM instead of 4 pM), although the approach could be further optimized (choice of oil, generating a more stable surface chemistry, etc.). Nonetheless, these studies indicate that devices can be pre-assembled and stored, effectively decoupling chip production and utilization.

2.3 - Conclusions

We developed a microfluidic device able to perform multiplexed analysis of up to 384 biomarkers in four samples for a total of 1'536 immunoassays per device. The consumption of antibodies is reduced to nanogram amounts, drastically decreasing assay cost. The primary hurdle to applying this platform to the detection of hundreds of protein biomarkers is the initial acquisition cost of a large number of antibody pairs, which was prohibitive for this proof-of-concept study. Nonetheless the drastically reduced antibody consumption of our platform means that once a library of antibodies is acquired it becomes a long-lasting resource sufficient for ~100'000 assays. Once initial antibody pairs are acquired and validated, they can be used for thousands of assays also eliminating problems associated with antibody batch-to-batch variability, which otherwise would require significant re-validation efforts especially in clinical settings. The platform can of course be used to measure a smaller number of biomarkers. For example, 96 antibody pairs can be spotted in quadruplicate to measure 96 biomarkers in four samples with higher accuracy than could be achieved with a single measurement. We recently demonstrated that each MITOMI button can be used to analyze 3 different samples [20], which when applied to the current device would increase the sample throughput from 4 to 12 samples and 4'608 assays per device.

To validate the platform, four human antigens IL-6, IL-1 β , TNF- α , and PSA were detected achieving LODs in the range of 4-30 pM. We also applied the platform to a high-throughput combinatoric screen to identify functional antibody combinations. We showed that the chip can be stored after assembly for extended periods of time in adverse conditions (40°C) enabling the possibility to deploy such devices as academic or clinical research tools. All remaining processing steps are readily automated, and the final method only requires

user intervention to introduce a wash solution and samples onto the device. With our current device the antibody derivatization steps require a significant amount of time (2-3 hours). These steps could be drastically accelerated by including active mixing on the device [28], [29]. Active mixing could reduce each step to below 10-15 minutes, allowing the entire assay to be performed in less than 1-2 hours. These results show that MITOMI based high-throughput protein quantitation is an appealing approach for applications in clinical and basic research. Potential applications of the technology include the analysis of cellular signaling pathways [30] and analysis of clinical samples. A number of clinical investigations are currently underway with the aim to perform full genome and microbiome sequencing coupled to the analysis of a large number of serum proteins [31]. The technology presented here should be an appealing choice for the comprehensive analysis of medium to large panels of protein biomarkers in clinical samples, particularly since we recently demonstrated that a similar microfluidic platform was applicable to measuring protein biomarkers in clinical serum samples [16].

2.4 - Materials and methods

2.4.1 - Device fabrication

The device is composed of two PDMS layers (control and flow layer) aligned to an epoxy-functionalized microscope slide. The devices were fabricated by multilayer-soft-lithography [18]. SU8 GM1060 photoresist was used to pattern the 30 μm high control layer, which was spin coated first for 10 s at 500 rpm, then for 20.3 s at 2527 rpm, once more at 2527 rpm for 40 s, then for 1 s at 3527 rpm, followed by 1 s at 2527 rpm. After a soft bake step the wafer was exposed on a MA6 mask aligner for 8 s followed by a post exposure bake. The exposed wafer was developed in PGMEA, followed by a hard bake at 160°C. AZ9260 photoresist was used for the 10 μm high flow layer. It was spin coated for 10 s at 800 rpm, followed by 40 s at 1800 rpm. After a soft bake the wafer was exposed on an MA6 mask aligner for two intervals of 18 s. The flow layer mold was annealed at 180°C for 30 minutes to round the flow channels. 20:1 and 5:1 ratios of elastomer (Sylgard 184) were used for the flow and the control layer, respectively. These were cured at 80°C for 30 minutes and then aligned. After aligning the flow and control layer were bonded at 80°C for 1.5 hours.

2.4.2 - Epoxy-silane coated glass slide

The protocol consists of two parts: cleaning of the glass slides followed by coating them with epoxy silane. In the first step a solution of milli-Q water and ammonia solution (NH_4OH 25%) in a 5:1 ratio was heated to 80°C. When the solution reached said temperature, 150 ml of hydrogen peroxide (H_2O_2 30%) was added to the bath. The glass slides were immersed in this solution for 30 minutes. Glass slides were then rinsed with milli-Q water and dried with nitrogen. In the second step the slides were submerged in a 1% solution of 3-Glycidioxypropyl-trimethoxymethylsilane (97% pure) in toluene for 20 minutes. The slides are then rinsed with fresh toluene to remove any unbound 3-GPS,

dried with nitrogen and followed by a baking step at 120°C for 30 minutes. The glass slides were sonicated in fresh toluene for 20 minutes and afterwards rinsed with isopropanol and dried. The epoxy-coated slides were stored in a vacuum chamber at room temperature until used.

2.4.3 - Microarray spotting

A high-throughput microarray platform (Genetix QArray2) was used to array the reagents. Depending on the experiment a combination of primary, secondary, tertiary antibody, and sample were spotted. A 4.9 nL delivery-volume spotting pin (946MP8XB, Arrayit, USA) was used to array all samples. Each spot was spotted 5 times to increase reagent concentrations. After each sample the pin was washed 3 times using dH₂O for 500 ms, between each washing step the pin was dried for 500 ms. The humidity in the spotting robot was set to 60%.

2.4.4 - Antibodies and proteins

Biotinylated goat polyclonal antibody to GFP was purchased from Abcam (ab6658), EGFP from Biovision (4999-100) and the anti Penta-His Alexa Fluor 647 conjugate was purchased from Qiagen (35370). A matched monoclonal anti human-PSA antibody pair and purified native human PSA were purchased from Fitzgerald Industries International (MA, USA) (10-P20E, 10-P20D, 30C-CP1017U). Anti-PSA antibodies were purchased from Abcam (ab53774, ab76113, ab19554) and from Fitzgerald (70R-35481). Anti-PSA biotin conjugated antibodies were purchased from Abcam (ab182031, ab77310, ab182030) and from Abcore (1B-289). The anti-cytokine antibodies were purchased from eBioscience: IL-6 biotin-conjugate, IL-1 β biotin-conjugate, TNF- α , (13-7068-81, 13-7016-81, 16-7384-85). The anti human-IL-6 (12-7069-81), IL-1 β (13-7016-81), TNF- α (12-7349-81) labeled with phycoerythrin (PE), human IL-6 protein standard (39-8069-65), human IL-1 β protein standard (39-8018-65), human TNF- α protein standard (39-8329-65) were purchased from eBioscience. Goat anti-Rabbit IgG labelled with phycoerythrin (Pe) were purchased from Abcam (ab72465, ab97070) and from Life-Technologies (P2771MP), Goat anti-Rabbit IgG labelled with Alexa Fluor 546 from Life-Technologies (A-11010). Neutravidin biotin-binding protein and the biotinylated bovine serum albumin BSA were purchased from Thermo Scientific (29130 and 31000 respectively).

Primary antibodies for PSA (10-P20D) and TNF- α were biotinylated using a ChromaLink One-Shot Antibody Biotinylation kit (Solulink) according to the manufacture instructions. Anti human PSA (10-P20E) was labeled with PE using the R-PE Antibody All-in-One Conjugation kit (Solulink) according to the supplied protocol.

2.4.5 - Device operation

Microfluidic control channels were primed with dH₂O (or oil: Fluorinert FC-40) starting at 5 psi, once the channels were completely filled, the pressure was increased to 15 psi to close the fluidic valves and to 20 psi to actuate the MITOMI button membranes. All reagents were

aspirated into Tygon tubing (i.d. 0.51 mm, o.d. 1.52 mm) and connected to the flow channels, and the flow-channel pressure was set at 3.5 psi [15].

2.4.6 - Data analysis

The microfluidic device was scanned using a fluorescent microarray scanner (ArrayWorx e-Biochip Reader, Applied Precision, USA). The images were exported as 16-bit TIFF files and analyzed using microarray image analysis software (GenePix Pro v6.0, Molecular device). Non-linear regression analysis of the data was performed using Prism 5.0 (GraphPad).

2.5 - Supplementary

2.5.1 - Representative fluorescent image of the unit cell of the multiplex detection

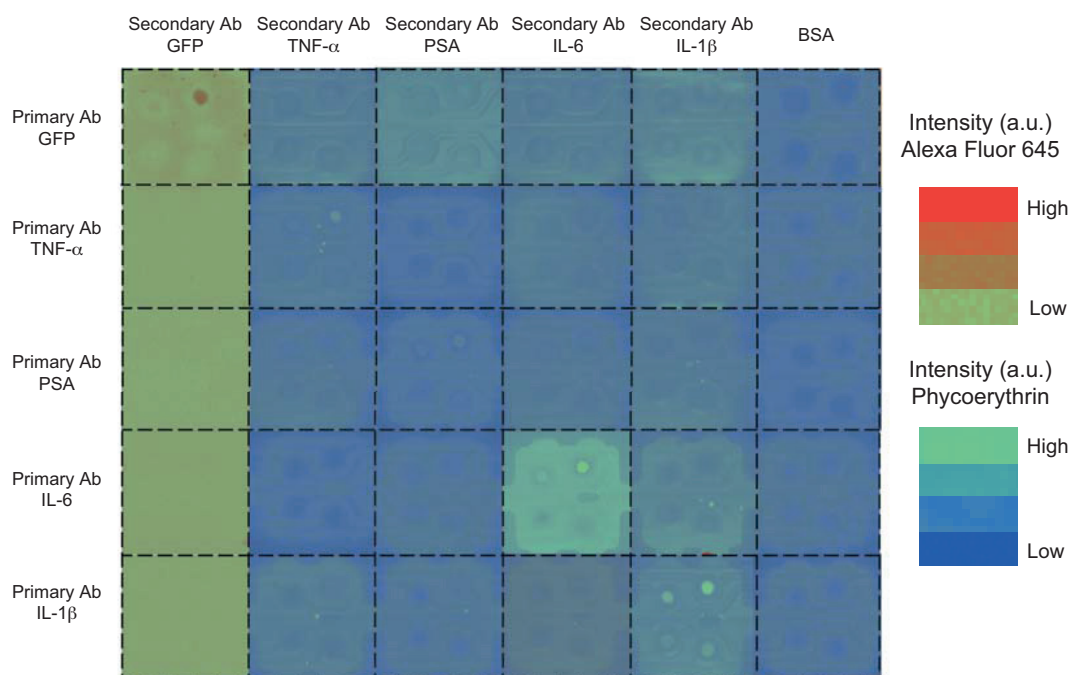


Figure SI 2.1: **Fluorescent images of some of the unit cells on the device.** All combinations of the five different primary antibodies and secondary antibodies were tested. A negative control (2% BSA in PBS) and a cocktail of proteins in buffer (GFP, IL-6, IL-1b, TNF-a, and PSA), at three different concentrations (5, 20, 100 pM), were sequentially flowed. The color bars indicate the relative fluorescence intensity.

2.5.2 - Multiplexed assay spotting 2 nM concentration secondary antibody

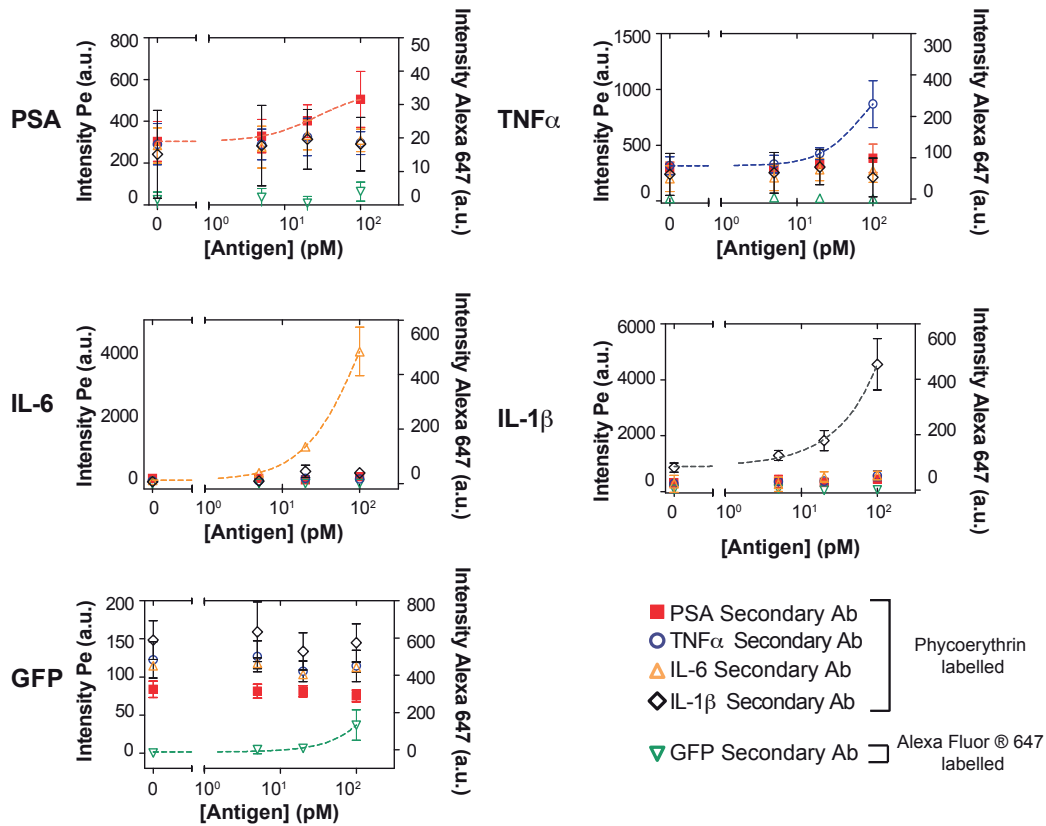


Figure SI 2.2: **Multiplexed assay and antibody cross-reactivity testing.** Fluorescent signal and binding curves for 5 different proteins (PSA, TNF- α , IL-6, IL-1 β , and GFP) quantitated in parallel on a single device. Concentrations for the primary and secondary antibodies used in this experiment were 600 nM and 6 nM, respectively. Each panel shows the signal obtained from the specific primary antibody to the given antigen detected with the various secondary fluorescently labeled detection antibodies. The results show that each antigen was specifically detected by the correct antibody pair and that no significant cross reactivity occurred between the antigens and antibodies tested in this experiment. Left y-axis: phycoerythrin labeled secondary antibody signal; right y-axis: Alexa Fluor 647 labeled secondary antibody signal (error bars are std. dev. n=7).

2.5.3 - Stability on the surface chemistry

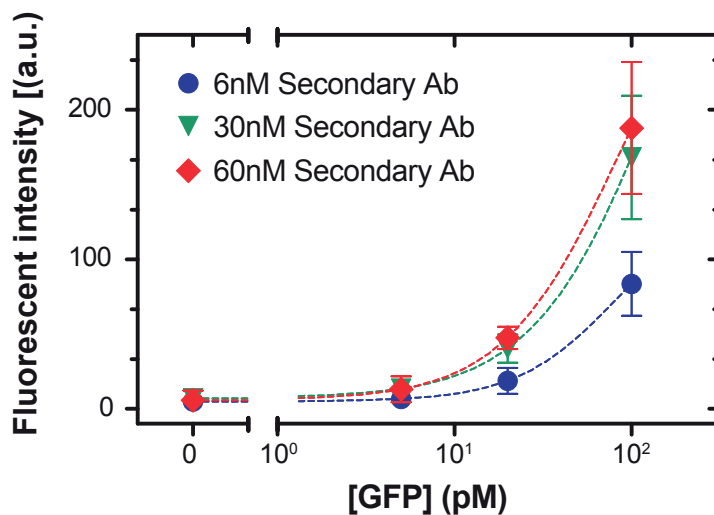


Figure SI 2.3: **Stability on the surface chemistry.** Fluorescent intensity as a function of GFP concentration 1 day after generating the surface chemistry on the device (error bars are std. dev., $n=9$). The control lines were filled with oil (Fluorinert FC-40), and the functionalization of the surface was performed, as described. Next, the flow layer was dried by pushing air through the channel at 3.5 psi for 30 minutes. The chip was then stored in a vacuum chamber at room temperature for 1 day. To perform the immunoassay the chambers containing the spotted antibodies against GFP were filled with PBS in order to re-hydrate the spots. The unit cells were then isolated and the primary antibody allowed to diffuse into the reaction chamber. After a washing step, four different concentrations of GFP were flowed in sequence, one for each button. Finally, the secondary antibody was allowed to diffuse into the reaction chamber and the device was scanned.

Bibliography

- [1] M. J. Lee *et al.*, “Sequential Application of Anticancer Drugs Enhances Cell Death by Rewiring Apoptotic Signaling Networks,” *Cell*, vol. 149, no. 4, pp. 780–794, May 2012.
- [2] R. Fan *et al.*, “Integrated barcode chips for rapid, multiplexed analysis of proteins in microliter quantities of blood,” *Nat. Biotechnol.*, vol. 26, no. 12, pp. 1373–1378, Dec. 2008.
- [3] A. M. Gonzalez-Angulo, B. T. J. Hennessy, and G. B. Mills, “Future of Personalized Medicine in Oncology: A Systems Biology Approach,” *J. Clin. Oncol.*, vol. 28, no. 16, pp. 2777–2783, Jun. 2010.
- [4] A. Bange, H. B. Halsall, and W. R. Heineman, “Microfluidic immunosensor systems,” *Biosens. Bioelectron.*, vol. 20, no. 12, pp. 2488–2503, Jun. 2005.
- [5] A. Singhal, C. A. Haynes, and C. L. Hansen, “Microfluidic measurement of antibody-antigen binding kinetics from low-abundance samples and single cells,” *Anal. Chem.*, vol. 82, no. 20, pp. 8671–8679, Oct. 2010.
- [6] C. Zheng *et al.*, “High-throughput immunoassay through in-channel microfluidic patterning,” *Lab. Chip*, vol. 12, no. 14, pp. 2487–2490, Jul. 2012.
- [7] A. H. C. Ng, U. Uddayasankar, and A. R. Wheeler, “Immunoassays in microfluidic systems,” *Anal. Bioanal. Chem.*, vol. 397, no. 3, pp. 991–1007, Jun. 2010.
- [8] A. Bernard, B. Michel, and E. Delamarque, “Micromosaic immunoassays,” *Anal. Chem.*, vol. 73, no. 1, pp. 8–12, Jan. 2001.
- [9] R. Wilson, A. R. Cossins, and D. G. Spiller, “Encoded microcarriers for high-throughput multiplexed detection,” *Angew. Chem. Int. Ed Engl.*, vol. 45, no. 37, pp. 6104–6117, Sep. 2006.
- [10] H. Lee, J. Kim, H. Kim, J. Kim, and S. Kwon, “Colour-barcoded magnetic microparticles for multiplexed bioassays,” *Nat. Mater.*, vol. 9, no. 9, pp. 745–749, Sep. 2010.
- [11] S.-H. Kim, J. W. Shim, and S.-M. Yang, “Microfluidic Multicolor Encoding of Microspheres with Nanoscopic Surface Complexity for Multiplex Immunoassays,” *Angew. Chem. Int. Ed.*, vol. 50, no. 5, pp. 1171–1174, 2011.
- [12] M. Pla-Roca *et al.*, “Antibody Colocalization Microarray: A Scalable Technology for Multiplex Protein Analysis in Complex Samples,” *Mol. Cell. Proteomics MCP*, vol. 11, no. 4, Apr. 2012.
- [13] M. F. Ciaccio, J. P. Wagner, C.-P. Chuu, D. A. Lauffenburger, and R. B. Jones, “Systems analysis of EGF receptor signaling dynamics with microwestern arrays,” *Nat. Methods*, vol. 7, no. 2, pp. 148–155, Feb. 2010.
- [14] S. J. Maerkl and S. R. Quake, “A Systems Approach to Measuring the Binding Energy Landscapes of Transcription Factors,” *Science*, vol. 315, no. 5809, 2007.
- [15] J. L. Garcia-Cordero, C. Nembrini, A. Stano, J. A. Hubbell, and S. J. Maerkl, “A high-throughput nanoimmunoassay chip applied to large-scale vaccine adjuvant screening,” *Integr. Biol. Quant. Biosci. Nano Macro*, vol. 5, no. 4, pp. 650–658, Apr. 2013.
- [16] J. L. Garcia-Cordero and S. J. Maerkl, “A 1024-sample serum analyzer chip for cancer diagnostics,” *Lab. Chip*, vol. 14, no. 15, pp. 2642–2650, Jul. 2014.
- [17] L. M. Fidalgo and S. J. Maerkl, “A software-programmable microfluidic device for automated biology,” *Lab. Chip*, vol. 11, no. 9, pp. 1612–1619, May 2011.
- [18] M. A. Unger, H.-P. Chou, T. Thorsen, A. Scherer, and S. R. Quake, “Monolithic Microfabricated Valves and Pumps by Multilayer Soft Lithography,” *Science*, vol. 288, no. 5463, pp. 113–116, Apr. 2000.
- [19] S. Rockel, M. Geertz, and S. J. Maerkl, “MITOMI: a microfluidic platform for in vitro characterization of transcription factor-DNA interaction,” *Methods Mol. Biol. Clifton NJ*, vol. 786, pp. 97–114, 2012.
- [20] J. L. Garcia-Cordero and S. J. Maerkl, “Multiplexed surface micropatterning of proteins with a pressure-modulated microfluidic button-membrane,” *Chem. Commun.*, vol. 49, no. 13, pp. 1264–1266, Jan. 2013.
- [21] K. Limmer, D. A. Pippig, D. Aschenbrenner, and H. E. Gaub, “A Force-Based, Parallel Assay for the Quantification of Protein-DNA Interactions,” *PLoS ONE*, vol. 9, no. 2, p. e89626, Feb. 2014.

- [22] S. Rockel, M. Geertz, K. Hens, B. Deplancke, and S. J. Maerkl, “iSLIM: a comprehensive approach to mapping and characterizing gene regulatory networks,” *Nucleic Acids Res.*, vol. 41, no. 4, p. e52, Feb. 2013.
- [23] M. Geertz, D. Shore, and S. J. Maerkl, “Massively parallel measurements of molecular interaction kinetics on a microfluidic platform,” *Proc. Natl. Acad. Sci.*, vol. 109, no. 41, pp. 16540–16545, Oct. 2012.
- [24] P. M. Fordyce *et al.*, “De novo identification and biophysical characterization of transcription-factor binding sites with microfluidic affinity analysis,” *Nat. Biotechnol.*, vol. 28, no. 9, pp. 970–5, Sep. 2010.
- [25] L. Martin *et al.*, “Systematic reconstruction of RNA functional motifs with high-throughput microfluidics,” *Nat. Methods*, vol. 9, no. 12, pp. 1192–1194, Dec. 2012.
- [26] S. Einav *et al.*, “Discovery of a hepatitis C target and its pharmacological inhibitors by microfluidic affinity analysis,” *Nat. Biotechnol.*, vol. 26, no. 9, pp. 1019–1027, Sep. 2008.
- [27] D. Gerber, S. J. Maerkl, and S. R. Quake, “An in vitro microfluidic approach to generating protein-interaction networks,” *Nat. Methods*, vol. 6, no. 1, pp. 71–74, Jan. 2009.
- [28] H.-P. Chou, M. A. Unger, and S. R. Quake, “A Microfabricated Rotary Pump,” *Biomed. Microdevices*, vol. 3, no. 4, pp. 323–330, Dec. 2001.
- [29] H. Niederholtmeyer, V. Stepanova, and S. J. Maerkl, “Implementation of cell-free biological networks at steady state,” *Proc. Natl. Acad. Sci.*, vol. 110, no. 40, pp. 15985–15990, Oct. 2013.
- [30] M. F. Ciaccio, J. P. Wagner, C.-P. Chuu, D. A. Lauffenburger, and R. B. Jones, “Systems analysis of EGF receptor signaling dynamics with microwestern arrays,” *Nat. Methods*, vol. 7, no. 2, pp. 148–155, Feb. 2010.
- [31] N. D. P. Leroy Hood, “Demystifying disease, democratizing health care,” *Sci. Transl. Med.*, vol. 6, no. 225, p. 225ed5, 2014.

Chapter 3

A digital-analog microfluidic platform for patient-centric multiplexed biomarker diagnostics of ultra-low volume samples

Reprinted with permission from: Francesco Piraino*, Francesca Volpetti*, Craig Watson and Sebastian J. Maerkl (2016) ACS Nano vol.10 pp. 1699–1710. Copyright (2016) American Chemical Society.

*Equally contributing authors

Detection of biomarkers is essential for the diagnosis of diseases. The use of microfluidics plays a key role for the future diagnostic platforms. A powerful platform should be able to combine low limit of detection LOD (sub-picomolar), high dynamic range (≥ 5 orders of magnitude), multiplexing capability (≥ 4) and use low volume samples ($< 5 \mu\text{l}$). Finally the setup should be portable to allow its use in a resource-limited environment.

We developed a two layers microfluidic device, composed of 16 independent assay units. In half of the units there are MITOMI (mechanically induced trapping of molecular interactions) buttons, for analog detection, and in the other half buttons patterned with femtowells, for digital detection. Analog detection is achieved observing the increase of fluorescent intensity due to the increase of concentration of the analyte. In digital-MITOMI the increasing analyte concentration gives rise to increasing number of positive wells. The combination of the two detection approaches allows achieving a broad dynamic range and low LODs. Single enzyme detection has been demonstrated using digital readout. Successively a digital immunoassay, detecting GFP in serum and in buffer, has been performed. The LODs achieved, with digital-analog detection, were 10 fM in buffer and 12fM in serum with a dynamic range of 5 orders of magnitude.

A portable and low cost microfluidic Diagnostic System (μFDS), composed of a microfluidic control system, a fluorescent USB microscope and a netbook, has been

assembled. Using the μ FDS we were able to detect human IL-6 levels in serum and achieve a LOD of 1 pM. We also measured levels of different species of anti IgG Ebola virus spiked in 5 μ l of whole blood. We conducted multiplexed assays over an IgG concentration range of 0.1-100 nM and we obtain a LOD of 100 pM-1 nM in whole blood.

In summary, we developed an integrated, multiplexed digital-analog device that can potentially be applied for point-of-care testing.

3.1 - Introduction

Management and prognosis of disease requires the measurement of biomarkers. Quantitative detection of low abundance biomarkers is of great interest for health monitoring and biological applications because protein biomarkers can be present at low concentrations of 10^{-15} to 10^{-12} M in biofluids [1]. Furthermore, detection of biomarkers in body fluids such as whole blood is very desirable. Next generation diagnostic platforms are eliciting considerable excitement as they promise a paradigmatic shift in how disease diagnosis and health monitoring is conducted in the near future [2].

Biomolecular detection of proteins has been carried out using nanostructured microelectrodes [3], nanoparticles probes [4], nanomaterials and biomaterials in electrochemical arrays [5]. Microfluidics has been developed to precisely manipulate low sample volumes, enable large-scale integration, and improve bioassay performance [6]. Numerous microfluidic systems have been developed for miniaturization of immunoassays over the years [7]. Although the microfluidic format has enhanced the performance of immunoassays considerably few microfluidic assays exist that simultaneously fulfill all of the following performance criteria: i) low Limit Of Detection (LOD, sub-picomolar), ii) high dynamic range (5 orders of magnitude or better), iii) multiplexed biomarker analysis (4 or more), and iv) compatible with ultra-low volume (<5 μ l) samples (Table 3.2).

A notable recent example is a platform developed by the Rusling group, which achieved outstanding sensitivity, high dynamic range (~5 orders of magnitude), and multiplexed detection of 4-6 analytes, but required dilution of samples prior to quantitation [8]. Another important and often overlooked aspect is the development of portable and low-cost device control and readout instrumentation. Another case of a multiplexed platform is the blood barcode chip reported by Fan *et al.* that achieved multiplexed protein biomarker detection from 10 μ l whole blood samples diluted to 90 μ l with buffer [9]. Device readout required an expensive research grade DNA microarray scanner restricting its use to point-of-care (POC) applications. A further report described a nanoplasmonic electrical field-enhanced resonating device (NE²RD), which achieved an impressive LOD of ~23 fM (400f g/ml) for detecting interferon- γ in human serum and a dynamic range of 8 orders of magnitude [10]. It thus meets the criteria of high LOD and dynamic range, but NE²RD doesn't support multiplexed analysis of biomarkers and requires a sample volume of 100 μ l per analyzed biomarker.

Research and clinical laboratories have extensively used Enzyme-Linked Immunosorbent Assays (ELISA) for protein detection. To enable the use of standard ELISA microplate based tests in resource-limited settings, Berg and coworkers created a hand-held cellphone-based colorimetric microplate reader, which illuminates a 96-well plate with a light-emitting-diode (LED) array. This LED light is transmitted through each well, and is then collected *via* 96 individual optical fibers. They tested this platform in a clinical microbiology laboratory using FDA-approved mumps IgG, measles IgG, and herpes simplex virus IgG (HSV-1 and HSV-2) ELISA tests [11]. However, the method uses standard ELISA assays for detection of the biomarkers, which require large sample and reagent volumes prohibiting multiplexed, sensitive analysis of ultra-low volume samples, and the assays require numerous pipetting steps.

Digital immunoassays have emerged as a robust technology for sub-picomolar detection of proteins [12][16]. These assays usually use beads placed into micrometer-sized wells or droplets to isolate individual target molecules. Rissin *et al.* used microbeads coupled with antibodies and enzymes to detect low-abundance proteins. Their digital ELISA approach detected proteins in 100 μ l serum sample at concentrations as low as 0.4 fM [12]. Their method was then extended to simultaneously detect TNF- α , IL-6, IL-1 α , and IL-1 β in human plasma at sub-femtomolar concentrations [13]. Shim *et al.* reported a microfluidic droplet-based approach enabling single-molecule-counting immunoassay. The femtoliter droplets produced with their device could be used to encapsulate single biomolecular complexes tagged with a reporter enzyme. Their prototype system was validated by detection of a biomarker for prostate cancer in buffer, down to a concentration of 46 fM [14]. Lastly, Ge *et al.* showed that the concept of Brownian trapping with drift could be applied to improve quantitative molecular measurements. Their approach has the potential to combine high-sensitivity, broad dynamic range, and end-point readout. This concept was tested with enzyme and TNF- α measurements in a microfluidic device [15]. Although many of the methods reported have the ability to digitally detect biomarkers, the number of unique digital units that in turn defines the dynamic range often limits them. One strategy to improve dynamic range for digital immunoassays involves combining digital readout with an analog readout into a digital-analog hybrid platform as demonstrated by Rissin *et al.* who achieved a dynamic range of 4 orders of magnitude [17].

In this paper we describe a multiplexed microfluidic platform that combines digital and analog detection based on mechanically induced trapping of molecular interactions (MITOMI) [18] to create a portable, integrated, digital-analog hybrid microfluidic device capable of detecting biomarkers with high-LOD and dynamic range. Our integrated microfluidic platform allows the multiplexed detection and quantitation of protein biomarkers in a 5 μ l serum or whole blood sample obtainable by a pinprick. We characterized our platform by performing single enzyme measurements, and digital immunoassays achieving single molecule detection and digital detection of 10 fM GFP in buffer and 12 fM GFP in human serum and a dynamic range of 5 orders of magnitude. We demonstrate the applicability of our platform to clinically relevant tests by performing

multiplexed digital detection of anti-Ebola antibodies in serum at concentrations down to 1 pM. Finally, we combine our microfluidic device with a low-cost, portable microfluidic control system and a fluorescence USB microscope to enable diagnostic testing at home, or in resource limited field-environment in addition to clinical point-of-care settings. Using our portable, field-compatible hardware we demonstrate the multiplexed detection of anti-Ebola IgGs in an ultra-low volume whole blood sample.

3.2 - Results and Discussion

3.2.1 - Microfluidic digital-analog device

The microfluidic device, fabricated by multilayer soft lithography [19], includes 16 independent assay units (Figure 3.1a). The assay chambers contain a deflectable (actuated by means of hydraulic pressure, ΔP) button membrane (analog MITOMI) in half of the assay units and a deflectable button membrane patterned with femtowells (digital MITOMI) in the other half (Figure 3.1b).

In digital-MITOMI, increasing analyte concentrations give rise to increasing numbers of positive wells containing one, two, or more molecules (Figure 3.1c, top row). Analog detection is achieved using our MITOMI mechanism where increasing analyte concentration results in increasing fluorescence signal density under the MITOMI button (Figure 3.1c, bottom row). The combination of digital and analog detection allow to have an increasing in the dynamic range (Figure 3.1d). We have previously shown that highly-multiplexed biomarker detection is possible using analog MITOMI, and that such devices can be pre-programmed with reagents and stored at elevated temperatures for at least 2-3 weeks[20]. In order to reduce assay time, we now incorporated active mixing using a simple serpentine-shaped (S-shaped) peristaltic pump [21]. The integrated peristaltic pump permits complete mixing of the spotted reagents in 1 minute, as opposed to 2.5 hours required when solely relying on passive diffusion [20], [22], [23] (Figure 3.2c).

Despite conventional peristaltic pump where 3 independent valves are actuated by three independent pressure sources, in the S-shape delay pump only one valve is actuated (Figure 3.2a, b). A single control channel crosses the flow channel three times in a serpentine path. The valve is split in four parallel channels in order to address the four columns. To characterize the mixing time the assay chamber has been filled with DI water and the spotting chamber with food dye color water and the pump has been activated with a period of closing and opening of 60 ms. A single unit has been imaged using high speed camera, and the signal has been analyzed in a portion of the assay chamber (Figure 3.2c).

Chapter 3 – A digital-analog microfluidic platform for patient-centric multiplexed biomarker diagnostics of ultra-low volume samples

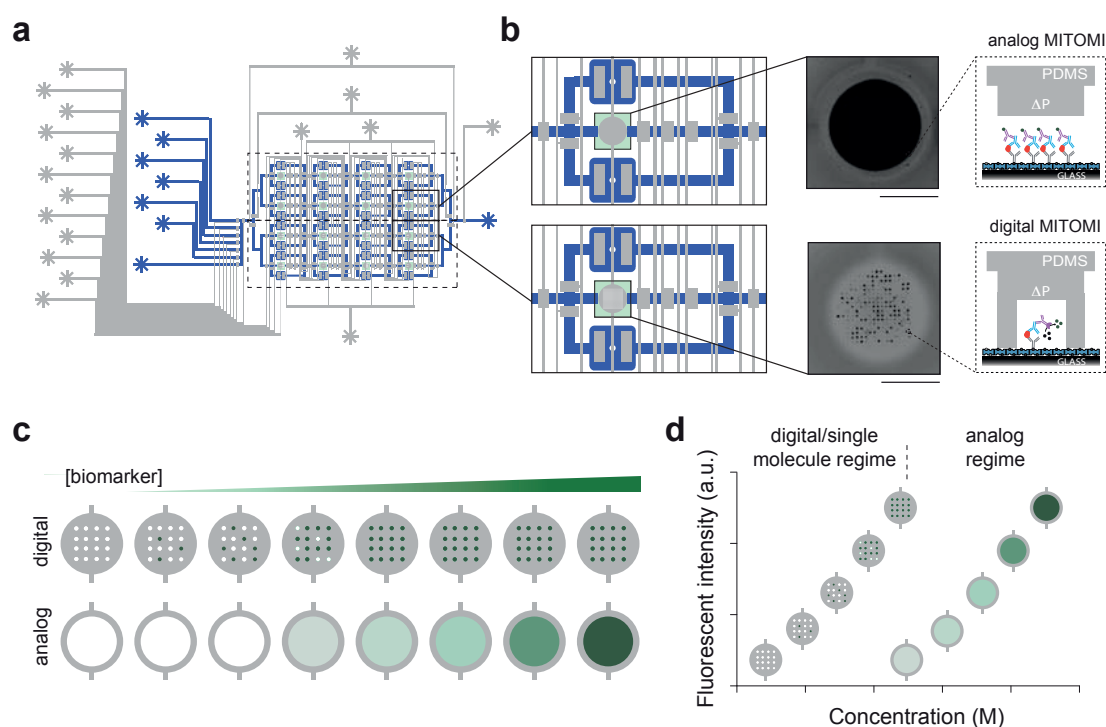


Figure 3.1: **The digital-analog hybrid, multiplexed microfluidic diagnostic device.** (a) Schematic of the device flow (blue) and control (grey) layers. The chip consists of four rows; each with four assay units allowing a total of 16 independent assays to be performed on each device. (b) Each assay unit contains two reagent chambers, an assay chamber, isolation valves, a peristaltic pump and a MITOMI button. Phase contrast and fluorescence images of the analog and the digital MITOMI buttons. Schematic cross-section of the MITOMI detection area: a sandwich immunoassay is performed with either fluorophore-labeled (analog MITOMI) or enzyme-conjugated (digital MITOMI) antibodies. (c) Increasing analyte concentrations lead to increasing numbers of positive femtowells in a digital measurement, and to increasing signal densities in analog measurements. (d) The schematic plot shows how a broad dynamic range can be achieved by combining digital and analog measurements in the hybrid device. Scale bars: 150 μm . Adapted from *ACS Nano* vol.10 pp. 1699-1710 © (2016).

The delay response of the pressure through the control channel is used instead of the time sequence used in the traditional peristaltic pump [24]. Valves placed in the intersection between spotting and assay chamber allow to mix separately the spots on the top and bottom chamber using only one S-shape delay valve (Figure 3.2d).

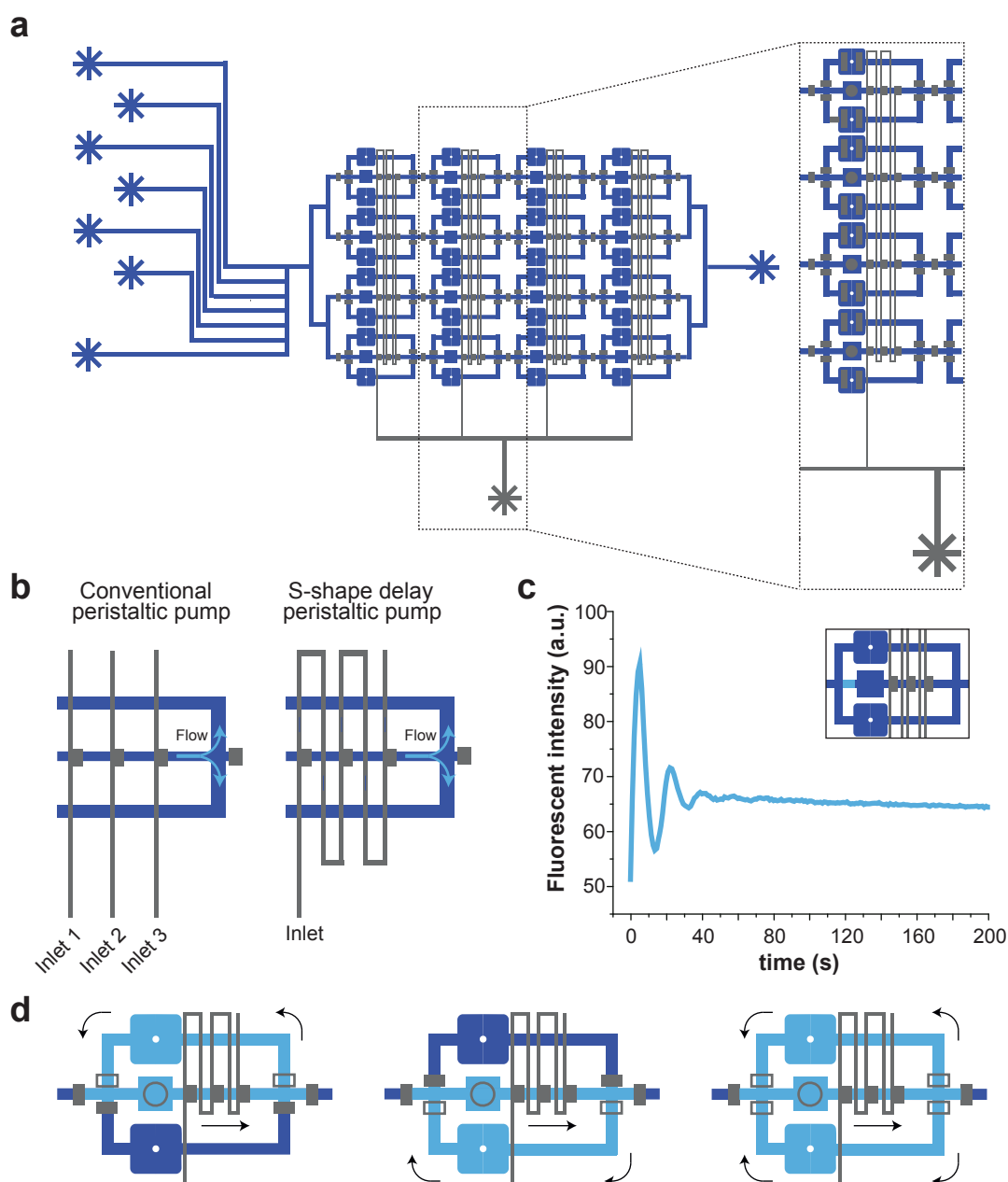


Figure 3.2: **Serpentine-shape (S-shape) delay peristaltic pump.** (a) Schematic of the S-shape delay peristaltic pump used in this study and magnified view of a single column. (b) Schematic illustrations of the difference between a conventional peristaltic pump, in which 3 independent valves are activated in sequence, and the S-shape delay peristaltic pump, in which a single channel is able to perform the mixing. (c) Cy3 labeled solution mixing measurement at a frequency of ~ 8.3 Hz ($t_{\text{open}} = t_{\text{close}} = 60$ ms) and $P = 25$ psi. (d) A schematic illustration of the possible flow modes. Adapted from *ACS Nano* vol.10 pp. 1699-1710 © (2016).

3.2.2 - Digital-MITOMI characterization

We first tested whether it is possible to count single enzyme molecules with our digital-MITOMI buttons[25] (Figure 3.3). We conducted our initial proof-of-concept tests with β -Galactosidase (β G) and Fluorescein di- β -D-galactopyranoside (FDG) in buffer.

In order to study the kinetics of substrate turnover by single β G molecules, an enzyme/substrate mixture (β G + FDG) (Figure 3.3a) was introduced on chip after surface derivatization. We then closed the digital MITOMI buttons and the fluorescent intensity in femtowells of 4 buttons (484 individual femtowells) was measured using a fluorescence microscope. The time elapsed between combining the enzyme-substrate solutions and acquiring the first image was 15 minutes and we imaged the buttons for 15 minutes with a frequency of 5 minutes. Wells that contained one or more active β G molecule displayed an increase in fluorescence intensity. Figure 3.2b shows histograms of the substrate turnover rates of β G molecules for different enzyme concentrations. The results were consistent with Poisson statistics (Figure SI 3.1)[25]–[27], as expected for a random distribution of molecules in the wells. We thus established that solution phase single enzyme counting could be performed on an integrated digital-MITOMI assay.

Having successfully conducted single enzyme counting we next sought to determine whether it is possible to also conduct digital immunoassays with our integrated digital-MITOMI platform. We developed a coupled analog-digital immunoassay and detected his-tagged GFP using a surface immobilized primary goat anti-GFP antibody, an Alexa Fluor 555 labeled mouse anti-Penta-His antibody (analog MITOMI detection), which in turn is detected using a β G conjugated goat anti-mouse IgG antibody (digital and analog amplification detection) (Figure 3.4a). Analog MITOMI is a direct detection mechanism that doesn't rely on signal amplification. In analog MITOMI a specific antibody labeled with \sim 1-4 fluorophores detects an immobilized antigen. Analog MITOMI thus requires a fairly high density of antigens/detection antibodies on the surface in order to reach the detection limit of a standard epi-fluorescent microscope setup. Digital MITOMI, on the other hand, relies on enzyme based signal amplification and small volume traps. Here an enzyme-conjugated antibody binds the antigen.

The enzyme is capable of turning over a non-fluorescent substrate to a fluorescent product, and does so many thousands of times, giving rise to a high level of signal amplification. In addition, since the product molecules are confined to a small volume they will reach a high concentration/density, which is readily detectable with a standard epi-fluorescent microscope. We were able to detect as low as \sim 10 fM (330 fg/ml) GFP in a buffer solution using digital-MITOMI (calculated LOD: 2.6 fM (86 fg/ml)), which is an improvement of 2-3 orders of magnitude compared to detection of GFP with analog-MITOMI (LOD: 1.7 pM (55.59 pg/ml)) (Figure 3.4b).

Chapter 3 – A digital-analog microfluidic platform for patient-centric multiplexed biomarker diagnostics of ultra-low volume samples

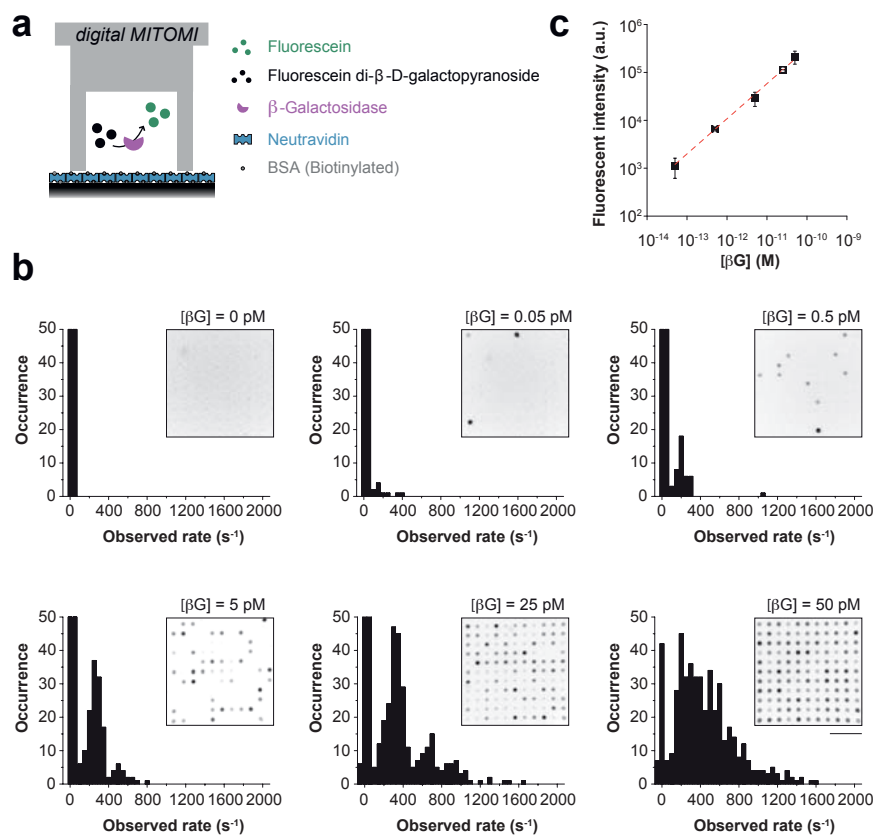


Figure 3.3: **Single enzyme counting with digital-MITOMI.** (a) Schematic of the β -Galactosidase (βG) assay in which βG is free in solution and detected by fluorescein di- β -D-galactopyranoside (FDG) substrate turnover to fluorescein. (b) Histograms of observed turnover rates for individual femtowells. The bin size for all histograms is 50 s⁻¹. Insets show representative microscope images of individual digital-MITOMI buttons. Scale bar: 50 μm . (c) The sum of turnover rates plotted against βG concentration. Data represent means ($n=3$). Error bars correspond to the standard deviation of the means. The dashed red line is a linear fit to the data ($R^2=0.99$). Adapted from *ACS Nano* vol.10 pp. 1699-1710 © (2016).

Digital-MITOMI thus leads to a significant increase in LOD for microfluidic immunoassays. To test whether digital-MITOMI is compatible with clinical samples we detected GFP in human serum and were able to detect 12 fM (400 fg/ml) GFP (Figure 3.4c). Combining digital-MITOMI and analog-MITOMI detection on a single platform increases the dynamic range, in this case covering a range ~ 5 orders of magnitude between 10 fM (330 fg/ml) to at least 5 nM (164 ng/ml) without requiring any sample dilutions or other additional on- or off-chip processing steps.

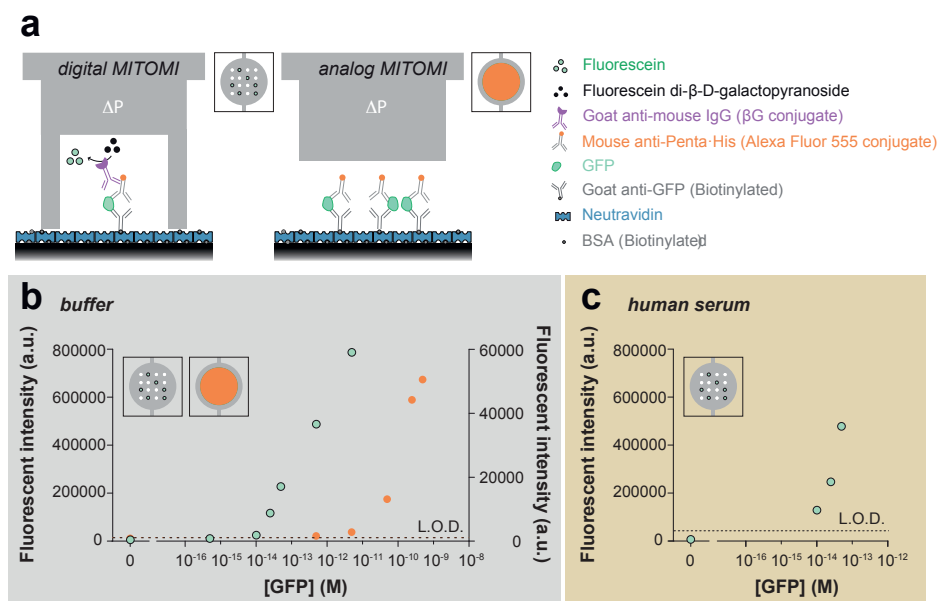


Figure 3.4: **Digital-MITOMI Immunoassay.** (a) Schematic of the GFP sandwich assays performed on the microfluidic device and detected with digital-MITOMI and analog-MITOMI. (b) Digital-MITOMI GFP immunoassay in buffer. Plotted is the sum of slopes of femtowells above background as a function of GFP concentration. Plotted is the intensity of Cy3 signal as function of GFP concentration. (c) Digital-MITOMI detection of GFP in human serum over concentrations ranging from 12 fM to 50 fM. Intensity of fluorescein signal is plotted as function of GFP concentration. Data were obtained with a research grade fluorescence microscope. LODs were determined from the signal of a negative control plus 3 standard deviations. Adapted from *ACS Nano* vol.10 pp. 1699-1710 © (2016).

3.2.3 - Multiplexed digital assay in serum

After digital detection of GFP in human serum we tested whether digital detection in human serum was also possible for a clinically relevant biomarker. We chose to diagnose Ebola virus infection by detecting the presence of anti-Ebola virus glycoprotein (GP) IgG antibodies [27][29]. Infectious hemorrhagic fevers caused by the Ebola virus results in mortality rates of up to 90% [31], and no effective vaccines or therapeutics are currently available. The highly infectious and lethal nature of this virus requires the development of novel diagnostic methods in order to monitor and control outbreaks [32], [33]. Although anti-Ebola IgG levels begin to rise 8-10 days after disease onset [34], detection of IgG antibodies does represent a viable diagnostic test for symptomatic and asymptomatic individuals [35], [36]. To demonstrate the multiplexing capability of the platform, we programmed a single device with Ebola GPs from 3 virus species (Bundibugyo, Reston, and Zaire) plus a negative control and performed 4 technical replicates of each on a single device (Figure 3.5a, b).

Chapter 3 – A digital-analog microfluidic platform for patient-centric multiplexed biomarker diagnostics of ultra-low volume samples

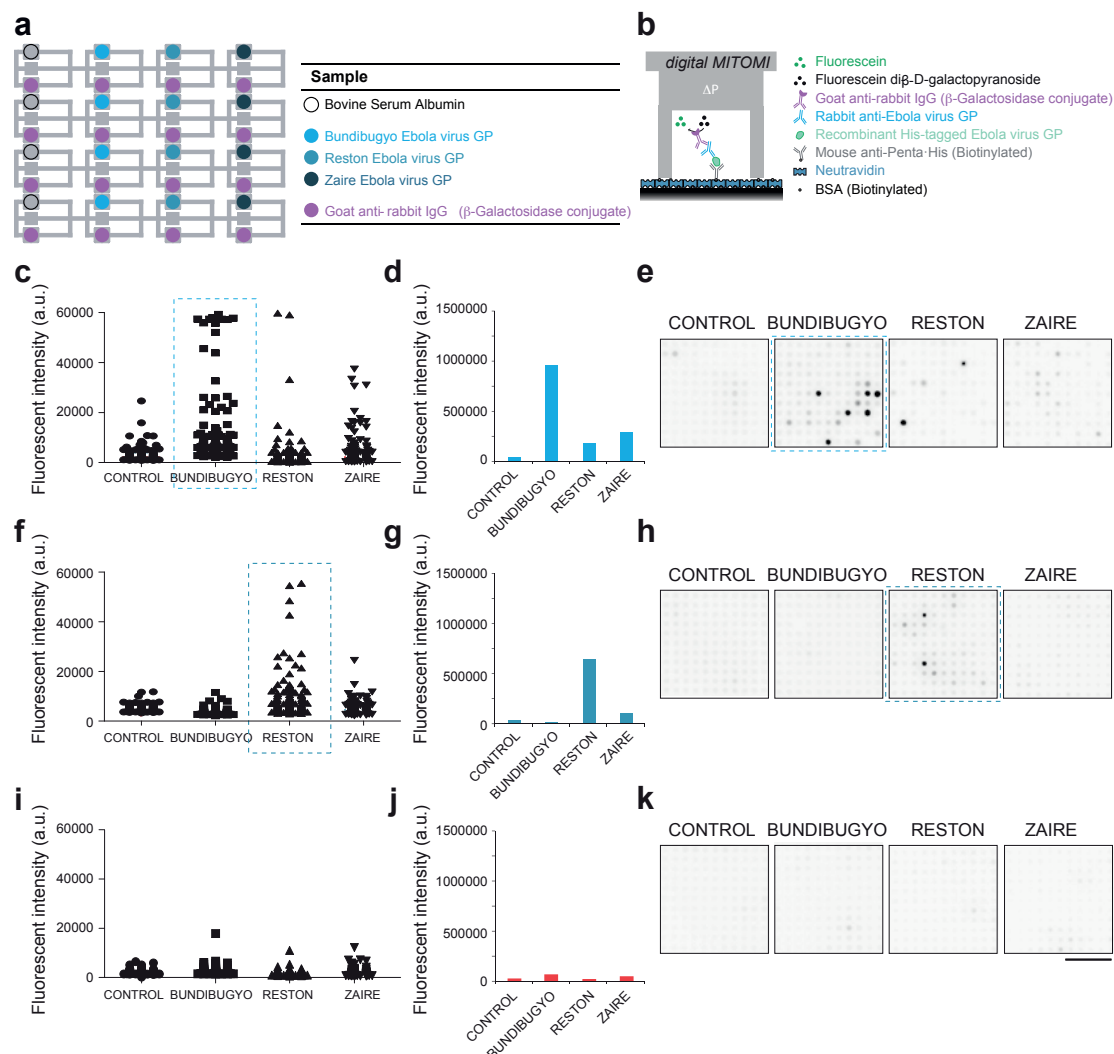


Figure 3.5: **Multiplexed digital Ebola diagnostics in human serum.** (a) Schematic of assay reagents allocation on the device. (b) Schematic of the assay for digital-MITOMI anti-Ebola virus detection. (c-e) 5pM anti-Bundibugyo Ebola GP IgG antibody, (f-h) 1pM anti-Reston Ebola GP IgG antibody, and (i-k) a negative control were measured on 3 independent devices. Shown are the signals obtained from individual femtowells (c,f,i), the sum of the signal in positive femtowells (d,g,j), and examples of a digital-MITOMI button for each sample (e,h,k). All measurements were performed in human serum. Scale bar: 700µm. Adapted from *ACS Nano* vol.10 pp. 1699-1710 © (2016).

Human sera containing 5 pM (75 pg/ml) anti-Bundibugyo GP IgG, 1pM (15 pg/ml) anti-Reston GP IgG, and a negative control sample were measured on 3 independent chips (Figure 3.5c-k). For each test we analyzed the femtowells of 4 digital-MITOMI buttons of the corresponding capture agents (Bundibugyo GP, Reston GP, Zaire GP, and BSA). When the human serum sample was spiked with anti-Bundibugyo IgG a large number of femtowells programmed with Bundibugyo GP were positive (Figure 3.5c-e). Summing the

fluorescence signal of positive wells for the 3 GPs and the negative control results in a clear signal for Bundibugyo, low signals for Reston and Zaire, and baseline levels for the negative control. A similar result was obtained when testing the presence of anti-Reston GP IgG, which was more specific (Figure 3.5f-h). The negative control sample showed no appreciable signal for any of the viral species tested (Figure 3.5i-k). Digital-MITOMI thus provides a sensitive approach for rapid multiplexed diagnostic testing of biomarkers in human serum samples in a point-of-care setting. By increasing the sample flow times from the above used 10 minutes to 60 minutes drastically improve the observed signal for 1 pM anti-Reston GP IgG and allowed us to readily detect a concentration as low as 100 fM.

3.2.4 - Portable microfluidic diagnostic system

To enable the use of our microfluidic devices for diagnostic testing in a home-based setting, or in a resource-limited environment we designed and built a portable microfluidic Diagnostic System (μ FDS). The μ FDS consists of a microfluidic control system (MCS) similar to a system developed by Li et al.[37], a low-cost fluorescence USB microscope, a netbook, and the microfluidic device (Figure 3.6). Blood sample can be picked directly from the finger using a micro hematocrit capillary tube (Figure 3.6a).

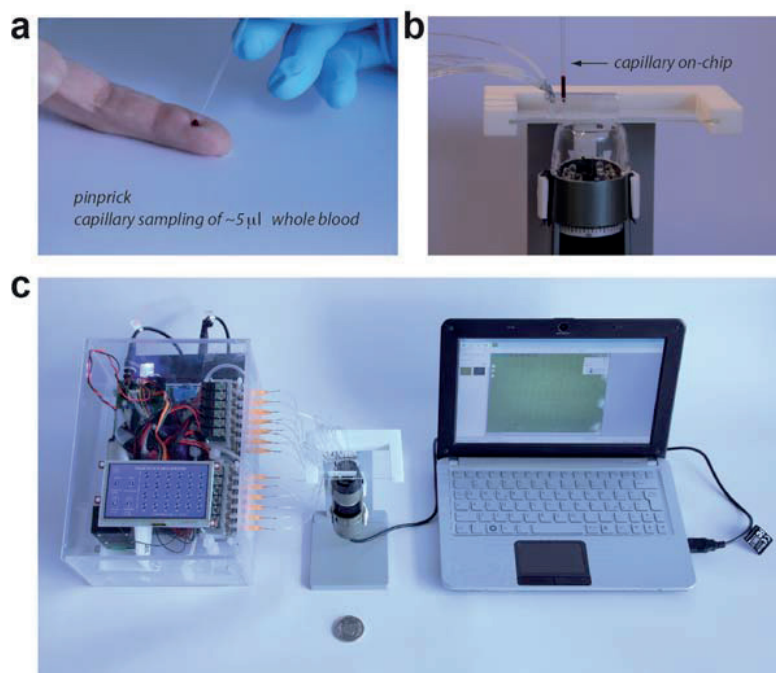


Figure 3.6: **Portable, low-cost μ Fluidic Diagnostics System.** (a) $\sim 5 \mu\text{l}$ of a whole blood sample obtained by a pinprick is aspirated with a micro hematocrit tube and (b) transferred to a single use microfluidic diagnostic device. (c) Image of the μ Fluidic Diagnostic System consisting of a microfluidic control system, a fluorescence USB microscope, a device, and a netbook. Adapted from *ACS Nano* vol.10 pp. 1699-1710 © (2016).

Chapter 3 – A digital-analog microfluidic platform for patient-centric multiplexed biomarker diagnostics of ultra-low volume samples

A touch screen allow to toggle each valves, the compressor and the vacuum pump. The interface presents 5 screen: the home screen (Figure 3.7a), one screen for switching on and off each solenoid valves, the compressor and the vacuum pump (Figure 3.7b), one screen for setting the desired pressure (Figure 3.7c), and one for selecting the routine which you want to run for GFP, IgE (see Appendix1) and IgG measurements (Figure 3.7d). Using commercially available electronic components our MCS costs 1666USD (Table 3.1). The fluorescence USB microscope and netbook cost 828USD and 134USD, respectively, bringing the hardware cost of the complete μ FDS to 2628USD.

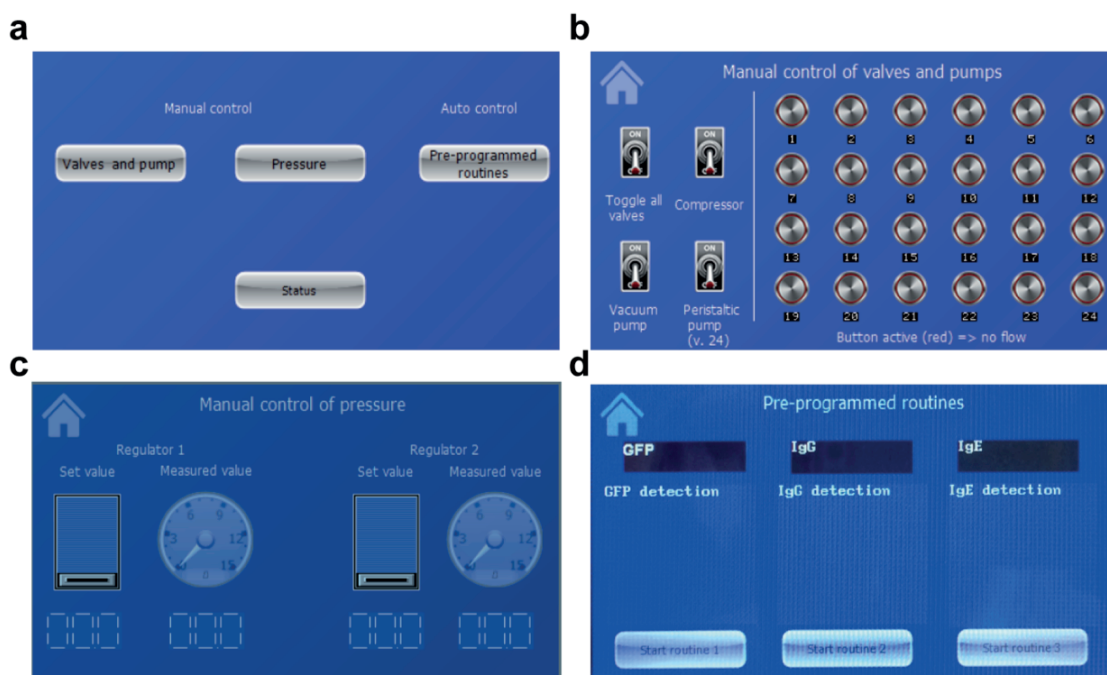


Figure 3.7: **Graphical user interface.** (a) Home screen, (b) screen for controlling each solenoid valves, compressor and vacuum pump, (c) screen for the pressure regulation and (d) the screen for the automatic routine. Adapted from *ACS Nano* vol.10 pp. 1699-1710 © (2016).

We tested whether we could readout our devices using a low-cost, commercially available fluorescence USB microscope. The lowest magnification of the USB microscope that allowed us to image the whole device did not permit to resolve the femtowells of our digital-MITOMI buttons, excluding the possibility to use digital-MITOMI. Nonetheless the USB microscope was able to detect GFP *via* analog-MITOMI, but the LOD of this approach was relatively poor with a LOD of 562 pM (18.37 ng/ml). In order to improve LOD we decided to perform a standard ELISA, using β G and FDG turnover for signal amplification. Combining on-chip signal amplification with a USB microscope allowed us to detect GFP at concentrations as low as 5 pM (163.5 pg/ml) with a theoretical LOD of 1.9 pM (62.13

Chapter 3 – A digital-analog microfluidic platform for patient-centric multiplexed biomarker diagnostics of ultra-low volume samples

pg/ml). This performance is comparable to that previously achieved by analog-MITOMI and an expensive, research grade optical microscope [20] (Figure 3.8b).

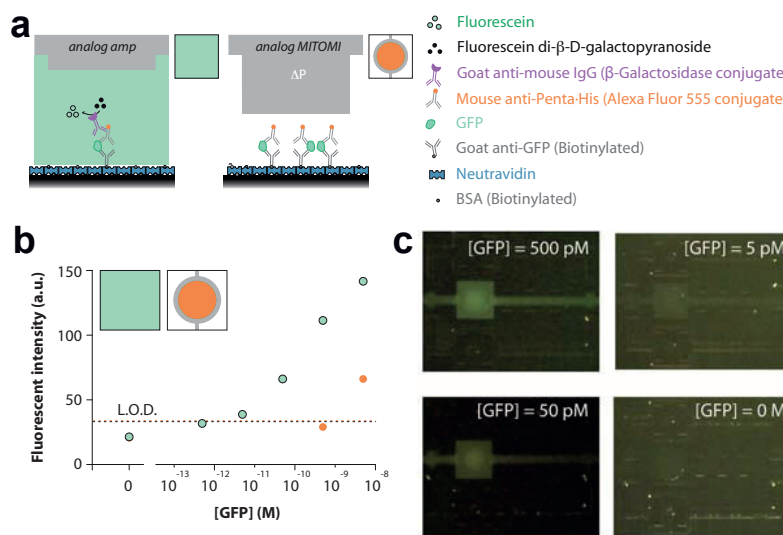


Figure 3.8: **GFP analog-amp and analog MITOMI assay.** (a) Schematic of the GFP sandwich assays performed on the microfluidic device and detected with analog amplification, and analog MITOMI. (b) Detection of GFP in 2% BSA PBS buffer solution with concentrations ranging from 500 fM to 5 nM. Analog amplification and analog MITOMI detection of GFP. Data were obtained with a fluorescence USB microscope. LODs were determined from the signal of a negative control plus 3 standard deviations. (c) Representative fluorescence images of one assay unit taken with the USB microscope for different concentrations of GFP in 2% BSA PBS using the analog amplification method. Scale bar: 350 μm . Adapted from *ACS Nano* vol.10 pp. 1699-1710 © (2016).

We also detected human IL-6 in human serum with the same approach. Biotinylated primary antibody and secondary antibody against human IL-6 were spotted on the glass slide. The human serum was spiked with human IL-6, four different concentrations were sampled in 4 independent microfluidic chips. After the secondary antibody was pumped in the chamber the tertiary antibody β -galactosidase labeled was flowed through the channels. The signal from the turn over of the FDG has been measured using the USB microscope. The LOD (1 pM (21 pg/ml), (Figure 3.9) was also comparable to results previously achieved by analog/MITOMI and a research grade optical microscope [20]. Serum levels of IL-6 in patients with oral cancer are 20 pg/ml, while healthy persons are below 6 pg/ml [38], [39].

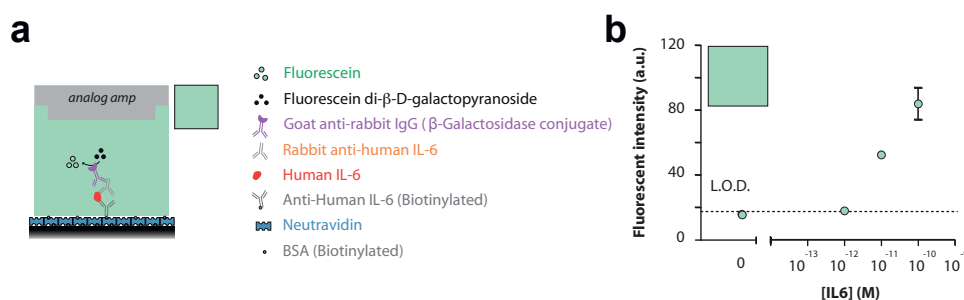


Figure 3.9: **IL-6 detection** (a) Schematic of the IL-6 sandwich assays performed on the microfluidic device and detected with analog amplification. (b) Detection of IL-6 in human serum with concentrations ranging from 100 pM to 1 pM. Data were obtained with a fluorescence USB microscope. LODs were determined from the signal of a negative control plus 3 standard deviations. Adapted from *ACS Nano* vol.10 pp. 1699-1710 © (2016).

3.2.5 - Multiplexed Ebola diagnostic in whole blood sample

To test whether our platform could be used to detect Ebola specific IgG levels in a resource-limited setting we measured anti-Ebola IgG antibodies spiked into whole blood samples and used our μ FDS for device readout. The average quantitative load of specific IgG molecules during a viral infection ranges from 6.6 nM-6.6 μ M (1-1000 μ g/ml) [40], [41], which defines the concentration range that our platform needs to be able to detect.

Sample volumes for our device can be as small as 5 μ l of whole blood obtainable by a pinprick (Figure 3.1a). The blood sample is aspirated and transferred to the device by means of a micro hematocrit tube (Figure 3.1b). To introduce the sample onto the device we employ vacuum based loading, by applying vacuum to the outlet of the device and drawing the blood sample into and through the microfluidic device. We found that we could load a whole blood sample directly onto the device and perform on-chip biomarker quantitation without requiring any sample-pretreatment or removal of hematocytes. Previously, microfluidic approaches generally relied on off-chip hematocyte removal or integrated on-chip separation approaches [42], [43], which complicated chip design and assay implementation. Here we show that cell-separation [44], [45][46] is not necessary in turn simplifying the assay and enabling multiplexed biomarker detection from an ultra-low volume whole blood sample.

We conducted multiple measurements (1 experiment per concentration for a total 10 independent experiments) over an IgG concentration range of 0.1-100 nM for the three Ebola species, Bundibugyo, Reston, and Zaire (Figure 3.10a-d). Using analog-MITOMI we were able to detect IgG antibodies specific to all three species at levels of 100 nM, with the exception of anti-Zaire IgG, which could be detected to a concentration of 1 nM. Employing on-chip enzymatic signal amplification improved the detection limit for all species to 10 nM and 0.1 nM for Zaire.

Chapter 3 – A digital-analog microfluidic platform for patient-centric multiplexed biomarker diagnostics of ultra-low volume samples

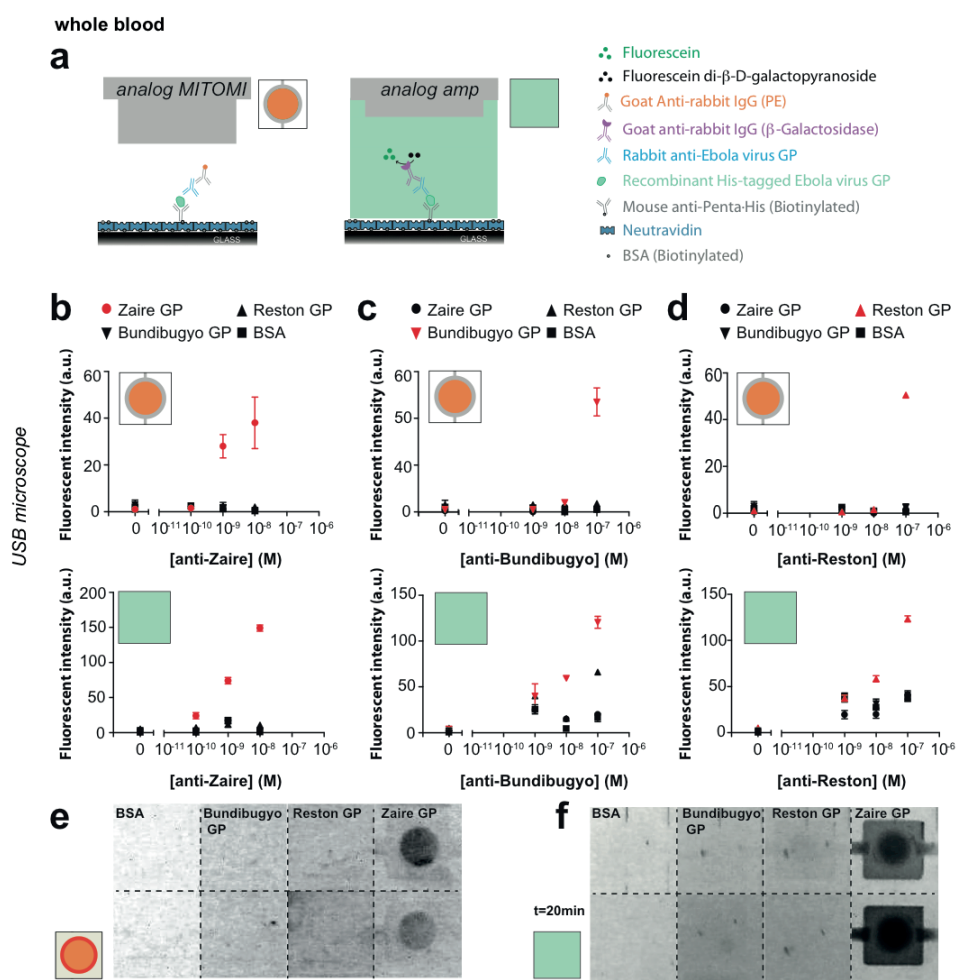


Figure 3.10: **Multiplexed Ebola diagnostics in whole blood using the μ FDS.** (a) Schematic of the assay for anti-Ebola virus detection in a whole blood sample. Data for different concentrations of (b) anti-Zaire Ebola GP IgG antibody, (c) anti-Bundibugyo Ebola GP IgG antibody, and (d) anti-Reston Ebola GP IgG antibody spiked in whole blood. Zaire, Bundibugyo and Reston glycoproteins are spotted in quadruplicate to yield two repetitions for the analog and the analog amplification detection mechanisms. Goat anti-rabbit IgG PE conjugated antibody and goat anti-rabbit IgG β -Galactosidase conjugated antibody were spotted in the top and bottom part of the chip, respectively, to allow the use of both detection methods on the same device. Data represent means ($n=2$). Error bars correspond to the standard deviation of the means. (e-f) Representative fluorescent images of 10 nM anti-Zaire Ebola GP IgG antibody spiked in whole blood. (e) The analog-MITOMI signal imaged using a fluorescence USB microscope with a 570 nm emission filter. (f) Amplified analog signal detected with a fluorescence USB microscope using a 510 nm emission filter. Scale bar: 350 μ m. Adapted from *ACS Nano* vol.10 pp. 1699-1710 © (2016).

Actual micrographs obtained with the fluorescence USB microscope for 10 nM anti-Zaire Ebola IgG are shown for the analog-MITOMI (Figure 3.10e) and the analog amplification based method (Figure 3.10f). A dynamic range of 3 orders of magnitude can be achieved in

the range of 100 pM (0.15 $\mu\text{g/ml}$) to 100 nM (150 $\mu\text{g/ml}$) in unprocessed whole blood using a USB microscope, which effectively covers the clinically relevant range.

3.3 - Conclusions

Here we described the development of an integrated digital-analog microfluidic diagnostic platform capable of performing multiplexed detection of ultra-low volume human serum samples. Digital MITOMI improved the limit of detection by 3 orders of magnitude to ~ 10 - 12 fM, compared to previous MITOMI based immunoassays, which is a significant improvement and will further enhance the plethora of assays MITOMI has thus far been applied to including Protein-DNA, Protein-Protein, Protein-RNA, and immunoassay based measurements [18]. By combining digital-MITOMI with standard analog-MITOMI on the same device we increase the dynamic range of our measurement reaching 5 orders of magnitude in this study. Importantly, these levels of LOD and dynamic range can be achieved for a multiplexed analysis of a single, ultra-low volume (~ 5 μl) serum sample.

We also developed a (Do-It-Yourself) DIY microfluidic control system, which can be assembled by a master student from commercially available components. The current cost of the MCS is 1666 USD, which could be further reduced to 1145 USD by eliminating the expensive pressure regulators and touch display. For device readout we demonstrate that a low-cost USB fluorescence microscope provides sufficient resolution to quantitate microfluidic diagnostic tests based on fluorescence readout.

We have recently shown that MITOMI devices can be pre-programmed with antibody reagents and consequently stored at elevated temperatures of 40°C for at least 2 weeks without loss of function [20], making the microfluidic device itself a self-contained reagent reservoir with a good shelf-life. Long-term storage of enzyme-based reagents has also been shown previously [54]. We achieved similar sensitivities with the μFDS as with expensive research grade fluorescence microscope and we showed that we could detect IgG antibody levels down to 100 pM in a 5 μl whole blood sample that can be obtained by a simple pinprick.

In summary, we present an integrated, multiplexed digital-analog microfluidic diagnostic platform with novel performance characteristics that can potentially be applied to measurements in clinical point-of-care settings. We also demonstrate that the same device can be controlled and interrogated with low-cost off-the-shelf hardware, making it a viable diagnostic test in home-based, field-based, or resource-limited settings. The platform is applicable to any protein biomarker or molecule that can be detected *via* an immunoassay based affinity reagent, which encompasses an extremely broad range of possible tests that the platform can perform. Our platform thus represents a basis for developing new assays to meet the increasing demand for on-site clinical diagnostic testing, companion diagnostics, generic health monitoring, as well as applications in biodefense.

3.4 - Methods

3.4.1 - Reagents, antibodies, proteins, and clinical samples

Chlorotrimethylsilane (92360), 2-propanol (IPA) (I9516), β -Galactosidase from *Escherichia coli* (β G) (G3153), phosphate buffered saline (PBS) (P5244), β -mercaptoethanol (P6250), bovine serum albumin (BSA) (A3912), Tween 20 (P1379) and human serum (H4522) were purchased from Sigma-Aldrich. Fluorescein di- β -D-galactopyranoside (FDG) (F-1179) and goat anti-rabbit IgG PE conjugate (P-2771MP) were bought from Life Technologies. Goat anti-GFP antibody biotin conjugate (ab6658), goat anti-human IgG Fc (SureLight® PE) (ab131612), anti-IL-6 (ab6672), goat anti-rabbit IgG β G conjugate (ab136774), and rabbit anti-goat IgG β G conjugate (ab136712) were obtained from Abcam. Rabbit anti-Bundibugyo Ebola virus glycoprotein IgG (BVGP41-A), rabbit anti-Reston Ebola virus glycoprotein peptide IgG (RVGP31-A), recombinant Bundibugyo-Ebola virus glycoprotein (BVGP45-R-10) and recombinant Reston-Ebola virus glycoprotein (RVGP35-R-10) were acquired from Alpha Diagnostics. Anti-human IL-6 biotin conjugate (13-7068-81) and human IL-6 (39-8069-65) were purchased from Affymetrix eBioscience. Biotinylated BSA (29130), and neutravidin (31000) were purchased from Thermo Fisher Scientific. Mouse anti-Penta-His biotin conjugate (34440) and Mouse anti-Penta-His Alexa Fluor 555 conjugate (35310) were purchased from Qiagen. Rabbit anti-Ebola virus GP (1501003) and recombinant Ebola virus glycoprotein (0501-015) were purchased from IBT Bioservices. Goat anti-mouse IgG β G conjugate (401607) was bought from Merck Millipore and Enhanced Green Fluorescent Protein (EGFP) (4999100) from BioVision. Biotinylated natural Ara h2 (BI-AH2-1), recombinant Fel d1 (LTR-FD1D-1), and recombinant Der p2 (RE-DP2A-1) were purchased from INDOOR biotechnologies. Human clinical samples were purchased from PlasmaLab International. Micro hematocrit capillary tubes (7493 11) were purchased from VWR International.

3.4.2 - Blood specimens

Animals and their care were handled in compliance with institutional guidelines as defined in international laws and policies (EEC Council Directive 86/609, OJ L 358. 1, December 12, 1987 Standards for the Care and Use of Laboratory Animals - UCLA, US National Research Council, Statement of Compliance A5023-01, November 6, 1998).

3.4.3 - Microfabrication

The microfluidic device consists of a flow and a control layer. Molds for each layer were fabricated using standard lithography techniques on 4" silicon wafers. After exposure to O₂ plasma the control layer mold was patterned with GM1050 SU-8 photoresist (Gersteltec Sarl, Switzerland) to a height of 30 μ m. The mold for the fluidic layer was fabricated by a three-step lithography process. Briefly, a micropost array (patterned to a height of 5 μ m using GM1040 SU8 (Gersteltec Sarl, Switzerland)) was patterned on top of a \sim 10 μ m high SU8 layer. Then, \sim 15 μ m high channel features were patterned with AZ9260 photoresist

(Gersteltec Sarl, Switzerland). Devices were cast in polydimethylsiloxane (PDMS) using multilayer soft lithography.⁶ PDMS was prepared at a 20:1 ratio and spin-coated on the flow layer mold at 1900 rpm. PDMS at a 5:1 ratio was cast on the control layer mold to a thickness of ~4 mm. Both layers were baked at 80°C for 30 minutes. The control layer was peeled off from its mold and manually aligned to the flow layer mold, followed by a baking step at 80°C for 90 minutes. The femtowells for digital-MITOMI were 5 µm wide and 5 µm tall, giving a volume of 100 fl, with a pitch of 10 µm.

3.4.4 - MicroFluidic Diagnostic System

The system consists of an electronic printed circuit board (PCB, designed in Altium and printed by Euro Circuits) coupled with an Arduino (Arduino Mega 2560 R3, Distrelec), two pressure controllers (990-005103-015, Parker), an air pump (TM40a, TOPSFLO), a vacuum pump (E163-11-120, Parker), a touch screen (uLCD-43DT, 4D Systems), a pneumatic control subsystem (S14-2936, Pneumadyne), and a PDMS device. The cost of each part of microfluidic diagnostic system is listed in Table 3.1.

Chapter 3 – A digital-analog microfluidic platform for patient-centric multiplexed biomarker diagnostics of ultra-low volume samples

Part description	Vendor	Part no.	Unit price (USD)	Quantity	Total (USD)
<i>6 valve manifold</i>	<i>Pneumadyne</i>	<i>S14-2936</i>	<i>174.35</i>	<i>4</i>	<i>697.40</i>
Vacuum pump	Parker	E163-11-120	68.57	1	68.57
Air pump	Amazon	TM40-A	66.35	1	66.35
<u>Electronic P controllers</u>	<u>Parker</u>	<u>990-005103-015</u>	<u>185.71</u>	<u>2</u>	<u>371.41</u>
Arduino Mega 2560	Amazon	642819	37.76	1	37.76
Printed Circuit Board	Euro Circuits	Custom	65.09	1	65.09
Locking male header, 2-pin	Digi-Key	A1921-ND	0.12	2	0.24
Locking male header, 4-pin	Digi-Key	A19431-ND	0.18	4	0.72
Header pins	Digi-Key	S1012E-36-ND	1.61	2	3.22
Capacitors	Digi-Key	399-10449-1-ND	0.39	4	1.55
Diodes	Digi-Key	641-1017-1-ND	0.28	2	0.56
Power jack 2.1mm	Digi-Key	CP-002A-ND	0.96	1	0.96
Resistors	Digi-Key	P1.0KJCT-ND	0.10	4	0.40
DC/DC converter 5V out	Digi-Key	945-1395-5-ND	9.03	1	9.03
DC/DC converter 12V/3A out	Digi-Key	945-1729-5-ND	24.54	1	24.54
Transistor arrays (ULN2803)	Digi-Key	296-15777-2-ND	0.99	3	2.97
Transistors (for compressors)	Digi-Key	Z3099-ND	12.67	2	25.34
<u>4.3" LCD module w/ Res Touch</u>	<u>Mouser</u>	<u>uLCD-43PT</u>	<u>150.18</u>	<u>1</u>	<u>150.18</u>
Rechargeable Battery	BixPower	Bat-MP100-24V	139.95	1	139.95

<i>Microfluidic Control System</i>					1666.24
USB microscope	VWR International	AM4113T-FBW	827.84	1	827.84
Netbook	Amazon	n/a	134.31	1	134.31

Table 3.1: Cost table of μ Fluidic Diagnostic System.

3.4.5 - Device function and operation

Control lines on the device were primed with Phosphate Buffered Saline (PBS) at 5 psi. When the control lines were fully primed the pressure was increased to 25 psi. Flow lines were operated at 3 psi. For the initial surface derivatization steps the neck valves remained closed to avoid liquid from entering the chambers containing the spotted reagents. First, the surface area was derivatized by flowing a solution of either biotinylated BSA resuspended to 2mg/ml in H₂O resuspended to 1 mg/ml in H₂O for 10 minutes, followed by a 5 minutes 0.005% Tween 20 in PBS. Next a 500 μ g/ml neutravidin solution in PBS was flown for 10 minutes, followed by a 5 minutes 0.005% Tween 20 in PBS wash. The buttons were closed and all remaining accessible surface area was passivated with the same biotinylated solution as above for 10 minutes, followed by a 5 minutes 0.005% Tween 20 in PBS wash.

To perform resuspension and mixing of the spotted reagents and the assay chamber we first closed valve 2 (Figure SI 3.3), in order to isolate each unit, followed by opening valves 3 and 4, to allow mixing between the top spotting chamber and the assay chamber. Then the MITOMI button was opened and the pump activated. Once the mixing was completed, button and valves 3 and 4 were closed sequentially. The same procedure was followed for mixing the bottom chamber, using valves 5 and 6 instead of 3 and 4 (Figure 3.2).

3.4.6 - Digital enzyme measurements

After surface derivatization various concentrations of β G ranging from 0.05 pM (0.02 ng/ml) to 50 pM (23.26 ng/ml) and 50 μ M of FDG were mixed and then flowed through the device. FDG was resuspended in a 100mM phosphate buffer, including 1mM MgCl₂ and 50 μ M β -mercaptoethanol. As a final step, the MITOMI buttons were actuated at 25 psi. Bright field and fluorescent images were taken 15 minutes after the closure of the buttons with an exposure time of 2000 ms. To establish a calibration curve with known β G we summed the observed rates of all wells above a threshold defined by the negative control and plotted the sum of rates versus β G concentration.

3.4.7 - Microfluidic digital and analog immunoassay

For the GFP immunoassay 15 μ l of each reagent were loaded into tygon tubing, connected to the device and flowed in sequence at 3 psi. After surface functionalization, a 66.7 nM (10 μ g/ml) biotinylated goat anti-GFP solution in 2% BSA was flowed for 10 minutes and immobilized in the button region coated with neutravidin. To generate the standard curves, various concentrations of GFP ranging from 5 fM (0.17 pg/ml) to 5 nM (166.67 pg/ml) in 2% BSA, and 12 fM (0.4 pg/ml) to 50 fM (1.67 pg/ml) in human serum were flowed through the device for 10 minutes. Next, a 13 nM (2 μ g/ml) mouse anti-Penta-His Alexa Fluor 555 conjugate solution in 2% BSA was flowed for 10 minutes. After, a 100 pM (0.015 μ g/ml) goat anti-mouse IgG β G conjugate solution in 2% BSA was flowed for 8 minutes. The channels were washed with 0.005% Tween PBS flowed immediately after each reagent for 5 minutes. After the last washing step 50 μ M FDG was flowed for 4 minutes and buttons

closed with 25 psi pressure. Bright field and fluorescent images were taken 15 minutes after the closure of the buttons with an exposure time of 2000 ms.

3.4.8 - Multiplexed digital detection of anti-EBOLA antibodies in human serum

The recombinant virus antigens, along with the detection antibodies, were printed in a 4x4 format on epoxy slides. Briefly, we spotted 3 different Ebola virus GPs and a BSA negative control in all upper spotting chambers of the unit. Goat anti-rabbit IgG β G conjugated antibodies were printed in the lower spotting chamber of the unit cells.

After surface functionalization, 15 μ l of each reagent were loaded into individual tygon tubings, connected to the device and flowed sequentially at 3psi for 10 minutes. First, a 7 nM (0.45 μ g/ml) biotinylated mouse anti-Penta-His solution in 2% BSA was flowed and immobilized in the button region coated with neutravidin. Then, 1.9 μ M (136.8 μ g/ml) of recombinant Reston GP, 1.9 μ M (187.7 μ g/ml) of recombinant Bundibugyo GP, and 1 μ M (73 μ g/ml) of recombinant Zaire GP were pumped for 10 minutes. 5 pM (75 pg/ml) of rabbit anti-Bundibugyo and 1 pM (15 pg/ml) of rabbit anti-Reston in human serum were flowed for 8 minutes (one species per chip). Next, a 100 pM (15 ng/ml) goat anti-rabbit β G antibody 2% BSA was pumped for 10 minutes. The channels were washed with 0.005% Tween 20 in PBS flowed after each reagent for 5 minutes. After the last wash step 50 μ M FDG was flowed for 4 minutes and buttons were closed with 25 psi pressure. Bright field and fluorescent images were taken 15 minutes after the closure of the buttons with an exposure time of 2000 ms.

3.4.9 - Detection of human IL-6 in human serum

Biotinylated primary antibody and secondary antibody against human IL-6 were spotted on epoxy slide.

After surface functionalization, 15 μ l of each reagent were loaded into individual tygon tubing, connected to the device and flowed sequentially at 3psi for 10 minutes. First, 300 nM (43mg/ml) of primary antibody was pumped for 10 minutes and immobilized in the button region coated with neutravidin. Then, 1 pM (21 pg/ml), 10 pM (210 pg/ml) and 100 pM (2.1 ng/ml) of human IL-6 were spiked in human serum, was flowed in the chip. Next, secondary rabbit anti human IL-6 antibody (diluted 1:500 in 2% BSA in PBS) was pumped for 10 min. A 100 pM (15 ng/ml) goat anti-rabbit β G antibody was flowed for 10 min. The channels were washed with 0.005% Tween 20 in PBS flowed after each reagent for 5 minutes. At the end 50 μ M FDG was flowed for 4 minutes. Fluorescent images were taken using USB fluorescence microscope with the following exposure setting: Lowest, Luma 240.

3.4.10 - Multiplexed detection of anti-Ebola IgG in whole blood

In the multiplexed Ebola immunoassay we spotted 3 different Ebola virus GPs and a BSA negative control in the upper spotting chambers (Figure SI 3.3a *i*) of the unit cells.

Secondary antibodies were printed in the bottom spotting chambers (Figure SI 3.3a *ii*) of the units. PE conjugated antibodies were spotted in the top half of the chip, to allow analog detection while β G conjugated antibodies were spotted in the bottom half of the chip to allow analog-amp detection. After surface functionalization, 15 μ l of each reagent were loaded into tygon tubing, connected to the device and flowed sequentially at 3 psi for 10 minutes. First, a 7 nM (0.45 μ g/ml) biotinylated mouse anti-Penta-His solution in 2% BSA were immobilized in the button region coated with neutravidin. Then, 1.9 μ M (136.8 μ g/ml) of recombinant Reston GP, 1.9 μ M (187.7 μ g/ml) of recombinant Bundibugyo GP, and 1 μ M (73 μ g/ml) of recombinant Zaire GP were pumped for 10 minutes. To generate the standard curves, different concentrations, ranging from 0.1 nM (0.15 μ g/ml) to 100 nM (150 μ g/ml), of anti-Bundibugyo, anti-Reston, and anti-Zaire were spiked in mouse whole blood. A final volume of 3.5 μ l was then flown through the device from a hematocrit tube that in turn was plugged into the device. The mouse whole blood sample from the hematocrit tube was loaded into the device by vacuum suction (8 minutes at - 2.5 psi) as opposed to pressure driven flow. Next, 30 nM (11.7 μ g/ml) goat anti-rabbit IgG PE conjugated antibody and 2 nM (0.3 μ g/ml) of goat anti-rabbit β G antibody in 2% BSA were pumped for 10 minutes in the upper and lower half of the device, respectively. The channels were washed with 0.005% Tween 20 in PBS immediately after each reagent for 5 minutes. After the last washing step 50 μ M FDG was flowed and buttons immediately closed with 25 psi pressure. Bright field and fluorescent images were taken with the USB fluorescence microscope 15 minutes after the closure of the buttons with the following exposure settings: Lowest, Luma 240.

3.4.11 - Image acquisition, quantification and data analysis

Pumping and mixing sequences were recorded with a Hamamatsu ORCA-Flash4.0 camera (C11440). Mixing time was determined by analyzing fluorescent intensity changes over time in a portion of the microfluidic channel during pumping (ImageJ, plugins stacks \rightarrow Measure hyperstack) (Figure 3.2c). The sandwich valve was closed and a Cy3 labeled solution was pumped in the assay chamber containing buffer.

Fluorescent images were obtained Nikon ECLIPSE *Ti* microscope equipped with LED Fluorescent Excitation System, Cy3 and FITC filter sets, and a Hamamatsu ORCA-Flash4.0 camera (C11440). Images were taken with a 40x objective lens (Nikon, SPlan Fluor, ELWD 40x/0.60, ∞ /0.2, WD 3.6-2.8). Alternatively, fluorescent images were taken with a Cy3 (AM4113T-YFBW) or FITC (AM4113T-GFBW) Dino-Lite USB fluorescence microscopes.

The resulting TIFF-images were analyzed with a microarray image analysis software (GenePix Pro v6.0, Molecular Devices), ImageJ, Fiji or Matlab (Mathworks). Averages, SDs and linear fits were calculated with Microsoft Excel. Vertical scatterplots, histograms and statistical analysis were created and performed in Prism (Prism v5.0, Graphpad).

3.5 - Supplementary

3.5.1 - Single enzyme counting and activity traces

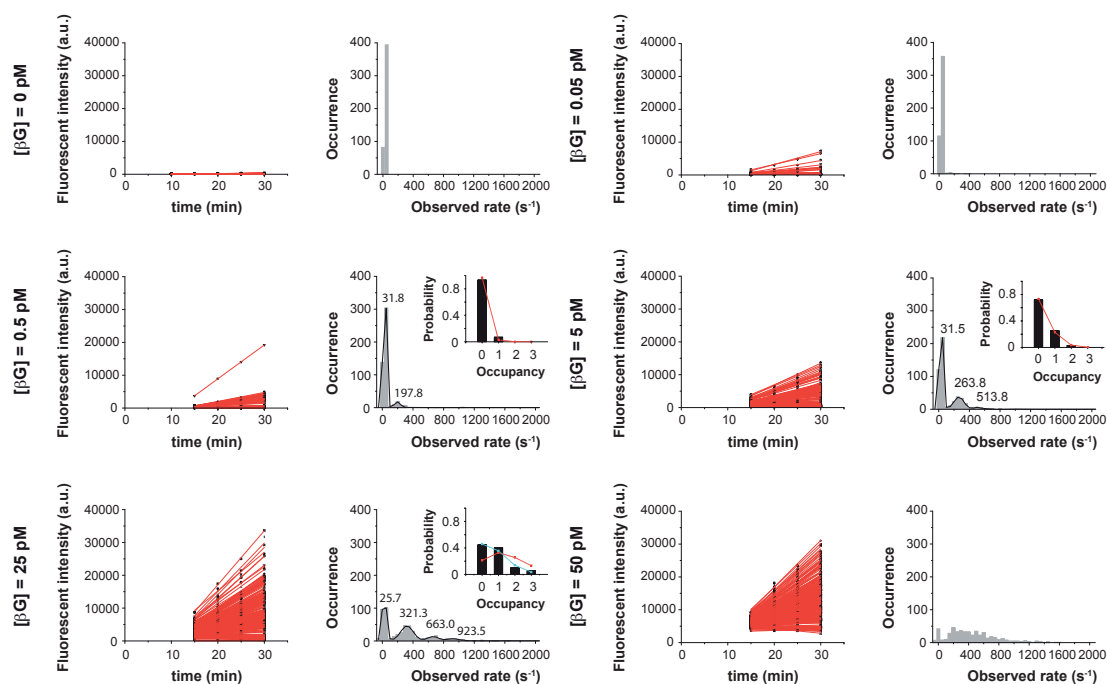


Figure SI 3.1: Activity traces and observed turnover rates of enzymes for the β G assay. Activity traces of enzymes for the β G assay. Turnover rates are determined by linear regression fitting (solid red lines) to the fluorescence trajectories after background subtraction. Histograms of observed turnover rates for individual femtowells. The numbers of wells are plotted versus the increase in observed rate. For 0.5, 5, and 25 pM the peaks were fitted with a sum of Gaussians. The values displayed above each peak are the centers of these Gaussians. The inserts show the probability distribution. The black bars represent the experimentally obtained probability distributions calculated from the Gaussian fits. Red data points represent the values obtained from the Poisson distribution $f(k;\lambda)=\lambda^k e^{-\lambda}/k!$ with the parameter λ equal to the expected number of enzymes per chamber for 0.5, 5, and 25 pM of β G. Blue data points are the values obtained from the Poisson distribution for 12.5 pM of β G. The bin size for all histograms is 50 s^{-1} . Adapted from *ACS Nano* vol.10 pp. 1699-1710 © (2016).

3.5.2 - Microfluidic control system

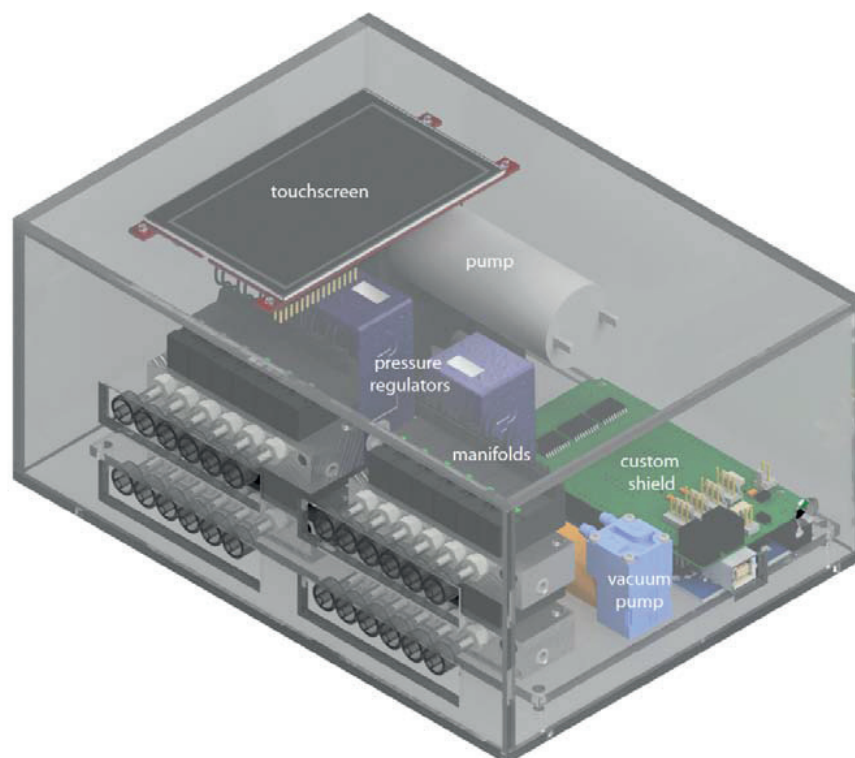
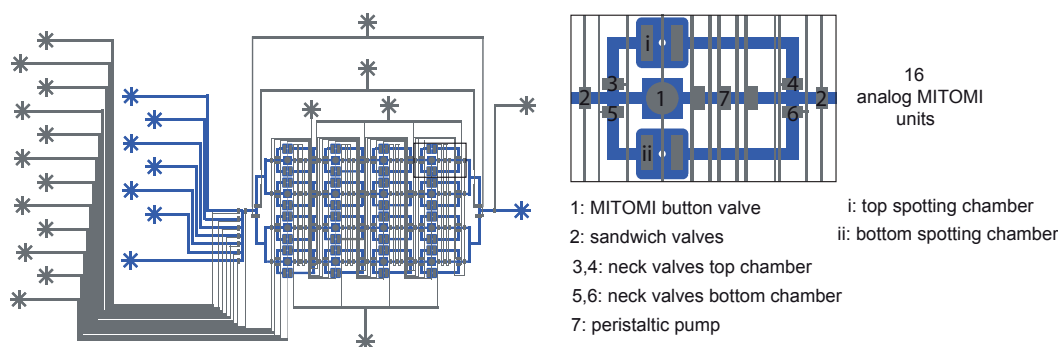


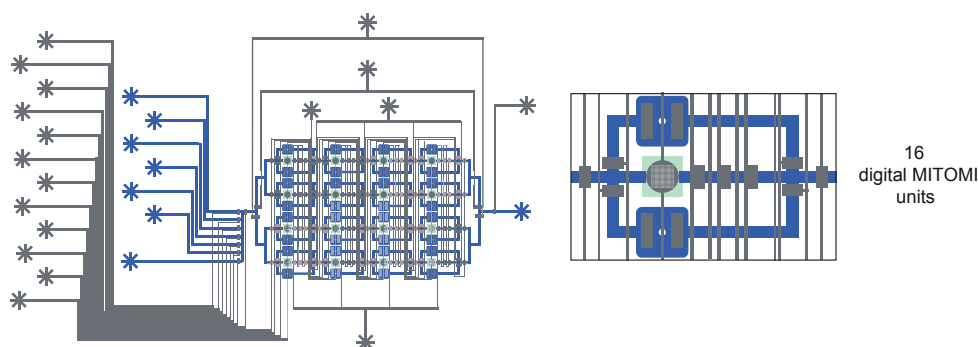
Figure SI 3.2: **3D rendering, of the MSC.** 3D rendering of the MSC showing how the different components were arranged. Adapted from *ACS Nano* vol.10 pp. 1699-1710 © (2016).

3.5.3 - Microfabricated diagnostic design

a Analog MITOMI



b Digital MITOMI



c Digital-Analog MITOMI

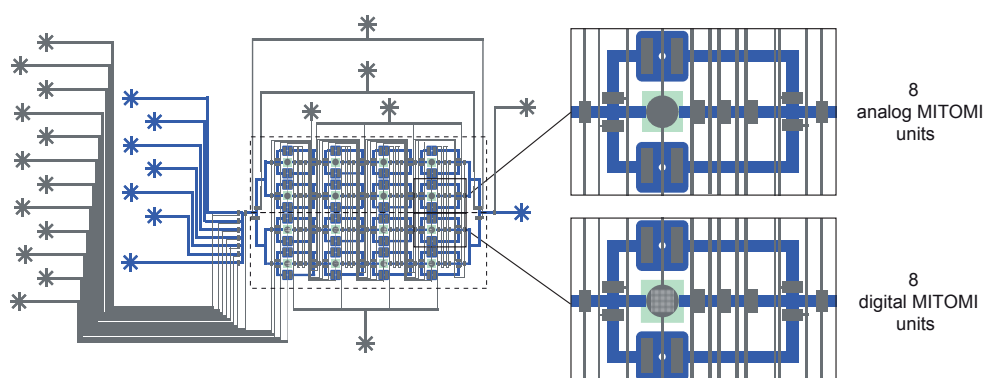


Figure SI 3.3: **Microfabricated diagnostic devices used in this study.** (a) Design schematic of the analog MITOMI microfluidic device showing flow (blue) and control (grey) layers. The device has four rows; each row contains four unit cells for a total of 16 analog assay units. Each assay unit (inset) contains: a MITOMI button valve (1), a sandwich valve (2), two neck valves (3, 4) for the top chamber (i) and two (5, 6) for the bottom one (ii), and a peristaltic pump (8). (b) Digital MITOMI device. (c) Digital-analog hybrid MITOMI device, with 8 digital and 8 analog units. Adapted from *ACS Nano* vol.10 pp. 1699-1710 © (2016).

3.5.4 - Platform technologies for biomarker diagnostic

	Digital	Analog	Limit of detection	Dynamic range [order of magnitude]	Sample volume [μ l]	Dilution required	Multiplexing [units]
This study	✓	✓	~330fg/ml	5	5	-	16
Wu <i>et al.</i> ¹	✓	x	1fg/ml-0.09pg/ml	>4	100	1:4	10
Rissin <i>et al.</i> ²	✓	x	~6-10fg/ml	4	100	1:4	2
Rissin <i>et al.</i> ³	✓	x	3fg/ml	4	100	-	4
Inci <i>et al.</i> ⁴	x	✓	400 fg/ml	8	\leq 100	1:10	-
Fan <i>et al.</i> ⁵	x	✓	17.5 pg/ml	4	10	1:10	12
Kadimisetty <i>et al.</i> ⁶	x	✓	10-100 fg/ml	5	5-10	1:30-500	6
Krause <i>et al.</i> ⁷	x	P	10-40fg/ml	3	5	1:30	4

Table 3.2: Comparison of the μ FDS with the microfluidic platform technologies for biomarker diagnostics.

3.5.5 - Digital-MITOMI immunoassay steps

	Reagent	time (min)
1	BSA (Biotinylated)	10
2	PBS-tween	5
3	Neutravidin	10
4	PBS-tween	5
5	BSA (Biotinylated)	10
6	PBS-tween	5
7	Goat anti-GFP (Biotinylated)	10
8	PBS-tween	5
9	GFP	10
10	PBS-tween	5
11	Mouse anti-Penta His (Alexa Fluor 555 conjugate)	8
12	PBS-tween	5
13	Goat anti-mouse IgG (bG conjugate)	10
14	PBS-tween	5
15	FDG	4

Table 3.3: Liquid handling sequence for the digital-MITOMI immunoassay

3.5.6 - IL-6 immunoassay steps

	Reagent	time (min)
1	BSA (Biotinylated)	10
2	PBS-tween	5
3	Neutravidin	10
4	PBS-tween	5
5	BSA (Biotinylated)	10
6	PBS-tween	5
7	Anti-Human IL-6 (Biotinylated)	10
8	PBS-tween	5
9	Human IL-6	10
10	PBS-tween	5
11	Rabbit anti-Human IL-6	8
12	PBS-tween	5
13	Goat anti-rabbit IgG (bG conjugate)	10
14	PBS-tween	5
15	FDG	4

Table 3.4: **Liquid handling sequence for the analog-amp IL-6 MITOMI immunoassay**

3.5.7 - Multiplex Ebola immunoassay steps

	Reagent	time (min)
1	BSA (Biotinylated)	10
2	PBS-tween	5
3	Neutravidin	10
4	PBS-tween	5
5	BSA (Biotinylated)	10
6	PBS-tween	5
7	Mouse anti-Penta His (Biotinylated)	10
8	PBS-tween	5
9	Pumping GP	10
10	PBS-tween	5
11	Sample	8
12	PBS-tween	5
13	Pumping secondary antibody	10
14	PBS-tween	5
15	FDG	4

Table 3.5: **Liquid handling sequence for the multiplex MITOMI immunoassay**

Bibliography

- [1] P. R. Srinivas, B. S. Kramer, and S. Srivastava, “Trends in biomarker research for cancer detection,” *Lancet Oncol.*, vol. 2, no. 11, pp. 698–704, Nov. 2001.
- [2] L. Hood and N. D. Price, “Demystifying disease, democratizing health care,” *Sci. Transl. Med.*, vol. 6, no. 225, p. 225ed5, Feb. 2014.
- [3] A. T. Sage, J. D. Besant, B. Lam, E. H. Sargent, and S. O. Kelley, “Ultrasensitive Electrochemical Biomolecular Detection Using Nanostructured Microelectrodes,” *Acc. Chem. Res.*, vol. 47, no. 8, pp. 2417–2425, Aug. 2014.
- [4] S. I. Stoeva, J.-S. Lee, J. E. Smith, S. T. Rosen, and C. A. Mirkin, “Multiplexed detection of protein cancer markers with biobarcode nanoparticle probes,” *J. Am. Chem. Soc.*, vol. 128, no. 26, pp. 8378–8379, Jul. 2006.
- [5] J. F. Rusling, G. W. Bishop, N. M. Doan, and F. Papadimitrakopoulos, “Nanomaterials and biomaterials in electrochemical arrays for protein detection,” *J. Mater. Chem. B*, vol. 2, no. 1, pp. 12–30, Nov. 2013.
- [6] “Microfluidic Large-Scale Integration | Science.” [Online]. Available: <http://science.sciencemag.org/content/298/5593/580>. [Accessed: 23-Mar-2017].
- [7] K. N. Han, C. A. Li, and G. H. Seong, “Microfluidic Chips for Immunoassays,” *Annu. Rev. Anal. Chem.*, vol. 6, no. 1, pp. 119–141, 2013.
- [8] K. Kadimisetty *et al.*, “Automated Multiplexed ECL Immunoarrays for Cancer Biomarker Proteins,” *Anal. Chem.*, vol. 87, no. 8, pp. 4472–4478, Apr. 2015.
- [9] R. Fan *et al.*, “Integrated barcode chips for rapid, multiplexed analysis of proteins in microliter quantities of blood,” *Nat. Biotechnol.*, vol. 26, no. 12, pp. 1373–1378, Dec. 2008.
- [10] F. Inci *et al.*, “Multitarget, quantitative nanoplasmonic electrical field-enhanced resonating device (NE2RD) for diagnostics,” *Proc. Natl. Acad. Sci.*, vol. 112, no. 32, pp. E4354–E4363, Aug. 2015.
- [11] B. Berg *et al.*, “Cellphone-Based Hand-Held Microplate Reader for Point-of-Care Testing of Enzyme-Linked Immunosorbent Assays,” *ACS Nano*, vol. 9, no. 8, pp. 7857–7866, Aug. 2015.
- [12] D. M. Rissin *et al.*, “Single-molecule enzyme-linked immunosorbent assay detects serum proteins at subfemtomolar concentrations,” *Nat. Biotechnol.*, vol. 28, no. 6, pp. 595–599, Jun. 2010.
- [13] D. M. Rissin *et al.*, “Multiplexed single molecule immunoassays,” *Lab. Chip*, vol. 13, no. 15, pp. 2902–2911, Jul. 2013.
- [14] J. Shim *et al.*, “Ultrarapid generation of femtoliter microfluidic droplets for single-molecule-counting immunoassays,” *ACS Nano*, vol. 7, no. 7, pp. 5955–5964, Jul. 2013.
- [15] S. Ge, W. Liu, T. Schlappi, and R. F. Ismagilov, “Digital, ultrasensitive, end-point protein measurements with large dynamic range via Brownian trapping with drift,” *J. Am. Chem. Soc.*, vol. 136, no. 42, pp. 14662–14665, Oct. 2014.
- [16] D. Wu, M. D. Milutinovic, and D. R. Walt, “Single molecule array (Simoa) assay with optimal antibody pairs for cytokine detection in human serum samples,” *The Analyst*, vol. 140, no. 18, pp. 6277–6282, Sep. 2015.
- [17] D. M. Rissin *et al.*, “Simultaneous detection of single molecules and singulated ensembles of molecules enables immunoassays with broad dynamic range,” *Anal. Chem.*, vol. 83, no. 6, pp. 2279–2285, Mar. 2011.
- [18] J. L. Garcia-Cordero and S. J. Maerkl, “Mechanically Induced Trapping of Molecular Interactions and Its Applications,” *J. Lab. Autom.*, vol. 21, no. 3, pp. 356–367, Jun. 2016.
- [19] M. A. Unger, H.-P. Chou, T. Thorsen, A. Scherer, and S. R. Quake, “Monolithic Microfabricated Valves and Pumps by Multilayer Soft Lithography,” *Science*, vol. 288, no. 5463, pp. 113–116, Apr. 2000.
- [20] F. Volpetti, J. Garcia-Cordero, and S. J. Maerkl, “A microfluidic platform for high-throughput multiplexed protein quantitation,” *PloS One*, vol. 10, no. 2, p. e0117744, 2015.

Chapter 3 – A digital-analog microfluidic platform for patient-centric multiplexed biomarker diagnostics of ultra-low volume samples

- [21] Z.-H. Wang, Y.-H. Meng, P.-Q. Ying, C. Qi, and G. Jin, "A label-free protein microfluidic array for parallel immunoassays," *Electrophoresis*, vol. 27, no. 20, pp. 4078–4085, Oct. 2006.
- [22] J. L. Garcia-Cordero, C. Nembrini, A. Stano, J. A. Hubbell, and S. J. Maerkl, "A high-throughput nanoimmunoassay chip applied to large-scale vaccine adjuvant screening," *Integr. Biol. Quant. Biosci. Nano Macro*, vol. 5, no. 4, pp. 650–658, Apr. 2013.
- [23] J. L. Garcia-Cordero and S. J. Maerkl, "A 1024-sample serum analyzer chip for cancer diagnostics," *Lab. Chip*, Dec. 2013.
- [24] C.-H. Wang and G.-B. Lee, "Pneumatically driven peristaltic micropumps utilizing serpentine-shape channels," *J. Micromechanics Microengineering*, vol. 16, no. 2, p. 341, 2006.
- [25] Y. Rondelez *et al.*, "Microfabricated arrays of femtoliter chambers allow single molecule enzymology," *Nat. Biotechnol.*, vol. 23, no. 3, pp. 361–365, Mar. 2005.
- [26] S. Sakakihara, S. Araki, R. Iino, and H. Noji, "A single-molecule enzymatic assay in a directly accessible femtoliter droplet array," *Lab. Chip*, vol. 10, no. 24, pp. 3355–3362, Dec. 2010.
- [27] S. Ota, H. Kitagawa, and S. Takeuchi, "Generation of femtoliter reactor arrays within a microfluidic channel for biochemical analysis," *Anal. Chem.*, vol. 84, no. 15, pp. 6346–6350, Aug. 2012.
- [28] A. Macneil, Z. Reed, and P. E. Rollin, "Serologic cross-reactivity of human IgM and IgG antibodies to five species of Ebola virus," *PLoS Negl. Trop. Dis.*, vol. 5, no. 6, p. e1175, Jun. 2011.
- [29] T. Kamata, M. Natesan, K. Warfield, M. J. Aman, and R. G. Ulrich, "Determination of specific antibody responses to the six species of ebola and Marburg viruses by multiplexed protein microarrays," *Clin. Vaccine Immunol. CVI*, vol. 21, no. 12, pp. 1605–1612, Dec. 2014.
- [30] L. M. Rodríguez-Martínez *et al.*, "Antibody Derived Peptides for Detection of Ebola Virus Glycoprotein," *PLoS One*, vol. 10, no. 10, p. e0135859, 2015.
- [31] "WHO | Ebola virus disease," *WHO*. [Online]. Available: <http://www.who.int/mediacentre/factsheets/fs103/en/>. [Accessed: 23-Mar-2017].
- [32] G. Vogel, "Testing new Ebola tests," *Science*, vol. 345, no. 6204, pp. 1549–1550, Sep. 2014.
- [33] E. González-González *et al.*, "Anti-Ebola therapies based on monoclonal antibodies: current state and challenges ahead," *Crit. Rev. Biotechnol.*, vol. 37, no. 1, pp. 53–68, Feb. 2017.
- [34] T. G. Ksiazek *et al.*, "Clinical virology of Ebola hemorrhagic fever (EHF): virus, virus antigen, and IgG and IgM antibody findings among EHF patients in Kikwit, Democratic Republic of the Congo, 1995," *J. Infect. Dis.*, vol. 179 Suppl 1, pp. S177–187, Feb. 1999.
- [35] A. M. Casillas, A. M. Nyamathi, A. Sosa, C. L. Wilder, and H. Sands, "A current review of Ebola virus: pathogenesis, clinical presentation, and diagnostic assessment," *Biol. Res. Nurs.*, vol. 4, no. 4, pp. 268–275, Apr. 2003.
- [36] E. M. Leroy, S. Baize, P. Debre, J. Lansoud-Soukate, and E. Mavoungou, "Early immune responses accompanying human asymptomatic Ebola infections," *Clin. Exp. Immunol.*, vol. 124, no. 3, pp. 453–460, Jun. 2001.
- [37] B. Li *et al.*, "A smartphone controlled handheld microfluidic liquid handling system," *Lab. Chip*, vol. 14, no. 20, pp. 4085–4092, Oct. 2014.
- [38] C. E. Krause *et al.*, "Rapid microfluidic immunoassays of cancer biomarker proteins using disposable inkjet-printed gold nanoparticle arrays," *ChemistryOpen*, vol. 2, no. 4, pp. 141–145, Aug. 2013.
- [39] N. P. Sardesai, K. Kadimisetty, R. Faria, and J. F. Rusling, "A microfluidic electrochemiluminescent device for detecting cancer biomarker proteins," *Anal. Bioanal. Chem.*, vol. 405, no. 11, pp. 3831–3838, Apr. 2013.
- [40] O. Kavanagh *et al.*, "Serological responses to experimental Norwalk virus infection measured using a quantitative duplex time-resolved fluorescence immunoassay," *Clin. Vaccine Immunol. CVI*, vol. 18, no. 7, pp. 1187–1190, Jul. 2011.
- [41] M. C. Rodríguez-Barradas *et al.*, "IgG antibody to pneumococcal capsular polysaccharide in human immunodeficiency virus-infected subjects: persistence of antibody in responders, revaccination in nonresponders, and relationship of immunoglobulin allotype to response," *J. Infect. Dis.*, vol. 173, no. 6, pp. 1347–1353, Jun. 1996.

Chapter 3 – A digital-analog microfluidic platform for patient-centric multiplexed biomarker diagnostics of ultra-low volume samples

- [42] I. K. Dimov *et al.*, “Stand-alone self-powered integrated microfluidic blood analysis system (SIMBAS),” *Lab. Chip*, vol. 11, no. 5, pp. 845–850, Mar. 2011.
- [43] B. S. Ferguson *et al.*, “Real-time, aptamer-based tracking of circulating therapeutic agents in living animals,” *Sci. Transl. Med.*, vol. 5, no. 213, p. 213ra165, Nov. 2013.
- [44] M. R. Monroe, G. G. Daaboul, A. Tuysuzoglu, C. A. Lopez, F. F. Little, and M. S. Unlü, “Single nanoparticle detection for multiplexed protein diagnostics with attomolar sensitivity in serum and unprocessed whole blood,” *Anal. Chem.*, vol. 85, no. 7, pp. 3698–3706, Apr. 2013.
- [45] A. I. Barbosa, A. P. Castanheira, A. D. Edwards, and N. M. Reis, “A lab-in-a-briefcase for rapid prostate specific antigen (PSA) screening from whole blood,” *Lab Chip*, vol. 14, no. 16, pp. 2918–2928, Jul. 2014.
- [46] E. Stern *et al.*, “Label-free biomarker detection from whole blood,” *Nat. Nanotechnol.*, vol. 5, no. 2, pp. 138–142, Feb. 2010.
- [47] B. Hantusch *et al.*, “Affinity determinations of purified IgE and IgG antibodies against the major pollen allergens Phl p 5a and Bet v 1a: Discrepancy between IgE and IgG binding strength,” *Immunol. Lett.*, vol. 97, no. 1, pp. 81–89, Feb. 2005.
- [48] L. R. Hirsch, J. B. Jackson, A. Lee, N. J. Halas, and J. L. West, “A Whole Blood Immunoassay Using Gold Nanoshells,” *Anal. Chem.*, vol. 75, no. 10, pp. 2377–2381, May 2003.
- [49] T. Chinnasamy, L. I. Segerink, M. Nystrand, J. Gantelius, and H. A. Svahn, “A lateral flow paper microarray for rapid allergy point of care diagnostics,” *The Analyst*, vol. 139, no. 10, pp. 2348–2354, May 2014.
- [50] D. Pomponi *et al.*, “Allergen Micro-Bead Array for IgE Detection: A Feasibility Study Using Allergenic Molecules Tested on a Flexible Multiplex Flow Cytometric Immunoassay,” *PLoS ONE*, vol. 7, no. 4, p. e35697, Apr. 2012.
- [51] S. B. Lehrer, R. Reish, J. Fernandes, P. Gaudry, G. Dai, and G. Reese, “Enhancement of murine IgE antibody detection by IgG removal,” *J. Immunol. Methods*, vol. 284, no. 1–2, pp. 1–6, Jan. 2004.
- [52] M. Cretich *et al.*, “Detection of allergen specific immunoglobulins by microarrays coupled to microfluidics,” *Proteomics*, vol. 9, no. 8, pp. 2098–2107, Apr. 2009.
- [53] P. A. Eigenmann *et al.*, “The ImmunoCAP Rapid Wheeze/Rhinitis Child test is useful in the initial allergy diagnosis of children with respiratory symptoms,” *Pediatr. Allergy Immunol. Off. Publ. Eur. Soc. Pediatr. Allergy Immunol.*, vol. 20, no. 8, pp. 772–779, Dec. 2009.
- [54] S. Ramachandran, E. Fu, B. Lutz, and P. Yager, “Long-term dry storage of an enzyme-based reagent system for ELISA in point-of-care devices,” *The Analyst*, vol. 139, no. 6, pp. 1456–1462, Mar. 2014.

Chapter 4

A microfluidic biodisplay

Adapted from: Francesca Volpetti*, Ekaterina Petrova* and Sebastian J. Maerkl (2017)
bioRxiv doi:10.1101/112110.

*Equally contributing authors

Synthetically engineered cells are powerful and potentially useful biosensors, but it remains difficult to deploy such systems due to practical difficulties and biosafety concerns. To overcome these hurdles, we developed a microfluidic device that serves as an interface between an engineered cellular system, environment, and user. We created a biodisplay consisting of 768 individually programmable biopixels and demonstrated that it can perform multiplexed, continuous environmental monitoring. The biodisplay detected 10 $\mu\text{g/l}$ sodium-arsenite in tap water using a research grade fluorescent microscope, and reported arsenic contamination down to 20 $\mu\text{g/l}$ with an easy to interpret “skull and crossbones” symbol detectable with a low-cost USB microscope or by eye. The biodisplay was designed to prevent release of chemical or biological material to avoid environmental contamination. The microfluidic biodisplay thus provides a practical solution for the deployment and application of engineered cellular systems.

4.1 - Introduction

With the advent of synthetic biology, a number of biological sensors have been engineered that are capable of monitoring the environment [1], [2]. Although such synthetic biological systems are in principle extremely powerful sensors and information processing units, they often lack direct applicability because suitable interfaces between the environment, the user and the engineered biological system don't exist [3], [4]. The lack of such interfaces results in problems related to safely deploying genetically modified organisms (GMOs), while making it possible for them to interact with the environment and user [5]. Aside from safety

concerns, interfaces can solve practical problems such as keeping the engineered biological system alive for extended periods of time, automatic and frequent sampling of the environment, and facilitating readout.

Microfluidics originated as a tool to enable analytical measurements in chemistry and biology [6]. In the last decades, microfluidic devices have found a plethora of applications in biology spanning high-throughput screening [7], cell-based assays [8], [9], and molecular diagnostics [10]. The use of microfluidic devices increases throughput, reduces cost, and can enable novel measurements [11]. In most instances the purpose of microfluidics is to enable or conduct analytical measurements of molecules or cells. Few examples depart from this dogmatic application of microfluidics and instead employ microfluidic devices as soft robots capable of movement and camouflage [12], or as microfluidic games [13]. One recent example demonstrated how engineered biological systems can be deployed by combining bacterial sensors with passive microfluidic channels in a wearable hydrogel-elastomer hybrid device capable of sensing and reporting the presence of Diacetylphloroglucinol (DAPG), Isopropyl b-D-1thiogalactopyranoside (IPTG), Acyl homoserine lactones (AHL) and Rhamnose [14].

We have previously developed a method to culture and interrogate 1'152 *S. cerevisiae* strains on a microfluidic device. Each strain is cultured in a dedicated micro-chemostat and is interrogated optically to provide single-cell, phenotypic information on each strain. We applied this platform to the comprehensive, single-cell analysis of yeast proteome dynamics [15] and to the detailed characterization and modeling of transcriptional regulation in yeast [16]. Here we show that this approach can be used to generate a bacterial biodisplay. Unlike previous bacterial biodisplays [17], each of the 768 pixels can be independently programmed with a specific bacterial strain or clone. Once programmed, the device cultures cells for extended periods of time, while preventing contamination of the environment by GMOs contained on the device. We used the biodisplay to characterize the response of several engineered bacterial strains to small molecule analytes for extended period of time. To demonstrate environmental monitoring, we programmed the biodisplay with a “skull and crossbones” symbol using a bacterial arsenic sensor strain. The symbol is displayed when arsenic contaminated water is sensed by the biodisplay. We also demonstrate a multiplexed biodisplay that reports on the presence or absence of two small molecules: arabinose and arsenic. The use of an easy-to-interpret symbolic display drastically simplifies analysis, and is readily understood by a layman without any special hardware or analysis requirements. To enable field-deployment of our biodisplay we show that readout can be conducted using an off-the-shelf low-cost USB microscope, a cellphone, or direct visual inspection. Finally, to increase shelf-life and facilitate shipping / deployment of the biodisplay we programmed the device with *B. subtilis* spores, which allowed storage of the display at 80°C for 1 month without any detectable decrease in viability or sensing functionality.

4.2 - Results and Discussion

4.2.1 - Biodisplay programming, culturing, sampling and readout

The biodisplay has a resolution of 48 x 16 for a total of 768 programmable pixels with a density of 64 pixels per inch (PPI) (Figure 4.1a). Each pixel consists of a 250 μm square cell chamber, two side channels for medium and sample introduction, sandwich valves to isolate adjacent pixels and a neck valve to isolate the pixel from the side channels. Each pixel of the biodisplay can be programmed with a different bacterial strain. Standard microarray spotting was used to array bacterial cells or spores on an epoxy-coated glass slide. *E. coli* was spotted in medium containing 10% glycerol to preserve cell viability, as we observed that dried *E. coli* spots failed to regrow after spotting. *B. subtilis* spores could be spotted in water without addition of glycerol. The bacterial array was then aligned to the microfluidic chip and bonded at 37°C for 1 hour.

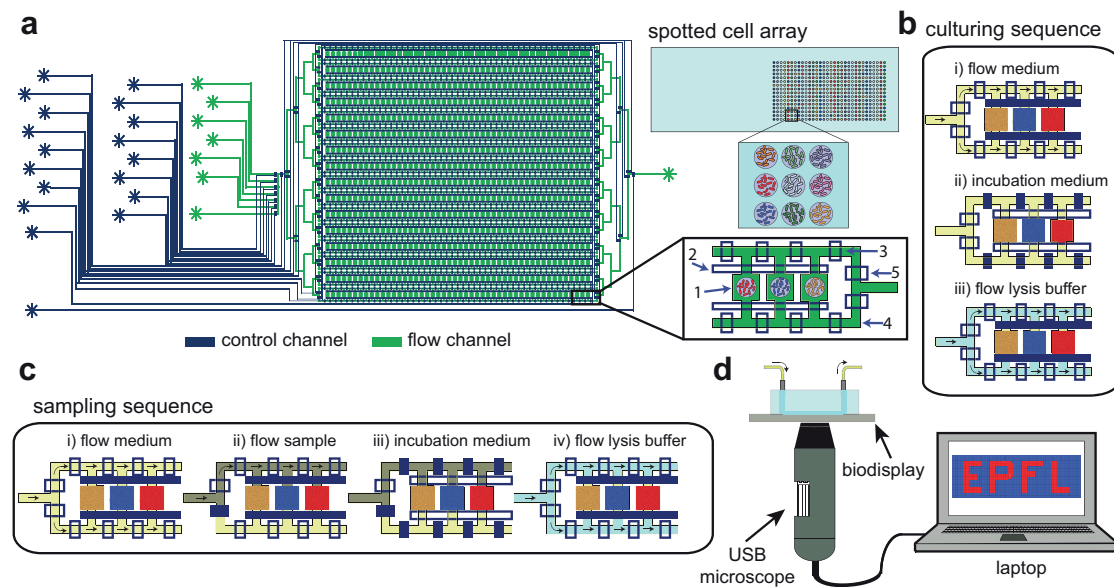


Figure 4.1: **Biodisplay schematic and use.** (a) Design of the two-layer microfluidic device (control channels in blue and flow channels in green). The device is composed of 16 rows and 48 columns for a total of 768 biopixels. Each pixel consists of a spotting chamber (1), chamber valve (2), sandwich valves (3) and side channels (4). The side channels in turn can be specifically addressed using the side channel valves (5). A bacterial cell array is spotted on a glass slide and aligned with the PDMS chip. (b) The culturing sequence consists of 3 steps: i) flowing medium with the chambers closed (10 minutes), ii) incubation with the sandwich valves closed and chamber valves open (45 minutes), and iii) flowing lysis buffer with the chamber closed (10 minutes). (c) The sampling sequence consists of 4 steps: i) flowing the medium in both side channels (10 minutes), ii) flowing the sample in one side channel (10 minutes), iii) incubation with both medium and sample (45 minutes), and iv) flowing lysis buffer (10 minutes). The sequence is then repeated continuously for the extent of the experiment. (d) The biodisplay can be imaged using a standard research grade epi-fluorescent microscope, a USB fluorescent microscope, a cellphone camera, or by eye.

After assembling and bonding the biodisplay, cells were allowed to recover overnight using an automated culturing routine (Figure 4.1b). A medium reservoir was attached to the device and the waste outlet was connected to a receptacle containing 70% aq. EtOH to immediately sterilize and contain the device outflow. First, the entire device was loaded with medium by outgas priming [18]. Once the device was fully primed with medium, cells were cultured with the following three-step culturing routine: i) flowing medium through the side channels (10 minutes), ii) allowing medium to diffuse into the biopixels (45 minutes) and iii) flowing lysis buffer through the side channels (10 minutes). Whenever fluid was flowed through the side channels, the biopixel chambers were sealed off from the side channels using a set of valves. In step (ii) the biopixel valves were opened to allow diffusion of molecules in and out of the biopixel chamber. During this step, individual pixels were isolated from one another by the sandwich valves. The lysis segment of the culturing routine prevented biofilm and microcolony formation outside of the biopixels [19]. By actively preventing accumulation and growth of cells in areas other than the biopixels we prevented device clogging and allowed experiments to proceed for several days; the longest experiment conducted here lasted one week. Culturing was performed at 37°C using a thermo glass plate (Okolab). Culturing at 37°C increases growth rate, leading to faster accumulation of biomass, but was otherwise not required and incubation at room temperature was also possible. After overnight culturing, each bacterial spot had outgrown, and populated its dedicated biopixel. We did not observe any contamination resulting from microarraying. Cells occasionally populated empty biopixels during culturing, which was avoided by spotting a non-fluorescent *E. coli* strain in otherwise empty biopixels.

Once the biodisplay was online, we switched from the culturing routine to a sampling routine that enables frequent testing of a liquid sample (Figure 4.1c). The sampling routine was identical to the culturing routine, with an additional step added prior to diffusive mixing of the pixel and side channels. After flowing medium through both side channels, the sample was flowed through one of the side channels. During the diffusion step, both the medium and the sample were allowed to diffuse into the biopixel chambers. This process allowed us to aspirate a sample directly from an environmental source, rather than having to premix it manually with the medium solution. By using a dedicated sampling port, it was possible to sample a source for extended periods of time in 75 minute intervals without user interference.

We employed a standard research grade epi-fluorescent microscope (Nikon) and a handheld, low-cost USB fluorescent microscope (Dino-Lite) for device readout and quantitation (Figure 4.1d). The standard epi-fluorescent microscope equipped with a motorized stage was programmed to image each biopixel individually whereas the handheld USB microscope could image either the entire display or acquire several sub-sections. Both approaches were used to acquire time course and endpoint measurements. We also demonstrated that the biodisplay could be observed directly by eye using a LED flashlight and an emission filter, and images could be acquired using a standard cellphone camera.

4.2.2 - Multiplexed characterization of bacterial strains

We tested the biodisplay device by culturing and characterizing nine *E. coli* strains engineered to induce GFP or RFP expression in response to arabinose (Table 4.1). These strains were obtained from the iGEM registry of standard biological parts and were generated by various student teams. The fluorescent protein genes were under the regulation of a pBAD promoter or derivatives thereof. We programmed the biodisplay with the nine strains, each strain filling 2 columns of the device for a total of 32 pixels per strain. Strains were induced with arabinose after overnight culturing at 37°C. Induction was performed at room temperature (23-24°C) (Figure 4.2a) or 37°C (Figure SI 4.1). Room temperature induction was used in order to assess the performance of the biodisplay and cell-based sensors at ambient temperature in order to reduce platform complexity by eliminating the need for a temperature control element.

We designed the biodisplay device so that it was possible to specifically address four sets of four rows with a different solution. We used this modality to characterize each strain against four arabinose concentrations: 0.006 mM, 0.066 mM, 0.666 mM, 6.66 mM (0.0001%, 0.001%, 0.01% and 0.1% w/v) arabinose in LB medium. Altogether, we tested 36 strain – inducer combinations by measuring nine strains in response to four arabinose concentrations with eight technical repeats for each combination. The biodisplay was placed on an automated research-grade fluorescent microscope and imaged over time.

We performed two consecutive 24 hour inductions, with the second induction starting 2.5 days after the end of the first (Figure 4.2). Upon induction we observed a measurable signal in all strains. All three of the GFP strains showed a strong response to 6.66 mM arabinose while only strain #3 induced highly in response to 0.666 mM. Strains #1 and #2 induced to low levels in response to 0.666 mM and failed to induce to appreciable levels at lower arabinose concentrations, whereas strain #3 also induced in the presence of 0.066 mM arabinose. These results showed that strains #2 and #3 could be used in combination to distinguish three different inducer concentrations ranging over 3 orders of magnitude. All RFP strains induced expression to differing degrees in response to 6.66 mM arabinose and in the cases of RFP strains #2-6 also to 0.666 mM arabinose. All strains, with the exception of strain GFP_1 slowly decreased in intensity during the 2.5 days de-induction period. Strain GFP_1 exhibited a transient expression profile with signal beginning to decrease during the induction phase. GFP_1 is also the only strain that failed to induce during the second induction when cultured at room temperature but induced well in the second induction when cultured at 37°C (Figure SI 4.1). The transient expression profile can be attributed to the DH5- α background used and the presence of a LVA protease tag which is not present in any of the other strains tested.

Using the same approach we tested nine engineered arsenic responsive bacterial strains [20], [21]. We chose arsenic responsive strains, for use in a biodisplay for low-cost, continuous environmental arsenic monitoring. After overnight growth, we flowed LB medium with 0 $\mu\text{g/l}$, 10 $\mu\text{g/l}$, 100 $\mu\text{g/l}$ and 500 $\mu\text{g/l}$ sodium-arsenite for 24 hours and quantitated GFP expression over time. The experiment was performed at room temperature. Strain EDI_as_4 in particular showed high expression of GFP and detected sodium-arsenite

down to 10 $\mu\text{g/l}$ (Figure SI 4.2). We thus chose this strain for all further arsenic sensing applications.

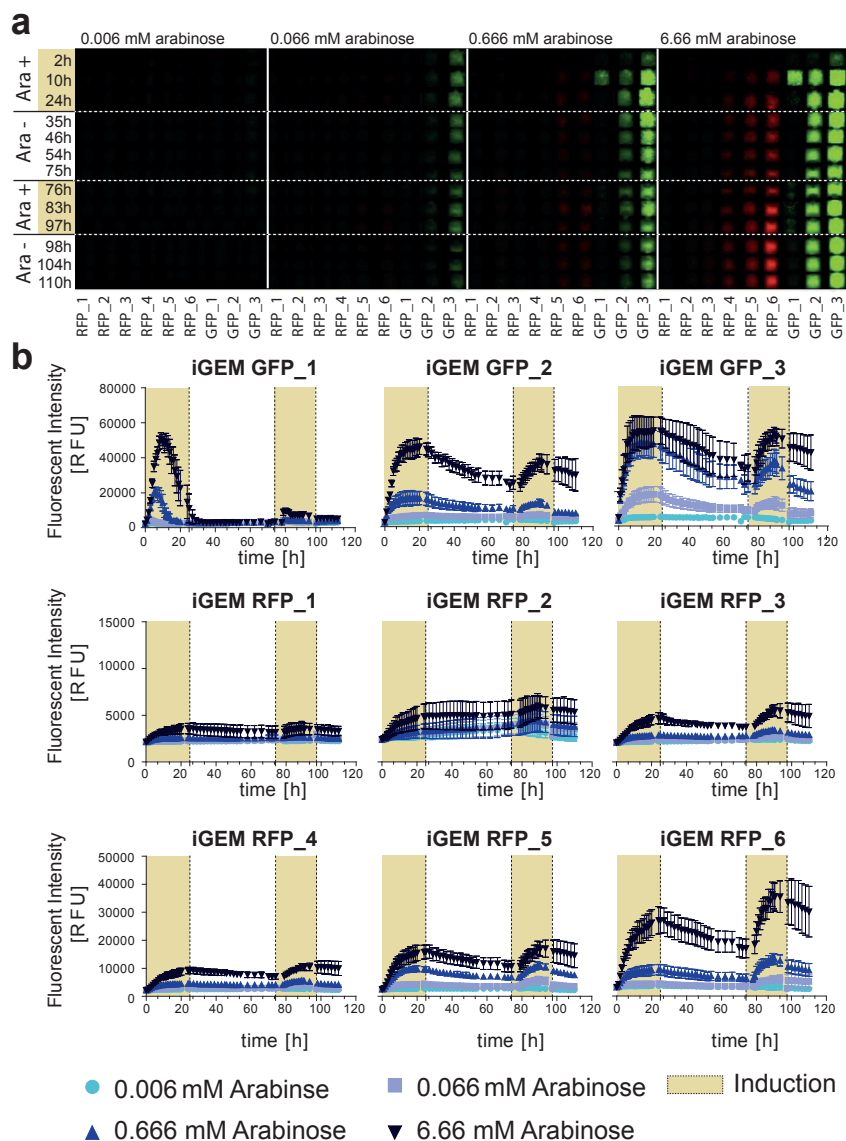


Figure 4.2: **Using the biodisplay for strain characterization.** (a) Fluorescence kymograms of nine arabinose-sensing *E. coli* strains. Shown is a representative biopixel for each strain and condition tested. The strains were induced twice for 24 hours with 0.006 mM, 0.066 mM, 0.666 mM and 6.66 mM arabinose. (b) Quantitative analysis of fluorescence pixel intensities for each strain under four arabinose concentrations. The yellow background denotes the two induction periods. Each data point represents the average of eight pixels with error bars representing to the std. deviation of the means.

This series of experiments demonstrated that our biodisplay is a viable high-throughput platform for long-term culturing and characterization of bacterial strains. Theoretically, up to 768 strains can be characterized in parallel on this platform under dynamically changing media conditions [15], which is otherwise difficult to achieve using standard microplate batch cultures or low-throughput microfluidic devices.

We also performed an experiment demonstrating that the biodisplay is able to sense arabinose after a period of continuous operation. The arabinose sensitive strains were spotted and four different concentrations of arabinose were flowed after 3 days (Figure 4.3).

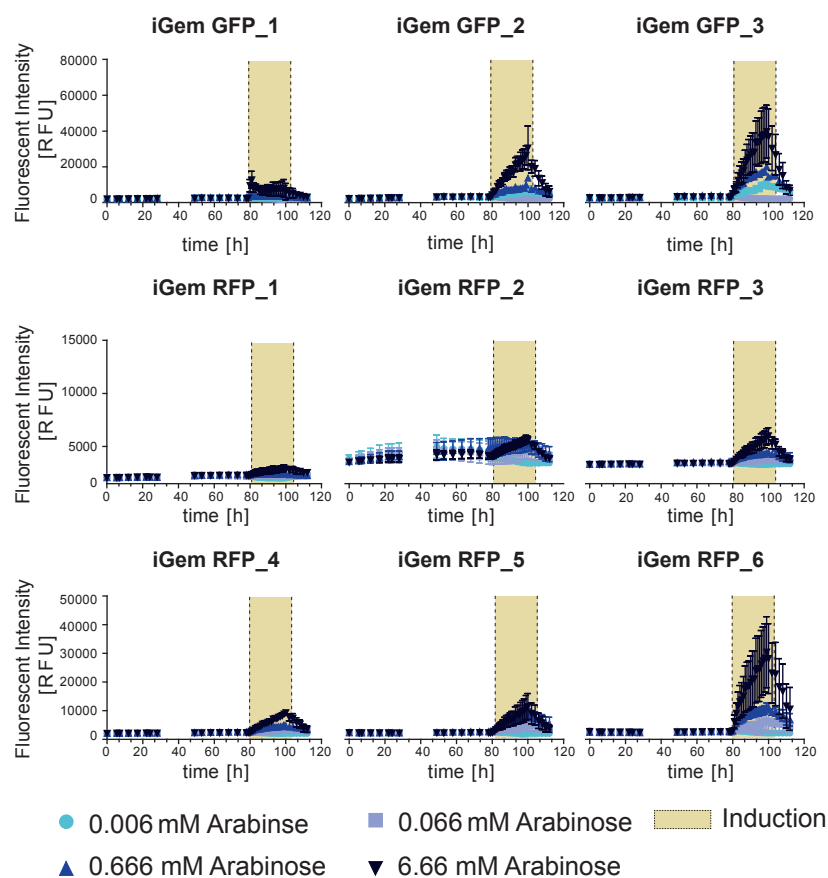


Figure 4.3: **One delayed arabinose induction.** Quantitative analysis of fluorescence pixel intensities for each strain under four arabinose concentrations. The yellow background denotes the induction period. Each data point represents the average of eight pixels with error bars representing to the std. deviation of the means.

The experiment has been performed at room temperature. An increase of the signal has been observed as soon as the medium spiked with different arabinose concentrations is flowed through the device.

4.2.3 - Biodisplay

High levels of arsenic in groundwater are common in a number of countries including China, India, and the USA. Not only is arsenic a concern in water supplies, high arsenic levels have also been found in a number of food sources [22], particularly rice [23], [24]. In Bangladesh, an estimated 20 – 45 million people are affected by arsenic levels that exceed the national standard of 50 $\mu\text{g/l}$ and the WHO / EPA standard of 10 $\mu\text{g/l}$ [25]. Worldwide it is estimated that over 200 million people are exposed to unsafe arsenic levels of 10 $\mu\text{g/l}$ or above [26]. Arsenic also tops the ATSDR substance priority list [27], which lists those substances “determined to pose the most significant and potential threat to human health”. Our biodisplay could serve as a continuous environmental water monitor that is low-cost, readily deployable in resource limited settings, and easy to interpret.

We programmed our biodisplay with an arsenic sensing *E. coli* strain (EDI_as_4) spelling “As”, the elemental symbol for arsenic, and a “skull and crossbones” symbol commonly used to warn of toxic substances (Figure 4.4). All pixels not programmed with the arsenic sensing strain were programmed with a non-fluorescent strain to prevent invasion and cross-contamination by the arsenic sensing strain. After overnight growth, sodium-arsenite in tap water was sampled by the device using the sampling routine described above. The biodisplay was kept at room temperature for the entire duration of the sampling routine. Using the research grade fluorescent microscope for readout, the biodisplay detected as little as 10 $\mu\text{g/l}$ sodium-arsenite, and 20 $\mu\text{g/l}$ sodium-arsenite was detected with the handheld low-cost fluorescent USB microscope (Figure SI 4.3). Fluorescent signal and the appearance of the “As” and “skull and crossbones” symbols was detected after 10 hours by the research grade microscope (Figure SI 4.4). After 24 hours a strong fluorescent signal had developed that could be easily imaged with a low-cost handheld USB microscope. A negative control biodisplay, which was run under identical conditions but exposed to tap water without added arsenic showed no detectable fluorescent signal.

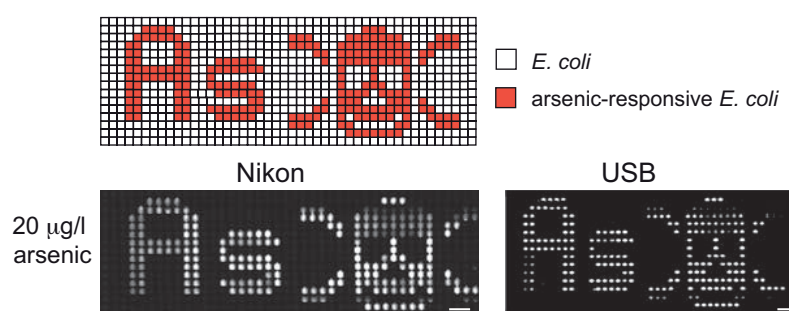


Figure 4.4: **Biodisplay for arsenic sensing.** Arsenic-responsive *E. coli* was spotted spelling “As” and forming a “skull and crossbones” symbol. 20 $\mu\text{g/l}$ of sodium-arsenite in tap water was sampled and images were acquired using Nikon and USB microscopes after 24 hours.

Given the large number of programmable pixels and high pixel density on our biodisplay we explored the possibility of generating a biodisplay that could sense and report the presence or absence of multiple substances in a sample (Figure 4.5a).

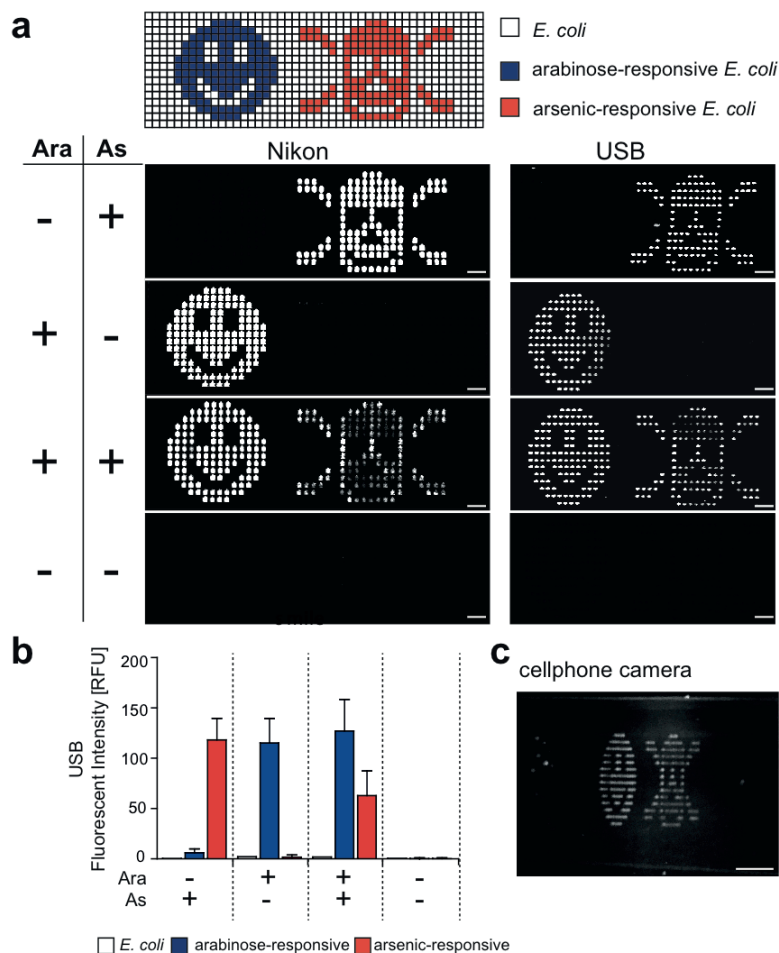


Figure 4.5: **Biodisplay for arabinose and arsenic sensing.** (a) Multiplexed detection of arabinose (blue) and arsenic (red) by two *E. coli* strains that were spotted to display a “smiley” and a “skull and crossbones” symbol, respectively. Nikon and USB images of the chip were acquired after flowing all combinations of 6.66 mM arabinose and 100 μ g/l sodium-arsenite in tap water in four independent experiments. Scale bars: 750 μ m (b) Quantitation of GFP intensity, after 24 hours of induction, measured using the USB microscope. (c) The device exposed to both arsenic and arabinose, was imaged using a mobile phone. The image was obtained using the illumination with blue LEDs and a band-pass filter, placed in front of the cellphone camera. Scale bar: 3.5 mm.

We selected the same arsenic sensing strain as above and the iGEM GFP_3 strain for arabinose sensing. The arsenic sensing strain was spotted in the form of a “skull and crossbones” pattern whereas the arabinose sensing strain was spotted in a “smiley” pattern. We performed four separate experiments exposing a new biodisplay to one of the four

possible combinations of arsenic and arabinose. After sampling for 24 hours, the biodisplay accurately reported on the presence / absence of these two small molecules (Figure 4.5a, b). We note that the arsenic-sensing strain used (EDI_as_4) was engineered to be tunable by arabinose, explaining the difference in intensity of the “skull and crossbones” symbol between experiments sampling arsenic and arabinose versus arsenic alone [20].

The patterns could be readily imaged using a research grade and USB fluorescent microscope. Because of the ease with which the symbols could be visualized we also tested whether the device could be imaged directly with a cellphone using a blue LED flashlight for illumination and a fluorescence emission filter held in front of the cellphone camera. Both symbols could readily be imaged with this simple setup (Figure 4.5c). The symbols could also be seen by eye using the flashlight and emission filter. Imaging was performed in an illuminated laboratory during daylight hours, with a small black curtain shielding the device from direct sunlight (Figure 4.5c, Figure SI 4.5).

4.2.4 - Spores enable long-term storage

In order to develop a biodisplay that can withstand long-term storage and shipping without requiring a cold chain or special conditions we explored the use of bacteria spores. Bacterial spores are well known for their incredible robustness to adverse environments [28], [29] and thus would be ideal for programming the biodisplay.

We generated spores from two *B. subtilis* strains, each containing a genomically integrated Phy-spark promoter driving the expression of either mCherry or GFP. The spores were spotted onto glass slides together with *B. subtilis* and *E. coli* cells. The slides were aligned and bonded to a microfluidic device. These biodisplays were then stored for one day or one month at 40°C and 80°C. After the storage period we introduced LB medium (Figure 4.6a, b). Neither *E. coli* nor *B. subtilis* cells could be recovered after any storage condition tested. Only when spotted in the presence of glycerol and without an extended storage period could *E. coli* and *B. subtilis* cells be recovered. *B. subtilis* spores, on the other hand, germinated after all storage conditions, notably even after incubation at 80°C for one month. Germination was observed as early as 1.5 hours after the start of the culturing routine. To test whether a spore-based biodisplay retains sensing capability after storage at 80°C for one month, we induced expression with 1 μ M IPTG and observed a rapid increase of fluorescence within 90 minutes. *B. subtilis* biopixels not exposed to IPTG remained non-fluorescent (Figure 4.6c).

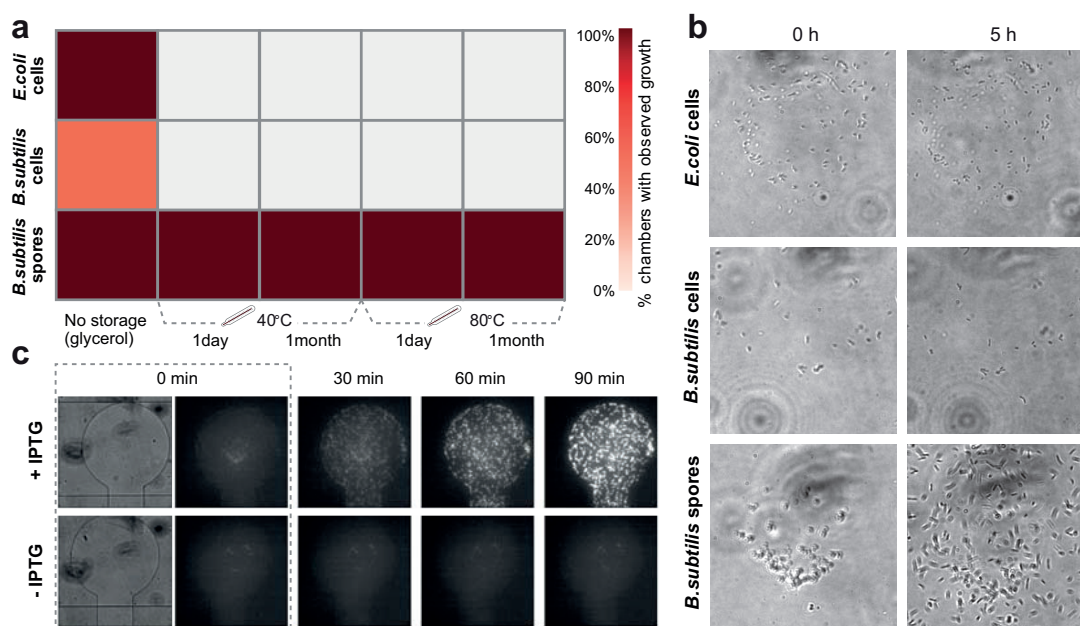


Figure 4.6: **Spore biodisplay.** (a) Comparison of *E. coli* cell, *B. subtilis* cell and *B. subtilis* spore recovery under different storage conditions. Each table entry represents the number of chambers with observed growth divided by the total number of spotted chambers for a specific temperature and time condition. (b) Bright-field images of a magnified view of the central part of representative pixels after storage at 80°C for 1 month. Images were acquired immediately after spots were resuspended in medium and after 5 hours incubation at 37°C. (c) Time-lapse images of germinated Phy-spank-mCherry *B. subtilis* spores after storage at 80°C for one month. Cells were induced with 1 μ M IPTG.

To decrease the risk of environmental biological and chemical release, the whole spore biodisplay with attached tygon tubings to the inlets and outlets of the chip was embedded into PDMS (Figure SI 4.6a). No effect on the spore germination and *B. subtilis* cells induction was observed (Figure SI 4.6b, c). Increasing the flow pressure from 20 kPa to 140 kPa as well as the actuation pressure of the control valves from \sim 70 kPa to 172 kPa did not perturb the functionality of the device, demonstrating its improved tolerance to higher applied pressures.

4.3 - Conclusions

We developed a bio-hardware device by combining engineered bacterial strains with a microfluidic chip. The resulting biodisplay consists of 768 independently programmable biopixels and we showed that it can culture bacterial strains for extended periods of time. Continuous culturing, with the capability of dynamically changing media makes the biodisplay a useful platform for high-throughput bacteria cell analysis (manuscript arising) and may find application in high-throughput screening and characterization of synthetically engineered bacterial strains.

Biological systems are powerful sensors, but challenging to deploy for several reasons. First, engineered biological systems generally need to be cultivated under fairly well controlled conditions, and often require the presence of antibiotics in order to maintain the synthetic network. Second, a major concern limiting the applicability of synthetic systems is the possible escape of genetically modified cells into the environment. Not only is the escape of GMOs a concern, but also the release of genetic material, which could readily be taken up by environmental bacteria through horizontal gene transfer. Our biodisplay solves both issues by providing a platform that enables long-term culturing, while eliminating release of genetic and chemical material into the environment. The small scale of the device requires low quantities of medium and antibiotics: ~2 ml for a 6 day experiment. The device outflow is sterilized and collected to prevent environmental contamination of biological and chemical components.

The ability to culture bacterial sensors on the biodisplay for extended periods of time with frequent readout makes the biodisplay a useful environmental monitoring tool. We have shown that our biodisplay can detect arabinose and sodium-arsenite in tap water using bacterial strains previously engineered by other research groups [20], [30] and student teams [31]. A large number of heavy metal sensors have already been engineered, including arsenic [32] [33], mercury [33], and lead sensors [34]. Information processing systems also exist, including genetic toggle switches [35], logic functions [36], band-pass filters [37], and event counters [38]. By combining event counters or toggle switches with sensors it is possible to implement memory, which could be useful in instances when the biodisplay can be monitored only intermittently, but a transient contamination should be logged and reported. The use of band-pass filters would enable the development of a biodisplay that reports the concentration of an analyte without requiring quantitative analysis of the reported signal. The biodisplay can also reduce the complexity of engineered strains, since functions can potentially be distributed amongst several strains [39]. For example, to generate a sensor that senses and reports the presence/absence of three different substances wouldn't require incorporation of all three functions into a single strain but could instead be implemented in three individual strains. It should also be possible to develop chemiluminescent biodisplays or color biodisplays using chromogenic proteins. Communication between pixels as previously demonstrated using hydrogen peroxide [17] could also be used to couple sensing biopixels, logic biopixels, and reporter biopixels.

Unlike previous biopixel arrays [17] where each pixel contains the same bacterial strain, each pixel on our display can be specifically programmed with a different strain, drastically increasing the multiplexing capacity and information content of our biodisplay with a maximum of 768 unique strains, each of which could contain multiple, genetically encoded functions. A previous demonstration of integrating an *E. coli* arsenic biosensor in a microfluidic device was limited to a single culture, employed a complex scheme that decoupled culturing from measurement, and used a research-grade fluorescent microscope for readout [40]. A scheme called InfoBiology was used for the transmission of information using arrays of bacterial cells spotted on microtiter sized agar plates [41]. 144 colonies of a

handful of strains were spotted in this scheme, but lacked integration with a microfluidic device for cell culturing and environmental sampling.

We have previously developed a low-cost, portable hardware system that contains all necessary components for microfluidic device operation, making the biodisplay readily deployable in resource limited settings [42]. By using bacterial spores the biodisplay can be stored and shipped under ambient conditions and is viable for extended periods of time. The material cost of the biodisplay itself is negligible at less than 1 USD per device. In this particular example a bio-hardware platform applied to continuous environmental monitoring of arsenic levels in water could replace a 26'5000 USD instrument with an annual running cost of over 3'5000 USD (Oval7000, Modern Water Monitoring Limited). The relatively slow response time of our biodisplay is acceptable in this and other applications, where continued chronic exposure of a substance is to be avoided. For time critical applications the response time of the biosensors would need to be improved, for example by developing phosphorylation based sensors and reporters rather than transcriptional based genetic networks [43].

Programmable biopixel displays drastically simplify device readout and interpretation. Instead of reporting the presence of arsenic using a display-wide pattern of signal oscillations [17], our biodisplay generates an easy to understand “skull and crossbones” symbol. We showed that this concept can be easily multiplexed using different symbols to report the presence of multiple small molecules. The number of biopixels is scalable with previous work on two layer polydimethylsiloxane (PDMS) chips having demonstrated up to 4'160 unit cells per device [44], [45]. Immediate optical readout without specialized equipment combined with the fact that computing and decision-making steps are conducted by the biodisplay itself make it low-cost, easy to deploy, and easy to interpret. Bio-hardware hybrid devices therefore combine the advantages of biological systems with the advantages of mechanical, electrical and optical systems. The ability to engineer biological systems on the molecular level and combine them with novel hardware opens new opportunities for how biological, mechanical, electrical and optical systems are integrated and the types of functions they can perform.

4.4 - Methods

4.4.1 - Materials

All bacterial strains and plasmids used in the study are listed in Table 4.1. Cells for arsenic detection were a gift from Baojun Wang (University of Edinburgh): pBW103ParsR-Amp30C (Addgene plasmid # 78638), pBW300ParsR-Amp32T (Addgene plasmid # 78652), pBW102ParsR-Amp32C (Addgene plasmid # 78637) and pBW101ParsR-gfp (Addgene plasmid # 78636). LB medium was purchased from Applichem Panreac (A0954). L-(+)-Arabinose (A3256-100G), 0.05M (35000-1L-R) and chloramphenicol (23275) were purchase from Sigma. Kanamycin sulfate (T832.1) was bought from Carl Roth. Isopropyl- β -

D-thiogalactoside for spore induction was purchased from Roche. Schaeffer and Fulton Spore Stain Kit was bought from Sigma Aldrich.

4.4.2 - Device fabrication

Device molds were made using standard photolithography techniques. The mold for the control layer was made using GM 1070 SU-8 photoresist (Gersteltec Sarl, Switzerland) with a height of 30 μm . The flow layer was made with AZ9260 photoresist (Gersteltec Sarl, Switzerland) with a thickness of 14 μm . A Suss MJB4 single side mask aligner was used to expose the wafers. The flow mold was baked for 2 hours at 135°C to anneal the flow channels. The molds were then treated with chlorodimethylsilane (DMCS) prior to being exposed to PDMS (Sylgard 184). The double layer microfluidic device were made by using multilayer soft lithography [46]. For the flow layer, PDMS was prepared with a ratio of 20:1 (part A:B) and spin coated with a speed of 3000 rpm for 1 minute, in order to get a thickness in the range of 20 – 40 nm. The control mold was placed in a petri dish and coated with a 5:1 ratio of PDMS, in order to get a ~ 0.5 cm thick device. Both layers were baked for 30 minutes at 80°C. Then the control layer was cut and peel off from the petri dish and place on top of the flow. The alignment of the two layer was performed by eyes using a stereomicroscope; markers, placed all around the main structure of the device, help to understand when the alignment is done. After alignment the two PDMS layers were baked for an additional 1.5 hours at 80°C. The chip was then aligned to a spotted glass slide.

4.4.3 - Cell culture, transformation and spore formation

E. coli and *B. subtilis* cells were cultured in LB medium at 37°C and 200 rpm with appropriate antibiotics, when required. All plasmid transformation and *E.coli* cell studies were performed in DH5- α cells. *B. subtilis* sporulation was performed as described previously [47]. For spore enrichment, a three day old *B. subtilis* cell suspension was centrifuge for 1 min at 15000 rpm, the pellet was washed three times with water and Schaeffer and Fulton spore staining was performed to verify the presence of spores.

4.4.4 - Cell arraying

Overnight cultures of *E. coli* and *B. subtilis* were centrifuged for 5 min at 3000 rpm. For the *E. coli* display the cell pellet was resuspended in 100 μl LB with 10% glycerol and appropriate antibiotics. For the spore biodisplay spores were resuspended in water. Cell suspensions and *B. subtilis* spore solutions were plated in conical, polypropylene 96-well plates. The samples were spotted with a 0.7 nl delivery volume pin (946MP2B Arrayit) on a glass slide by using a microarray robot (QArray2, Genetix). Glass slides were coated with epoxysilane (3-Glycidoxypropyl-dimethoxymethylsilane 97% AC216545000 Acros organic). The spotting parameters were as follows: 100 ms inking time, 10 ms stamping time, max number of stamps per ink 30. A wash procedure was included that consisted of washing the spotting pin with 70% ethanol for 2 s, washing with water for 2 s each followed by pin drying. Depending on the spotting pattern and number of samples used the spotting time varied between 10 to 20 minutes.

4.4.5 - Cell-display culturing

The *E. coli* array was aligned to a PDMS chip and incubate for 1 hour at 37°C. The spore-array was aligned to a MITOMI [48] PDMS chip and incubated depending on the experimental procedure as follows: 40°C for 1 day, 40°C for 1 month, 80°C for 1 day, or 80°C for 1 month. After the incubation step the devices were placed on a temperature-controlled glass plate (H401-NIKON-TI_SR_GLASS/H401_T_CONTROLLER; Okolab) at 37°C. Tygon tubes were filled with deionized water and connected to inlets of the control lines, pressure was applied in order to actuate the valves. For the *E. coli* display 68.9 kPa and 13.8 kPa were used, for the control and flow lines respectively. For the spore-display 103.4 kPa and 24.1-27.5 kPa were used instead. For the spore display we used a 768 unit cell MITOMI chip[48], but performed the same culturing routine as on the biodisplay device. For the cell-culturing and sampling routines a custom-written LabVIEW program was used. During the culturing, LB medium with appropriate antibiotics and lysis buffer containing 30 mM of NaOH (06203-1KG Sigma Aldrich) and 12% SDS (L3771-100G Sigma) was used. Depending on the experimental procedure LB medium or water was supplemented with arabinose, sodium-arsenite, or IPTG. The level of arsenic in the tap water was measured by a colorimetric arsenic stip test kit (MQuant™ Arsenic Test , Sigma Aldrich) with LOD of 5 µg/l. No levels of arsenic, in the tap water, were detected by the kit.

4.4.6 - Imaging

Image acquisition was performed on a Nikon ECLIPSE *Ti* automated microscope equipped with a LED Fluorescence Excitation System and a Hamamatsu ORCA-Flash 4.0 camera controlled by NIS Elements. Images were taken at 40x magnification (SPlan Fluor, ELWD 40x/0.60, ∞/0.2, WD 3.6-2.8, Nikon) in fluorescent and bright field mode. Images of all biopixel units were stitched together using either the Grid/Collection Stitching plugin in Fiji or a custom-written Python script. Fluorescent measurements were performed using Genepix software. A FITC USB fluorescent microscope (AM4113T-GFBW, Dino-Lite) was used to acquire fluorescent images. Images of 9 sub-sections of the device were taken, using lower magnification (10x), and stitched. Pictures were also taken using a cellphone camera. A band-pass filter, centered at 530 nm with a 40 nm bandwidth, was placed in front of the camera of the mobile phone, and the LEDs of the FITC USB microscope were used for illumination of the biodisplay.

4.5 - Supplementary

4.5.1 - Biodisplay for strain characterization at 37°C

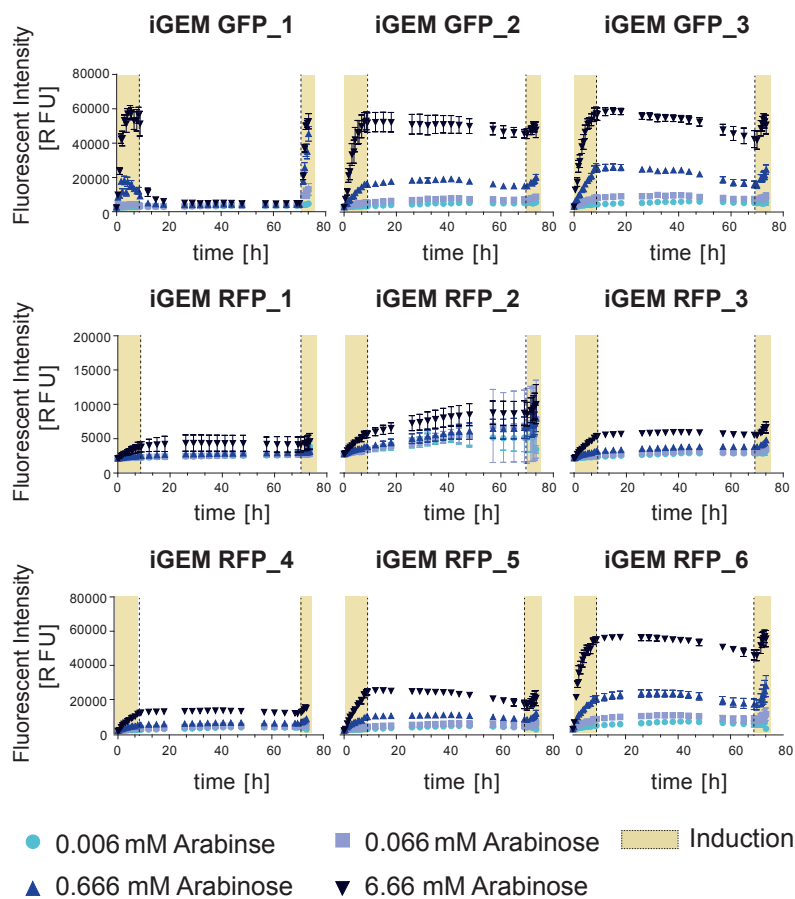


Figure SI 4.1: **Biodisplay for strain characterization at 37°C**. Fluorescent intensity of GFP or RFP expression of nine different arabinose sensitive *E. coli* strains. The cells were induced twice with 4 different concentrations of arabinose (0.006 mM, 0.066 mM, 0.666 mM and 6.66 mM). The yellow background indicates the induction intervals. The microfluidic chip was heated to 37°C during the experiment.

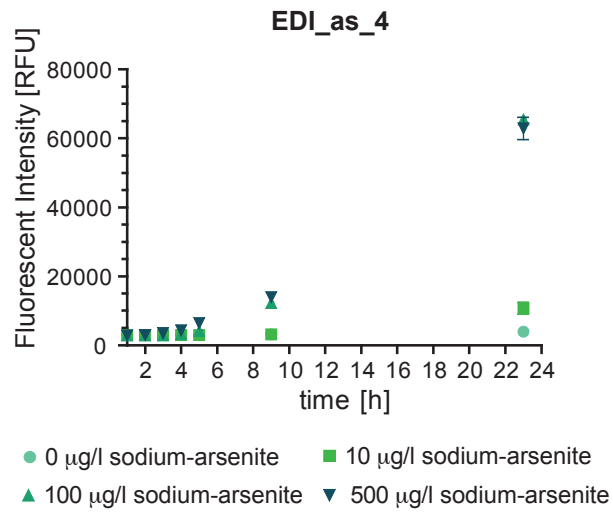
4.5.2 - Arsenic responsive *E. coli*

Figure SI 4.2: **Arsenic-responsive *E. coli***. EDI_as_4, was spotted on the chip and four different concentrations of sodium-arsenite in LB were sampled for 24 hours. GFP expression was monitored over time using a Nikon microscope.

4.5.3 - Arsenic biodisplay –different arsenic concentrations

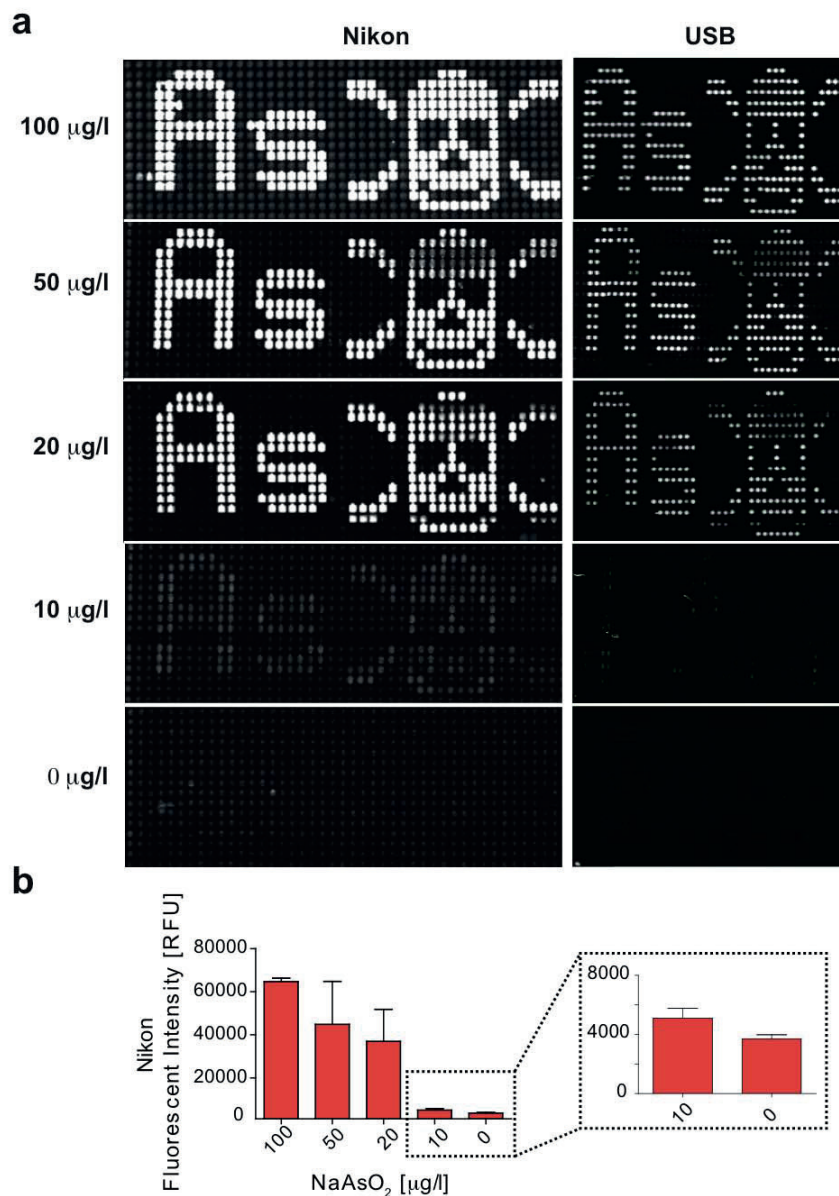


Figure SI 4.3: **Arsenic biodisplay.** (a) Fluorescent images taken using Nikon and USB microscope after 24 hours of induction with different concentrations of sodium-arsenite (100 $\mu\text{g/l}$, 50 $\mu\text{g/l}$, 20 $\mu\text{g/l}$, 10 $\mu\text{g/l}$ and 0 $\mu\text{g/l}$). Each concentration was sampled in different devices. (b) Quantitation of the fluorescent signal, after 24 hours of induction and measured with the Nikon microscope.

4.5.4 - Arsenic biodisplay over time

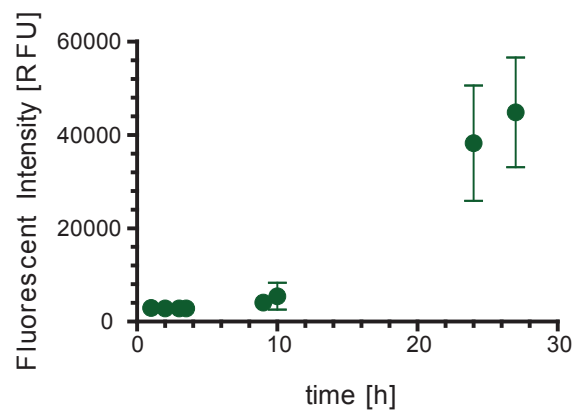


Figure SI 4.4: **Arsenic biodisplay over time.** Arsenic-responsive *E. coli* was spotted in a “As” and a “skull and crossbones” pattern. 20 $\mu\text{g/l}$ of sodium-arsenite in tap water was sampled and GFP expression monitored over time using a Nikon microscope.

4.5.5 - Cellphone image acquisition

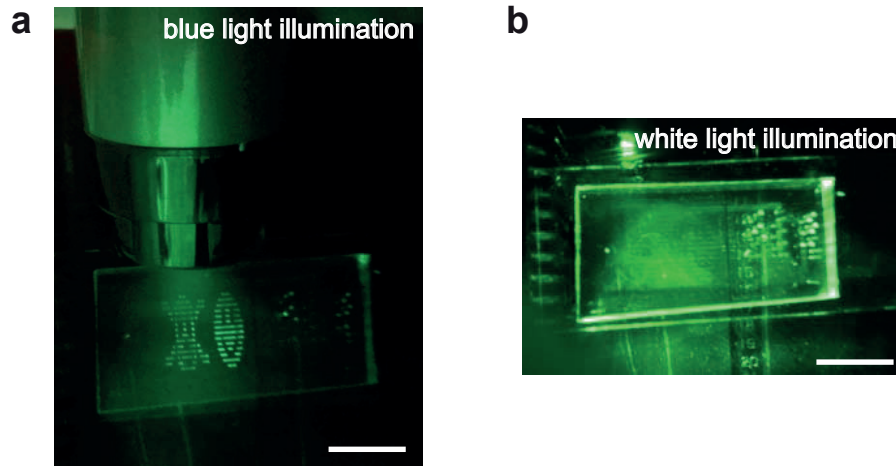


Figure SI 4.5: **Cellphone image acquisition.** (a) The microfluidic chip was illuminated using the LEDs of a USB microscope (excitation at 480 nm), a band-pass filter centered at 530 nm with a 40 nm bandwidth was placed in front of the camera of the cellphone. (b) The same device was illuminated by white light and imaged using the cellphone and emission filter as in (a). Scale bar 1 cm.

4.5.6 - Embedded device

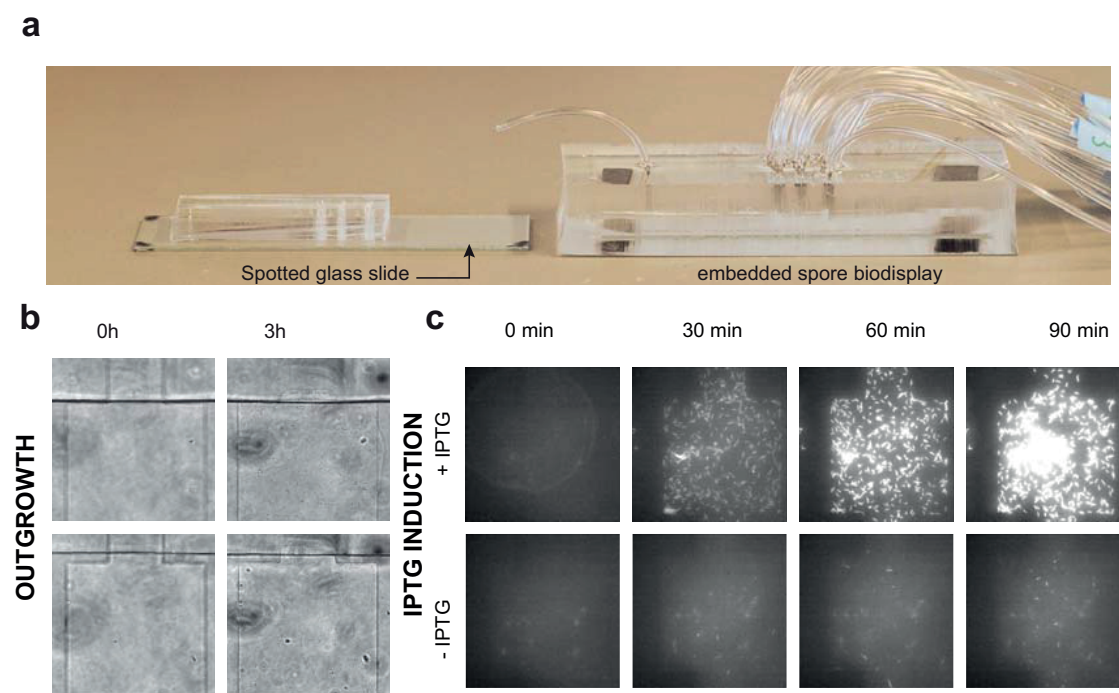


Figure SI 4.6: **Embedded spore biodisplay.** (a) Photos comparing the spore biodisplay and the embedded PDMS spore biodisplay. (b) Bright-field images of representative chambers showing the spores outgrowth. Images are acquired immediately after spot resuspension with medium and 3 hours incubation at 37°C. (c) Time-lapse images of germinated *Phy-spamCherry B. subtilis* spores after induction with 1 μ M IPTG.

4.5.7 - List of strains used in this work

Identifier	Name	Host Strain	Resistance	Inducer	Reporter
BBa_I13517	iGEM RFP_1	<i>E.coli</i> DH5 α	Chloramphenicol	Arabinose	RFP
BBa_K1333301	iGEM RFP_2	<i>E.coli</i> DH5 α	Chloramphenicol	Arabinose	RFP
BBa_K1333300	iGEM RFP_3	<i>E.coli</i> DH5 α	Chloramphenicol	Arabinose	RFP
BBa_K577004	iGEM RFP_4	<i>E.coli</i> DH5 α	Chloramphenicol	Arabinose	RFP
BBa_K577882	iGEM RFP_5	<i>E.coli</i> DH5 α	Chloramphenicol	Arabinose	RFP
BBa_I13516	iGEM RFP_6	<i>E.coli</i> DH5 α	Chloramphenicol	Arabinose	RFP
BBa_K750000	iGEM GFP_1	<i>E.coli</i> DH5 α	Chloramphenicol	Arabinose	GFP
BBa_K584000	iGEM GFP_2	<i>E.coli</i> DH5 α	Chloramphenicol	Arabinose	GFP
BBa_K577881	iGEM GFP_3	<i>E.coli</i> DH5 α	Chloramphenicol	Arabinose	GFP
pBW101ParsR-gfp (78636)	EDI_as_1	<i>E.coli</i> DH5 α	Kanamycin	Arsenic	GFP
pBW102ParsR-Amp32C (78637)	EDI_as_2	<i>E.coli</i> DH5 α	Kanamycin	Arsenic	GFP
pBW103ParsR-Amp30C (78638)	EDI_as_3	<i>E.coli</i> DH5 α	Kanamycin	Arsenic	GFP
pBW300ParsR-Amp32T (78652)	EDI_as_4	<i>E.coli</i> DH5 α	Kanamycin	Arsenic	GFP
pIIUN gfp	UNIL_1	<i>E.coli</i> DH5 α	Kanamycin	Arsenic	GFP
pAAUN gfp	UNIL_2	<i>E.coli</i> DH5 α	Kanamycin	Arsenic	GFP
pVUN gfp	UNIL_3	<i>E.coli</i> DH5 α	Kanamycin	Arsenic	GFP
pLtet0UN gfp	UNIL_4	<i>E.coli</i> DH5 α	Kanamycin	Arsenic	GFP
pPR arsR abs gfp	UNIL_5	<i>E.coli</i> DH5 α	Kanamycin	Arsenic	GFP
BGSC 3A40	Bacillus subtilis subsp. Subtilis amyE::Physpan k-mCherry	<i>B. subtilis</i> subsp. <i>subtilis</i>		IPTG	mCherry
BGSC 3A39	Bacillus subtilis subsp. Subtilis amyE::Physpan k-GFP	<i>B. subtilis</i> subsp. <i>subtilis</i>		IPTG	GFP

Table 4.1: List of plasmids and strains used in this work.

Bibliography

- [1] J. R. van der Meer and S. Belkin, “Where microbiology meets microengineering: design and applications of reporter bacteria,” *Nat. Rev. Microbiol.*, vol. 8, no. 7, pp. 511–522, Jun. 2010.
- [2] L. T. Bereza-Malcolm, G. Mann, and A. E. Franks, “Environmental Sensing of Heavy Metals Through Whole Cell Microbial Biosensors: A Synthetic Biology Approach,” *ACS Synth. Biol.*, vol. 4, no. 5, pp. 535–546, May 2015.
- [3] N. Szita, K. Polizzi, N. Jaccard, and F. Baganz, “Microfluidic approaches for systems and synthetic biology,” *Curr. Opin. Biotechnol.*, vol. 21, no. 4, pp. 517–523, Aug. 2010.
- [4] S. Gulati *et al.*, “Opportunities for microfluidic technologies in synthetic biology,” *J. R. Soc. Interface*, vol. 6, no. Suppl 4, pp. S493–S506, Aug. 2009.
- [5] O. Wright, G.-B. Stan, and T. Ellis, “Building-in biosafety for synthetic biology,” *Microbiol. Read. Engl.*, vol. 159, no. Pt 7, pp. 1221–1235, Jul. 2013.
- [6] G. M. Whitesides, “The origins and the future of microfluidics,” *Nature*, vol. 442, no. 7101, pp. 368–373, Jul. 2006.
- [7] S. J. Maerkl, “Integration column: Microfluidic high-throughput screening,” *Integr. Biol. Quant. Biosci. Nano Macro*, vol. 1, no. 1, pp. 19–29, Jan. 2009.
- [8] J.-B. Nobs and S. J. Maerkl, “Long-term single cell analysis of *S. pombe* on a microfluidic microchemostat array,” *PloS One*, vol. 9, no. 4, p. e93466, 2014.
- [9] M. R. Bennett and J. Hasty, “Microfluidic devices for measuring gene network dynamics in single cells,” *Nat. Rev. Genet.*, vol. 10, no. 9, pp. 628–638, Sep. 2009.
- [10] J. L. Garcia-Cordero and S. J. Maerkl, “A 1024-sample serum analyzer chip for cancer diagnostics,” *Lab. Chip*, vol. 14, no. 15, pp. 2642–2650, Aug. 2014.
- [11] J. L. Garcia-Cordero and S. J. Maerkl, “Mechanically Induced Trapping of Molecular Interactions and Its Applications,” *J. Lab. Autom.*, vol. 21, no. 3, pp. 356–367, Jun. 2016.
- [12] S. A. Morin, R. F. Shepherd, S. W. Kwok, A. A. Stokes, A. Nemiroski, and G. M. Whitesides, “Camouflage and display for soft machines,” *Science*, vol. 337, no. 6096, pp. 828–832, 2012.
- [13] I. H. Riedel-Kruse *et al.*, “Design, engineering and utility of biotic games,” *Lab Chip*, vol. 11, no. 1, pp. 14–22, 2011.
- [14] X. Liu, T.-C. Tang, E. Tham, H. Yuk, and S. Lin, “Stretchable Living Materials and Devices with Hydrogel-Elastomer Hybrids Hosting Programmed Cells,” *Proc. Natl. Acad. Sci.*, p. 201618307, Feb. 2017.
- [15] N. Dénervaud *et al.*, “A chemostat array enables the spatio-temporal analysis of the yeast proteome,” *Proc. Natl. Acad. Sci. U. S. A.*, vol. 110, no. 39, pp. 15842–7, Sep. 2013.
- [16] A. S. Rajkumar, N. Dénervaud, and S. J. Maerkl, “Mapping the fine structure of a eukaryotic promoter input-output function,” *Nat. Genet.*, vol. 45, no. 10, pp. 1207–1215, Aug. 2013.
- [17] A. Prindle, P. Samayoa, I. Razinkov, T. Danino, L. S. Tsimring, and J. Hasty, “A sensing array of radically coupled genetic ‘biopixels,’” *Nature*, vol. 481, no. 7379, pp. 39–44, Dec. 2011.
- [18] C. L. Hansen, E. Skordalakes, J. M. Berger, and S. R. Quake, “A robust and scalable microfluidic metering method that allows protein crystal growth by free interface diffusion,” *Proc. Natl. Acad. Sci. U. S. A.*, vol. 99, no. 26, pp. 16531–6, Dec. 2002.
- [19] F. K. Balagaddé, L. You, C. L. Hansen, F. H. Arnold, and S. R. Quake, “Long-term monitoring of bacteria undergoing programmed population control in a microchemostat,” *Science*, vol. 309, no. 5731, pp. 137–140, 2005.
- [20] B. Wang, M. Barahona, and M. Buck, “Engineering modular and tunable genetic amplifiers for scaling transcriptional signals in cascaded gene networks,” *Nucleic Acids Res.*, vol. 42, no. 14, pp. 9484–9492, Aug. 2014.
- [21] D. Merulla, V. Hatzimanikatis, and J. R. van der Meer, “Tunable reporter signal production in feedback-uncoupled arsenic bioreporters,” *Microb. Biotechnol.*, vol. 6, no. 5, pp. 503–14, Sep. 2013.
- [22] H. N. Lynch, G. I. Greenberg, M. C. Pollock, and A. S. Lewis, “A comprehensive evaluation of inorganic arsenic in food and considerations for dietary intake analyses,” *Sci. Total Environ.*, vol. 496, pp. 299–313, 2014.

- [23] I. Hojsak *et al.*, “Arsenic in Rice,” *J. Pediatr. Gastroenterol. Nutr.*, vol. 60, no. 1, pp. 142–145, Jan. 2015.
- [24] A. A. Meharg *et al.*, “Inorganic arsenic levels in rice milk exceed EU and US drinking water standards,” *J. Environ. Monit.*, vol. 10, no. 4, pp. 428–431, 2008.
- [25] “WHO | Arsenic,” *WHO*, 2016.
- [26] M. F. Naujokas *et al.*, “The broad scope of health effects from chronic arsenic exposure: update on a worldwide public health problem,” *Environ. Health Perspect.*, vol. 121, no. 3, pp. 295–302, Mar. 2013.
- [27] “Priority List of Hazardous Substances | ATSDR.”
- [28] P. Setlow, “Spores of *Bacillus subtilis*: their resistance to and killing by radiation, heat and chemicals,” *J. Appl. Microbiol.*, vol. 101, no. 3, pp. 514–525, Sep. 2006.
- [29] A. Atrih and S. J. Foster, “The role of peptidoglycan structure and structural dynamics during endospore dormancy and germination,” *Antonie Van Leeuwenhoek*, vol. 75, no. 4, pp. 299–307, 1999.
- [30] D. Merulla, V. Hatzimanikatis, and J. R. van der Meer, “Tunable reporter signal production in feedback-uncoupled arsenic bioreporters,” *Microb. Biotechnol.*, vol. 6, no. 5, pp. 503–514, Sep. 2013.
- [31] “parts.igem.org.”
- [32] H. Kaur, R. Kumar, J. N. Babu, and S. Mittal, “Advances in arsenic biosensor development – A comprehensive review,” *Biosens. Bioelectron.*, vol. 63, pp. 533–545, 2015.
- [33] O. Wright, M. Delmans, G.-B. Stan, and T. Ellis, “GeneGuard: A Modular Plasmid System Designed for Biosafety,” *ACS Synth. Biol.*, vol. 4, no. 3, pp. 307–316, Mar. 2015.
- [34] L. Bereza-Malcolm, S. Aracic, and A. E. Franks, “Development and Application of a Synthetically-Derived Lead Biosensor Construct for Use in Gram-Negative Bacteria,” *Sensors*, vol. 16, no. 12, Dec. 2016.
- [35] T. S. Gardner, C. R. Cantor, and J. J. Collins, “Construction of a genetic toggle switch in *Escherichia coli*,” *Nature*, vol. 403, no. 6767, pp. 339–42, Jan. 2000.
- [36] A. A. K. Nielsen *et al.*, “Genetic circuit design automation,” *Science*, vol. 352, no. 6281, p. aac7341-aac7341, Apr. 2016.
- [37] S. Basu, Y. Gerchman, C. H. Collins, F. H. Arnold, and R. Weiss, “A synthetic multicellular system for programmed pattern formation,” *Nature*, vol. 434, no. 7037, pp. 1130–1134, Apr. 2005.
- [38] A. E. Friedland, T. K. Lu, X. Wang, D. Shi, G. Church, and J. J. Collins, “Synthetic Gene Networks That Count,” *Science*, vol. 324, no. 5931, pp. 1199–1202, May 2009.
- [39] J. Shong, M. Rafael, J. Diaz, and C. H. Collins, “Towards synthetic microbial consortia for bioprocessing,” *Curr. Opin. Biotechnol.*, vol. 23, pp. 798–802, 2012.
- [40] N. Buffi *et al.*, “Development of a microfluidics biosensor for agarose-bead immobilized *Escherichia coli* bioreporter cells for arsenite detection in aqueous samples,” *Lab. Chip*, vol. 11, no. 14, pp. 2369–77, 2011.
- [41] M. A. Palacios *et al.*, “InfoBiology by printed arrays of microorganism colonies for timed and on-demand release of messages,” *Proc. Natl. Acad. Sci. U. S. A.*, vol. 108, no. 40, pp. 16510–4, Oct. 2011.
- [42] F. Piraino, F. Volpetti, C. Watson, and S. J. Maerkl, “A Digital–Analog Microfluidic Platform for Patient-Centric Multiplexed Biomarker Diagnostics of Ultralow Volume Samples,” *ACS Nano*, vol. 10, no. 1, pp. 1699–1710, Jan. 2016.
- [43] P. E. M. Purnick and R. Weiss, “The second wave of synthetic biology: from modules to systems,” *Nat. Rev. Mol. Cell Biol.*, vol. 10, no. 6, pp. 410–422, Jun. 2009.
- [44] P. M. Fordyce *et al.*, “De novo identification and biophysical characterization of transcription-factor binding sites with microfluidic affinity analysis,” *Nat. Biotechnol.*, vol. 28, no. 9, pp. 970–5, Sep. 2010.
- [45] J. L. Garcia-Cordero and S. J. Maerkl, “Mechanically Induced Trapping of Molecular Interactions and Its Applications,” *J. Lab. Autom.*, vol. 21, no. 3, pp. 356–367, Jun. 2016.

- [46] M. A. Unger, H.-P. Chou, T. Thorsen, A. Scherer, and S. R. Quake, “Monolithic Microfabricated Valves and Pumps by Multilayer Soft Lithography,” *Science*, vol. 288, no. 5463, pp. 113–116, Apr. 2000.
- [47] C. R. Harwood and S. M. Cutting, *Molecular biological methods for Bacillus*. Chichester ;New York: Wiley, 1990.
- [48] S. J. Maerkl and S. R. Quake, “Systems approach to measuring the binding energy landscapes of transcription factors,” *Science*, vol. 315, no. 5809, pp. 233–237, 2007.

Chapter 5

Conclusions and outlook

In this work, microfluidic platforms for multiplex immunoassay-based diagnostics and for environmental sensing have been developed. For both applications double layer microfluidic devices and spotting techniques have been exploited for creating multiplexed arrays of antibodies (for the immunoassay) and bacteria (for the environmental monitoring).

5.1 - Microfluidics for high-throughput immunoassay analysis

For the immunoassay application, we developed a high-throughput platform for protein interactions. The device enables 1'536 independent assays to be performed simultaneously. It is composed of 384 independent units, each of which can be addressed with a different antibody pair. Each unit contains four MITOMI buttons for analyzing four different samples. The stability of the device has been tested for long time periods (up to 1 month) at 40°C and according to performance tests, there is no significant difference between fresh and stored chips. The possibility to store the device for extended times, allows the device to be pre assembled before the analysis is performed making it suitable for academic and clinical applications.

The platform has been validated for the detection of four biomarkers and as well as for combinatorial analysis, in order to identify functional antibody pairs. Larger scale screening can be performed in the device, like the analysis of large protein libraries to search for new biomarkers for diagnosis, prognosis or to monitor therapy.

This platform would allow a drastic reduction in the cost of that study, not only for diagnostics but also for systems immunology and system biology applications. In fact the drastic reduction in the consumption of antibodies allows us to perform ~100'000 assays using ~100 µl of antibody stock solution.

Two drawbacks of the first generation of this system are the experimental time and the sensitivity. The long experimental time is mostly due to the diffusion time of the antibodies from the spotting to the reaction chamber. The total experimental time, considering the surface chemistry (1.5 hour), the incubation of primary and secondary antibodies (6.5 hours), the flowing of four samples (1.3 hours) and the washing steps, is about 10 hours. To overcome this limitation, a peristaltic pump, between the spotting chamber and the assay chamber, has been introduced in order to speed up the mixing of the antibodies instead of relying on diffusion. This second microfluidic chip design allowed us to perform the entire experiment in 2.5 hours.

Other requirements have been taken into consideration for the design of the second chip: low sensitivity, broad dynamic range, portability, and low sample volume. The device is composed of 16 independent units, each unit containing one MITOMI button. In order to improve the limits of detection a digital ELISA has been exploited and the MITOMI buttons have been patterned with femtoliter wells. The obtained sensitivity is in the femtomolar range, whereas the limits of detection using analog MITOMI buttons, is in the picomolar range, thus improving the limit of detection by 3 orders of magnitude.

Digital immunoassays are highly sensitive but do not allow the discrimination of high concentrations; indeed once the number of analytes increases, all the wells contain immunocomplexes and it is not possible to make a digital analysis (associating 1 to “on wells” and 0 to “off wells”). In order to increase the dynamic range, in one half of the device, the buttons were patterned with the digital wells and in the other half with standard analog MITOMI buttons. Combining the two techniques, digital detection for low concentrations and analog detection for high concentrations, we reached a dynamic range of 5 orders of magnitude.

Different kinds of sample matrices can be loaded into the device including, buffer, serum and whole blood. Only 5 μL sample are required to perform the analysis and the sample does not need any pretreatment and it can be directly loaded into the chip after blood sampling.

To make the employment of this platform feasible in a home-based setting or resource-limited environment, we built a portable microfluidic diagnostic system (μFDS) able to actuate the valves and control the flow of reagents. Using an Arduino interface it is possible to select the valves, regulate the pressure or start an automated program to perform the different assays (detection of an antigen or antibody for analog, amp, or analog-amp reactions). Furthermore, we employed a low cost and portable USB fluorescent microscope to image the chip. The entire cost of the microfluidic control system, the USB microscope and the netbook is \$2'628 USD, and the cost for the disposable microfluidic chip is \$1 USD. The cost could be further reduced by replacing some components, such as new generation solenoid valves, which are cheaper and more compact than those currently used.

In order to make the device more user-friendly, it could also be possible to replace the individual tubing for the control valves with “plug and play” multi-connectors, in order to interface the microfluidic device to multiple lines in a more convenient way.

So far the samples analyzed included mouse whole blood or human serum spiked with anti-Ebola, though it would also be interesting to test a clinical human sample. The platform could be applied further for the detection of multiple biomarkers, specific for a given disease especially for tests where the amount of sample is limited. For example, for the early diagnosis of Alzheimers, there is a set of biomarkers in the cerebrospinal fluid, which are recognized to be relevant [1], however the amount of available sample is too limited to conduct for several standard ELSA tests.

5.2 - Bacteria biodisplay

Multiplayer soft lithography has also been used for high-throughput culturing of bacterial cells. A different platform with 768 independent square units has been developed. Each chamber has been addressed with *E. Coli* cells using microspotting techniques. It is thus possible to have a multiplex array of cells with up to 768 different strains. After spotting the glass slide is aligned with a PDMS chip, stored for 1 h at 37°C and then connected with flow tubing, containing either media, lysis, or inducer solutions. The device can be employed for studying the high-throughput response of cells to different kinds or concentrations of inducer, in a unique device. A set of valves allows isolation of the chambers from each other and from the main channel, where the medium and lysis buffer are flown. Fresh medium and inducers diffuse periodically in the spotting cell, where the cells grow, and long term culturing is possible. As a proof of concept, nine different *E. coli* arabinose sensitive bacteria strains have been spotted. Different levels of the reporter protein have been observed depending on the different strain of cells and the concentration of arabinose. Different strains respond differently to the varying concentrations, such that low concentrations can only be detected from the more sensitive strains. Thus, it could be possible to spot different strains according to their sensitivity to obtain a progressive indication of the amount of an inducer molecule and discriminate the concentration in the sample based on which strain is producing the reporter protein.

E. coli strains sensitive to arsenate have also been employed to monitor the presence of this molecule in tap water. The cells were spotted according to a cross bone and skull pattern, and when a certain level of arsenate, 10 µg/L, is present in the solution (tap water), they produce GFP. The fluorescence signal can be detected using a low cost USB microscope making the entire system cheap and portable. Two different *E. coli* cells, sensitive to two different molecules (arabinose and arsenic) have been spotted in order to show the capability of performing multiplex detection.

Transmission of pathogenic through water is a global concern; and this platform can be used for a large screening of different heavy metals such as: arsenic, lead, mercury, and cadmium. Genetically engineered microorganisms for the detection of explosives have also been generated in order to detect 2,4,6-trinitrotoluene (TNT), for example[2]. Thus this device can be used to test the quality of groundwater reservoirs in the proximity of explosive manufacturing facilities, where the presence of residues of explosives could be found as a contaminant.

The device can also be employed for the detection of antimicrobials in food samples (such as milk, fish...). Several antibiotics are used by veterinarians or as food additives for growth promotion in the farming industry. Doses of antibiotics should be minimized to avoid resistance and to prevent the inclusion of allergenic antibiotics in the finished product, thus a control of food samples is necessary. For example, a bacterial strain sensitive to tetracycline can be employed for the detection of traces of the antibiotic in a fish sample [3] and the biodisplay could be used to perform the test.

There are systems for the detection of environmental samples that require one test vial and they can be performed in a short time periods, but on the other hand they do not allow a multiplexed and continuous analysis of a sample source. Instead, with the biodisplay platform multiplexed parameters could be monitored over time. The devices containing the bacterial spores can be stored for longer time periods, compared to those with *E. coli*, so further investigation of these devices could overcome the limitation of device storage.

In addition to its application towards environmental screening, the device can be employed for bacterial strain characterization. For example, it could be used as a tool for measuring expression dynamics in different cell strains [4], where screening a library of 768 different strains (8x96-well-plate) could be achieved on a single device.

Bibliography

- [1] B. Olsson *et al.*, “CSF and blood biomarkers for the diagnosis of Alzheimer’s disease: a systematic review and meta-analysis,” *Lancet Neurol.*, vol. 15, no. 7, pp. 673–684, Jun. 2016.
- [2] B. Shemer, N. Palevsky, S. Yagur-Kroll, and S. Belkin, “Genetically engineered microorganisms for the detection of explosives’ residues,” *Front. Microbiol.*, vol. 6, Oct. 2015.
- [3] T. Pellinen, G. Bylund, M. Virta, A. Niemi, and M. Karp, “Detection of Traces of Tetracyclines from Fish with a Bioluminescent Sensor Strain Incorporating Bacterial Luciferase Reporter Genes,” *J. Agric. Food Chem.*, vol. 50, no. 17, pp. 4812–4815, Aug. 2002.
- [4] A. Zaslaver *et al.*, “A comprehensive library of fluorescent transcriptional reporters for *Escherichia coli*,” *Nat. Methods*, vol. 3, no. 8, pp. 623–628, Aug. 2006.

Appendix A

A.1 - Multiplexed serological detection of IgE and IgG for Allergy detection

In vitro testing of specific IgE reactivities for diagnosis of allergies is a routine serological analysis, while IgG detection, as a diagnostic indicator for allergies, remains controversial. Due to the widespread incidence rate of allergies in the developed world there is considerable interest in developing novel assays and devices that perform sensitive, fast and multiplexed allergy tests [1]–[4] and do so in a POC or preferably a home-based setting. In serum the concentration of IgG is considerably higher than IgE, IgG thus readily outcompetes IgE for binding on the same immobilized allergen making IgE detection challenging [5], [6]. Commercial allergy tests are available based on lateral flow-based devices that allow the analysis of 10 IgE species, but require a large 110 μ l whole blood, a dedicated instrument for readout, and the quantification is qualitative or semiquantitative [7].

We employed the 16 units microfluidic chip, introduced in chapter 3, to perform allergy test. Since only analog detection has been exploited, all the 16 buttons are analog MITOMI buttons. To demonstrate the ability of our device to perform detection of allergen-specific IgE and IgG we tested a human serum sample obtained from a patient diagnosed with peanut allergy. In principle our device can measure up to 16 different allergens specific Ig or up to 8 different allergens for parallel quantitation of IgE and IgG. We programmed our device with two repeats of three different allergens: *Arachis hypogaea* allergen 2 (Ara h2), *Felis domesticus* allergen 1 (Fel d1), *Dermatophagoides pteronyssinus* allergen 2 (Der p2), and a negative control (Figure A.1a). The clinical serum sample (6 ml) was diluted 1:2 in an incubation buffer and flowed in the chip following the protocol described in the Materials and Methods section and IgE and IgG were detected as shown in Figure A.1b. In the top two rows of the device we measured allergen bound IgE and the bottom two rows of the device were used to detect IgG (Figure A.1c,d). We obtained clear signal for IgE and IgG bound to the recombinant allergen Ara h2, while the two other recombinant allergens Fel d1 and Der p2 showed no signal above the negative control. The signal obtained from IgG was

considerably stronger than that of IgE, as expected given the vastly different concentrations of these molecules in serum. Although we conducted readout of these devices with a research grade microscope, IgG levels were high enough to be observed directly using the fluorescence USB microscope indicating that a home-based, rapid allergy test could be developed. In the current form the diagnostic test is applicable in a POC setting to provide rapid and multiplexed analysis of a patient's allergic profile.

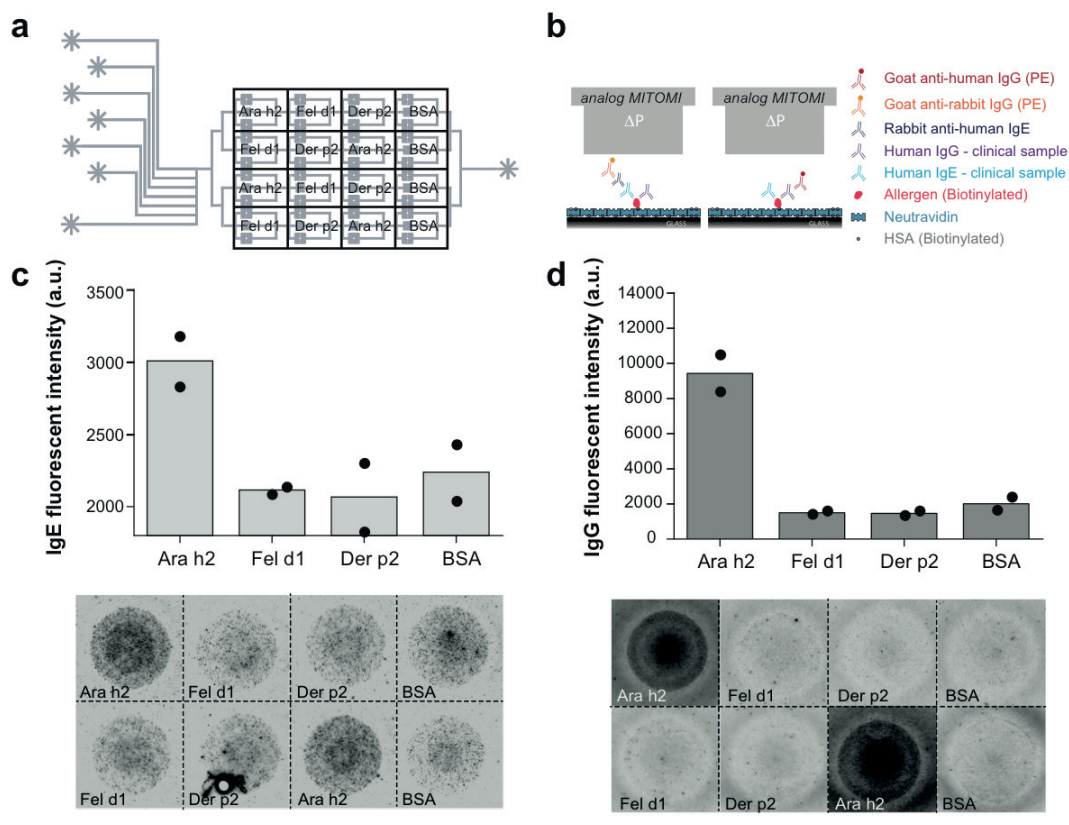


Figure A.1 **Allergy detection:** (a) Three biotinylated allergens (Ara h2, Fel d1, and Der p2) and a negative control (BSA) are spotted to allow multiplexed detection. (b) Schematic of the assay for the detection of IgG and IgE. (c) Quantification of IgE levels for a sample positive to peanuts allergy and the corresponding fluorescent images. (d) Quantification of IgG levels for a sample positive to peanuts allergy and the corresponding fluorescent images. Bars are means (n=2), with individual data points shown as dots (●).

A.1.1 - Materials and Methods

Three allergens: natural Ara h2, recombinant Fel d1, recombinant Der p2, and a BSA negative control were spotted in order to perform an allergy diagnostic test. The human clinical serum sample was diluted 1:2 (6.7 μ l in 13.4 μ l) with incubation buffer (0.05 M Tris/HCl pH 7.6, 0.15 M NaCl, Tween 20 0.02% v/v, BSA 1% w/v) [52]. After surface functionalization, 15 μ l of each reagent were loaded into tygon tubing, connected to the

device, and flowed sequentially at 3 psi for 10 minutes. First, 30.5 μM (0.55 mg/ml) of Ara h2, 41.15 μM (0.75 mg/ml) of Fel d1, and 42.8 μM (0.6 mg/ml) of Der p2 were circulated through each unit cell by the S-shaped peristaltic pump for 20 minutes and immobilized in the button region coated via neutravidin. Then the clinical sample was flowed for 5 minutes. Next, 1:100 rabbit anti-human IgE in 2% BSA and 30 nM (11.7 $\mu\text{g/ml}$) of anti-rabbit IgG PE conjugated antibody in 2% BSA were flowed on the top half of the device while 6 nM (2.4 $\mu\text{g/ml}$) of goat anti-human IgG PE conjugated antibody in 2% BSA was flowed on the lower half for 10 minutes. Channels were washed with 0.005% Tween 20 in PBS after each step for 5 minutes. After the last washing step the buttons were closed with 25 psi pressure. Bright field and fluorescent images were taken using the Nikon microscope with an exposure time of 2000 ms for IgE and 300 ms for IgG.

Bibliography

- [1] L. R. Hirsch, J. B. Jackson, A. Lee, N. J. Halas, and J. L. West, "A Whole Blood Immunoassay Using Gold Nanoshells," *Anal. Chem.*, vol. 75, no. 10, pp. 2377–2381, May 2003.
- [2] T. Chinnasamy, L. I. Segerink, M. Nystrand, J. Gantelius, and H. A. Svahn, "A lateral flow paper microarray for rapid allergy point of care diagnostics," *The Analyst*, vol. 139, no. 10, pp. 2348–2354, May 2014.
- [3] D. Pomponi *et al.*, "Allergen Micro-Bead Array for IgE Detection: A Feasibility Study Using Allergenic Molecules Tested on a Flexible Multiplex Flow Cytometric Immunoassay," *PLoS ONE*, vol. 7, no. 4, p. e35697, Apr. 2012.
- [4] D. M. Rissin *et al.*, "Simultaneous detection of single molecules and singulated ensembles of molecules enables immunoassays with broad dynamic range," *Anal. Chem.*, vol. 83, no. 6, pp. 2279–2285, Mar. 2011.
- [5] S. B. Lehrer, R. Reish, J. Fernandes, P. Gaudry, G. Dai, and G. Reese, "Enhancement of murine IgE antibody detection by IgG removal," *J. Immunol. Methods*, vol. 284, no. 1–2, pp. 1–6, Jan. 2004.
- [6] M. Cretich *et al.*, "Detection of allergen specific immunoglobulins by microarrays coupled to microfluidics," *Proteomics*, vol. 9, no. 8, pp. 2098–2107, Apr. 2009.
- [7] P. A. Eigenmann *et al.*, "The ImmunoCAP Rapid Wheeze/Rhinitis Child test is useful in the initial allergy diagnosis of children with respiratory symptoms," *Pediatr. Allergy Immunol. Off. Publ. Eur. Soc. Pediatr. Allergy Immunol.*, vol. 20, no. 8, pp. 772–779, Dec. 2009.

Francesca Volpetti

Address: Chemin de la Fourmi, 24-1010 Lausanne, Switzerland

Tel. +41 76 665 99 51

Email: francesca.volpetti@epfl.ch

Italian, Driving License, Work permit B

PhD in Microsystem and Microelectronics, Biomedical Engineer

Education

PhD Microsystems and Microelectronics – [EPFL, [Sep. 2012 — July 2017]
Lausanne, Switzerland]

Thesis: “High-throughput microfluidic platforms applied to immunoassay-based diagnostics and environmental monitoring”.

Design and fabrication of portable microfluidic device for immunoassay analysis in unprocessed human blood and analysis of environmental sample.

MSc Biomedical Engineering – [Sapienza University, Rome, [Jan 2010 — Jan 2012]
Italy]

Thesis: “Autonomous immunoassay in lab-on-chip for point-of-care analysis”.

Design and Fabrication of autonomous microfluidic device for sequential flow of different solution for diagnostics.

BSc – Clinical Engineering — [Sapienza University, Rome, [Oct 2006 — Nov 2009]
Italy]

Thesis: “Characterization of polydimethylsiloxane for biomedical application”

Study of long stability of PDMS for electrowetting.

Technical skills

Microfabrication: photolithography, soft lithography, e-beam lithography, thermal evaporation, atomic layer deposition, physical and chemical etching, design of electronic devices, transfer of 2D materials.

Characterization techniques: atomic force microscopy, electrical measurements, fluorescent microscopy.

Biological techniques: bacterial culture, bacterial transformation, immunoassay-based diagnostics.

Experience

Internship – [Janssen, pharmaceutical companies of [May 2012 — Jul 2012]
Johnson and Johnson, Latina (LT), Italy]

- Quality control in the area of packaging.

Master Internship — [INESC MN, Lisbon, Portugal] [Jul 2011 — Dec 2011]

- Design and fabrication of a microfluidic device based on capillarity effect for immunoassay analysis.

Bachelor Internship — [Sapienza University, Rome, Italy] [Jul 2009 — Oct 2009]

- Characterization of polydimethylsiloxane for electrowetting application.
- Fabrication and electrical characterization of electrowetting system.

Invention disclosures

- Piraino F, Volpetti F, Maerkl SJ, "A system, device and method for multiplexed biomarker diagnostics of ultra-low volume whole blood samples", US Provisional Patent Application n 62/267,959

- Novo P, Volpetti F, Chu V, Conde J, "Autonomous and programmable sequential flow of solutions in capillary microfluidics " WO 2013183013 A1

Languages and IT skills

Languages: *Italian* (Mother tongue), *English* (C2), *French* (A2).

IT: Matlab, LabView, Adobe Illustrator, MS Office, Mac OSX, AutoCad, Origin, Igor.

Extracurricular activities and interests

Swimming (4 years)
Ballet, modern and jazz dance (6 years)
Travelling and reading

List of publications

Volpetti F.*, Petrova E.*, Maerkl S.J. "A microfluidic biodisplay", under review

Piraino F.*, **Volpetti F.***, Watson C., Maerkl S.J. "A Digital–Analog Microfluidic Platform for Patient–Centric Multiplexed Biomarker Diagnostics of Ultralow Volume Samples", *ACS Nano*, 2016

Volpetti F. Garcia-Cordero J.L., Maerkl S. J. " A microfluidic platform for high- throughput multiplexed protein quantitation", *PLoS One*, 2015

Novo P., **Volpetti F.**, Chu V., Conde J. P. "Autonomous capillary microfluidic immunoassay with integrated detection using microfabricated photodiodes: towards a point-of-care device", *Transducers & Eurosensors XXVII: The 17th International Conference on Solid-State Sensors, Actuators and Microsystems (transducers & EUROSENSORS XXVII)*, 2013

Novo P.*, **Volpetti F.***, Chu V., Conde J. P. "Control of sequential fluid delivery in a fully autonomous capillary microfluidic device", *Lab on a chip*, 2012

***Equally contributing**

